LOW FREQUENCY WAVE RESONANCE ON FRINGING REEFS

Andrew William Mackay Pomeroy
4055292

The Erasmus Mundus MSc Coastal and Marine Engineering and Management
is an integrated programme organized by five European partner institutions,
coordinated by Delft University of Technology (TU Delft).
The joint study programme of 120 ECTS credits (two years full-time) has been
obtained at three of the five CoMEM partner institutions:

- Norges Teknisk- Naturvitenskapelige Universitet (NTNU) Trondheim, Norway
- Technische Universiteit (TU) Delft, The Netherlands
- City University London, Great Britain
- Universitat Politècnica de Catalunya (UPC), Barcelona, Spain
- University of Southampton, Southampton, Great Britain

The first year consists of the first and second semesters of 30 ECTS each, spent at
NTNU, Trondheim and Delft University of Technology respectively.
The second year allows for specialization in three subjects and during the third
semester courses are taken with a focus on advanced topics in the selected area of
specialization:
- Engineering
- Management
- Environment
In the fourth and final semester an MSc project and thesis have to be completed.
The two year CoMEM programme leads to three officially recognized MSc diploma
certificates. These will be issued by the three universities which have been attended by
the student. The transcripts issued with the MSc Diploma Certificate of each university
include grades/marks for each subject. A complete overview of subjects and ECTS
credits is included in the Diploma Supplement, as received from the CoMEM
coordinating university, Delft University of Technology (TU Delft).

Information regarding the CoMEM programme can be obtained from the programme
coordinator and director

Prof. Dr. Ir. Marcel J.F. Stive
Delft University of Technology
Faculty of Civil Engineering and geosciences
P.O. Box 5048
2600 GA Delft
The Netherlands

COASTAL AND MARINE ENGINEERING AND MANAGEMENT
COMEM

LOW FREQUENCY WAVE RESONANCE ON FRINGING REEFS

Andrew William Mackay Pomeroy

June 2011

Graduation Committee:
Prof.dr.ir. M.J.F. Stive   Chairman, Technische Universiteit Delft
Dr.ir. A.R. van Dongeren   Deltares
Dr.Ir. J.S.M. van Thiel de Vries   Deltares / Technische Universiteit Delft
Assoc. Prof. Dr. R.W.M.R.J.B. Ranasinghe   UNESCO | IHE / Technische Universiteit Delft
Dr.ir. M. Zijlema   Technische Universiteit Delft
Assoc. Prof. R. Lowe   The University of Western Australia

This thesis was prepared at the offices of:

Stichting Deltares

Rotterdamseweg 185, 2629HD,

Delft, the Netherlands

and is in partial fulfillment of the requirements of the degree of

Erasmus Mundus Master in Coastal and Marine Engineering and Management (CoMEM)

which is coordinated by

Prof.dr.ir. M.J.F. Stive

Faculty of Civil Engineering and Geosciences

Delft University of Technology (TU Delft)

Delft, The Netherlands

and includes the following educational institutions

Norwegian University of Science and Technology (NTNU)

Trondheim, Norway

Polytechnic University of Catalonia (UPC)

Barcelona, Spain

at which the graduate has studied.

CONTENTS

ABSTRACT

Reef systems have been estimated to exist along approximately 80% of the world's coastlines with living coral reefs, relic limestone platforms and submerged rock formations being the most common types observed. The influences of a reef on the hydrodynamics of the area play an important role in the distribution of nutrients, sediment and biological organisms as well as on the morphology and protection of the shoreline at their lee. This influence is complex and when compared to sandy coasts, little research has been undertaken to investigate the many processes that are hypothesised to occur in these environments.

The processes of wave breaking on a reef crest, setup on a reef and flow over and within a lagoon, have been the primary focus of research to date, while wave transformation shoreward of the reef crest and surf zone have also been studied. The propagation of low frequency waves has been shown to have a large influence on flow, sediment transport and morphology. Furthermore, it has been demonstrated that these waves may possess periods that, if closely correlated with the reef width and depth, may enter a standing wave type form and possibly resonate.

Aim

The aim of this study was to determine the indicators of low frequency resonance in field, laboratory or numerical model data, and to identify the influence of different geometric parameters on the generation of low frequency wave resonance on a fringing reef.

Methods

The indicators were tested by the use of the numerical model XBeach, which was demonstrated to consist of a numerical basis suitable for the analysis of reef systems. The model was calibrated with high-resolution field data obtained at the Ningaloo Reef (Western Australia).

The tested indicators were then applied to the Ningaloo Reef field data to determine if a resonance signal could be identified at the site. Finally, a geometric parameter sensitivity analysis was conducted with an idealised reef profile based upon the Ningaloo Reef. The wave boundary of the model was forced with a JONSWAP-type spectrum that characterised the peak of a storm at the site. The influence of different geometric parameters (in both non-frictional and frictional cases) was investigated and compared to an analytical model.

Results

For two time-series that are spatially lagged across a reef, three indicators need to be satisfied to demonstrate the presence of resonance. They are: the surface elevation variance across the basin must be coherent, a phase relationship associated with the mode of resonance considered must exist, and an amplification of the wave between two points considered at the frequency of resonance must occur.

The results of the indicator tests showed strong agreement with a simple basin analytical model that was adapted to include the effect of a lagoon. Strong amplification (resonant) peaks were observed for the first two standing waveforms. The frequency of these peaks was affected by the setup on a reef while the amplitude was affected by the influence of friction. It was shown that for frictional values consistent with Ningaloo Reef, the amplification peaks 'flatten' to magnitudes similar to the progressive waves in the spectrum.

The geometric sensitivity analysis indicated that the resonant frequency was more sensitive to the reef and lagoon length than the reef and lagoon depth. The amplification was greatest for the zero and first-mode of resonance. However this amplification was dampened with the introduction of friction. It was determined that resonance is not likely to occur on reef systems with the geometry, frictional characteristics and wave forcing similar to the studied section of Ningaloo Reef. Resonance may occur for reef systems with shorter reef and lagoon widths, lower frequency forcing and/or less frictional dissipation. The latter may occur for reefs that have a different roughness to Ningaloo Reef as well as for reef systems that are damaged or dying in which coral assemblages degrade into coral rubble.

KEYWORDS: low-frequency waves, infragravity waves, coral reef, resonance, standing wave

ACKNOWLEDGEMENTS

Ricardo, Tam, Weizhi, Will, Xuexue and Zeng) thank you for your friendship over the past two years. There have been many good times.

To my family, despite being far away, your encouragement and support has helped me very much. I have enjoyed our regular discussions, your visits to the various locations at which I have studied and the many random things that have arrived by post. I look forward to spending more time with you.

To Gundula, your questions and thoughts have contributed greatly to this thesis. I have also enjoyed the many cycling, surfing and snowboarding trips as well as the touring that we have undertaken. And of course, for the many coffees consumed. Thank-you.

Andrew WM Pomeroy

Delft, June 2011

Chapter 1

INTRODUCTION

1.1 Background

It has been estimated that reefs exist along approximately 80% of the world's coastlines (Emery and Kuhn, 1982). These reefs can be living coral reefs, relic limestone platforms or submerged rock-type formations and it is common to categorise these reef (particularly coral reefs) according to topography: fringing reefs, barrier reefs or atolls.

A fringing reef is characterised by a shallow lagoon (if one is present) and is typically located near to or directly connected to the shoreline. Darwin (1842) proposed that the submarine slope is important for the development of a fringing reef along with turbulent surf that does not promote high turbidity. This is consistent with well-developed fore and reef flats and the less developed reef in shallow water located far from the reef edge observed in the field.

A barrier reef differs from a fringing reef primarily by the presence of a wide deep lagoon that separates the reef from the shoreline. These reef are formed initially as fringing reef connected to a shoreline (often many thousands of years ago when the sea level was much lower) and then become detached from the coastline as the coral grows vertically along with the rise in sea level.

The same principles apply to atolls, which are characterised by a circular reef that encloses a lagoon. The formation of such a reef was explained by Darwin (1842) based upon observations made during the voyage of HMS Beagle. He proposed that an atoll forms by a gradual subsidence of an oceanic volcano. Analogous to a barrier reef, a fringing coral reef forms around the perimeter of the volcano and grows upwards as the volcano subsides. As the

subsistence continues, a lagoon is formed in the location of the original volcano and only the circular coral barrier remains.

The present study focused specifically on fringing reef and the generation of resonance in this context. Despite the extensive presence of fringing reefs along the coastlines of the world, little is known about these reef structures when compared to sandy coasts. The interaction between the waves and the reef environment is likely to be very different due to variations in bathymetry, breaking and roughness and therefore the scope for further research is very large.

A schematic description of the main elements of a typical fringing reef is shown in Figure 1-1.
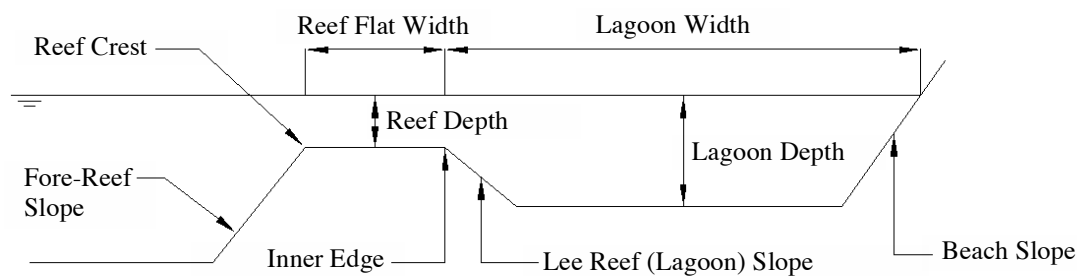
Figure 1-1: Key features of a schematic fringing reef

The majority of the investigations and studies that have been conducted with respect to reefs have focused on the processes and interactions of wave and current hydrodynamics in the presence of a reef. Specifically, the processes of energy dissipation (and the importance of wave breaking and bottom friction) along with the processes involved in circulation (primarily to understand the biological aspects of reefs) have been widely investigated (see Monismith (2007) for a review). One area that has received little attention has been the generation of resonance due to the interaction between low-frequency waves and reefs. Possible reasons for this include the lack of suitable data from field research and the absence of numerical models that explicitly model long waves.

One current tool (the numerical model XBeach) has the capability to simulate wave-group forced low-frequency waves and subsequently sediment transports. This model is an open-source tool under development by UNESCO-IHE, Deltares and the University of Miami (Roelvink et al., 2009). Trang (2010) recently examined the model to determine its capability to replicate a simple analytical reef model and reported good results.

Section 1.2 reviews the development of knowledge related to low-frequency waves. The key results of research related to the interaction between waves and reefs is summarised in Section 1.3 with the limited research undertaken related to low-frequency wave resonance on reefs discussed in Section 1.4. The scope and aims of the present study are outlined in Section 1.5 with the structure of the current report summarised in Section 1.6.

1.2 Low-Frequency waves

During a field study at Bikini Atoll, Munk (1949) observed low-frequency motion well outside the surf zone and postulated that this motion was likely to be caused by the variability in mass transported by the incident waves into the surf zone. This motion was referred to as 'Surf Beat'. Since this initial description, these waves have come to be known by many different names including: surf beat, infra-gravity waves, long waves, low-frequency waves and sub-harmonic waves. The term 'Low-Frequency Wave' will be used throughout this thesis. These waves are typically considered to be contained within the frequency band (0.004 Hz to 0.04 Hz), occur at beat frequencies of the shorter incident wind-generated waves and encompass bound and free components (Battjes, 2006).

On a beach at Perranporth (north coast of Cornwall), Tucker (1950) measured low-frequency waves well outside the surf zone and analysed the relationship between the short wave envelope and the long wave envelope at different time lags. A strong negative relationship was identified when the time lag was near zero. A strong positive relationship between the envelopes was identified when the time lag corresponded to the time taken for a short wave group to travel to the beach and for a free wave to travel back. Tucker (1950) suggested that the free waves travelling in the offshore direction were produced by groups of high waves breaking on the beach.

Longuet-Higgins and Stewart (1962) proposed the concepts of 'bound long waves', radiation stress and mass flux to explain the negative correlation between the short wave envelope and long wave elevation at zero time lag. They demonstrated that a group structure is created by superposition of short wave trains of different frequencies. This structure was shown to cause a small time varying modulation in mean surface elevation over the wave group – the so-called 'Bound Long Wave'. In this definition, the bound long waves must travel at the same velocity as the wave groups because the radiation stress and mass flux forces induced by the wave group structure force the waves. Longuet-Higgins and Stewart (1962) suggested that the free waves that radiated from the beach that were identified by Tucker (1950), were the reflected bound long waves that were released at some time within the surf zone. However the mechanism by which the bound long waves were released was not described.

Using a linear model, Symonds et al. (1982) proposed an alternative mechanism for low-frequency wave generation. They suggested that three zones existed: an outer surf zone, a transition zone and an inner surf zone. The assumptions made by Symonds et al. (1982) were such that outside the surf zone the horizontal variation of the radiation stress was negligible while in the inner surf zone the short waves are 'saturated'. This implies that the radiation stress

gradients were also constant in time as the variations on the wave group scale were considered to have vanished. In the transition zone, the breaking point of the waves moves (back and forth) over a finite distance. This is due to the larger waves breaking first, followed by smaller waves which induces a time varying radiation stress gradient. The forcing associated with the radiation stress gradient varies in the onshore and offshore direction and has been likened to the paddle of a wave maker. This produces onshore and offshore-directed waves. Symonds et al. (1982) suggested that the onshore wave was reflected at the beach and then travels offshore. The phase differences between the two offshore directed waves results in the combined (total) free wave being enhanced or dampened. This approach has become commonly known as the "Breakpoint Generation Mechanism".

Schaffer (1993) introduced a 'kappa' parameter that modelled the co-dependency of a dynamic breakpoint generation mechanism and the progression of groupiness into the surfzone. The introduction of this parameter (indirectly) resulted in the relaxation of the depth-limitation of breaking waves and consequently the 'saturated waves' assumption in the breakpoint generation mechanism proposed by Symonds et al. (1982). The results of Schaffer (1993) were shown to better represent laboratory experiments by Kostense (1984) as well as the original field results by Munk (1949) and Tucker (1950).

Janssen et al. (2003) demonstrated in their study that on a mild slope the incident bound long wave amplitude grows as the wave shoals. This was attributed to a net energy transfer from the incident short wave group to the forced bound long wave due to a phase lag that develops as the waves shoal. Battjes et al. (2004) showed that this energy transfer was a function of the relative slope and the phase difference between the wave group and the bound long wave. The growth in the bound long wave amplitude has been suggested to be greater than that experienced by free waves released within the surf zone or generated by the breakpoint mechanism. The dominance of the bound long waves on a mild slope is consistent with the findings of Symonds and Bowen (1984) in which on a mild slope the break point of the incident waves oscillates over a (relatively) large distance. This makes the breakpoint mechanism of generation ineffective. It was hypothesised by Battjes et al. (2004) that for steep slopes, the opposite could be expected.

Battjes et al. (2004) suggested that in the transition region between mild and steep slopes, a relative slope parameter (a function of the same elements as the Irribaren Number typically used for the separation of breaking and non-breaking wind waves on a slope) describes the degree of low-frequency wave reflection. Van Dongeren et al. (2007) demonstrated the importance of this parameter along with the relative influence of bed friction in relation to the reflection and breaking of these waves.

The importance of low-frequency waves has been recognised through the development of knowledge on these waveforms. The (relatively) small amplitudes and long wavelengths permit these waves to propagate and shoal over sloping bathymetry. The ability of these waves to dissipate (by bore type breaking) as well as (partially) reflect off a shoreline as free waves that subsequently travel offshore ('leaky waves') or become trapped in the near shore ('edge waves') presents an interesting field of investigation, particularly in relation to reefs where their interaction may be far different from sandy coasts.

1.3   Waves and reef interaction

The interaction between waves and reef structures is complex. The focus of research for the past 10 years has been confined to reef formation, energy dissipation and, flow and circulation. These processes are important to better understand the structural, biological and the coastal protection characteristics of reefs. However, limited research has been undertaken into the interaction of low-frequency waves with reefs.

Munk and Sargent (1948) identified a mean set up and wave dissipation during a field and desktop study at Bikini Atoll. It was determined that this set up was in the order of several decimetres. Longuet-Higgins and Stewart (1962) broadly explained this process in terms of the relationship between wave breaking and radiation stress.

Lee and Black (1978) studied the transformation in wave energy that occurs as incident waves interact with a reef during a field campaign on Oahu (Hawaii). This study was undertaken through an analysis of wave height and period data as well as the spectral distribution of energy. They demonstrated that offshore, the energy spectrum has low energy in the low and high frequencies. As the wave enters shallow water (on the reef), the energy shifts from the peak to the low and high frequencies. The low-frequency energy was shown to increase and was not attenuated on the reef. The high frequencies were shown to increase when the waves first enter the shallow zone but later break. Lee and Black (1978 pp. 597) argued, "the shift results in the production of multiple crests and periodic sea level changes at beat frequencies". Shoreward of the breaker zone, all frequencies were found to attenuate.

Field and laboratory measurements were used by Gerritsen (1980) to further investigate how to quantify water level setup and wave attenuation over a reef. Two damping factors were identified: wave breaking and friction. Parameterisations and indicative values for these damping factors were studied based upon the bore model for wave breaking and the linear friction model for friction. It was also suggested that setup on a shallow reef was governed by a parameter that took the form of a modified Ursell parameter. The results indicated that the redistribution of wave energy as the waves travel over a shallow reef were consistent with the

findings reported by Lee and Black (1978). Similarly, the results of Young (1989) also demonstrated a significant modification to the energy spectrum between deep water and the reef top. Young (1989) reported a relatively uniform spread of energy across all frequencies and that the significant wave height is dependent on the reef water depth and incident deep water wave energy.

Data obtained from a field experiment on the Great Barrier Reef was used by Hardy and Young (1996) to further investigate the importance of water depth on a reef's interaction with waves. Through the examination of the changes in wave energy, they found that when the water level was 'medium' to 'high', the energy spectra generally maintained the characteristics of the offshore spectrum. This was attributed to the absence of wave breaking (for which a wave breaking ratio between wave height to reef flat water level was established). At lower water levels, the spectrum was shown to flatten and broaden due to energy losses incurred via wave breaking. It was acknowledged that additional losses (not considered in the study) could be expected as a result of bottom friction, particularly on wider reef flats.

To understand the reef hydrodynamics, Symonds et al. (1995) formulated an analytical model based on linearized equations and radiation stress concepts. The model demonstrated that the magnitude of current and set up is dependent on the reef geometry (front face slope and reef width) and the magnitude of the forcing (defined by the depth at breakpoint and the water depth over the reef). An important result was that momentum flux could be partitioned into wave setup and onshore flow over a reef.

Lowe et al. (2005) returned to the question of energy dissipation and investigated the relative contributions of wave breaking and friction to the dissipation of incident wave energy. Based on field data, they suggested that the majority of wave energy is dissipated by bottom friction and that wave breaking is of lesser importance. This is a departure from the suggestions by other authors and the findings for coastal beaches where much of the research has been undertaken. Knowledge of energy dissipation mechanisms has been extended to explain flow over reefs and the circulation behind and within reef lagoons (eg. Lowe et al., 2009b).

The interaction between incident waves and reef structures is an area of ongoing research. Many of the investigations and studies that have been conducted with respect to reefs have focused on the process and interaction of wave and current hydrodynamics in the presence of a reef. In particular, the processes of energy dissipation (by breaking and friction) and frequency redistribution have been intensively studied with extension to explain processes involved in wave setup and circulation.

10

1.4 Low-Frequency wave resonance and reefs

Extensive research has been conducted with respect to low-frequency waves on sandy coasts. However, the importance of low-frequency waves with respect to reefs, despite being recognized by many authors in observed shifts in energy from the peak of the energy spectrum to the higher and lower frequencies, has not been studied in depth and is primarily confined to three works: Nakaza and Hino (1991), Péquignet et al (2009) and Nwogu and Demirbilek (2010). This is likely to be due to the difficulty in obtaining good data for low-frequency waves in these environments.

It is conceivable that in the presence of a reef, there could be a significant amount of energy that reaches the shoreline due to such low-frequency waves. This energy is likely to affect the shoreline morphology and if resonantly excited, could affect the coastal protection function of a reef that is often relied upon to protect coastal structures.

Nakaza and Hino (1991) were inspired by observations of resonant surf beat generation during typhoons and postulated that infragravity wave oscillations were responsible for coastal damage along the reef coasts of Japan. They studied, numerically and in the laboratory, the excitation of low-frequency waves ("surf beat") in the nearshore zone. It was demonstrated that for a nearshore zone that consists of a definite natural frequency (such as a coral reef with a long horizontal bottom), low-frequency waves could experience resonant excitation when the frequency of these waves approaches the natural frequency of the reef lagoon. It was suggested that the ability for these low-frequency waves to achieve a resonant frequency was primarily influenced by the time varying contributions of the radiation stress and the breakpoint that result from wave grouping. The form of the low-frequency oscillation in these experiments was found to change from a wave type form to a bore-like surge in which a steep forward face was exhibited.

Péquignet et al (2009), like Nakaza and Hino (1991), also observed low-frequency waves at near resonant oscillation in field data obtained during a tropical storm at Guam. The conditions that favour excitation were investigated with the hypothesis that the water depth along with the time series of forcing by the wave groups could lead to excitation. Consistent with Nakaza and Hino (1991), it was found that the natural resonance mode of the basin describes the capability for resonance to occur. The ability for the low-frequency wave to reflect of the shoreline was an important factor and was considered in the context of a standing wave pattern. The results of the study indicated that an increase in the water level caused by tropical storm Man-Yi enabled the resonant frequency to increase, become energised and approach a near resonance state.

Nwogu and Demirbilek (2010) investigated the ability for infragravity waves to resonate in experimental tests and a Boussinesq model based upon a Guam reef profile. It was shown that wave motions over the reef flat and at the shoreline were dominated by oscillations at low-frequency wave periods. It was found that most of the incident wave energy was dissipated within a few wavelengths of the reef face with low-frequency wave energy minimum at the reef crest which then increased as the wave propagated shoreward over the reef flat. The water level was shown to increase in a similar way. It was also demonstrated, in agreement with Péquignet et al (2009) and Nakaza and Hino (1991) that low-frequency waves could be resonantly amplified at the shoreline with the first reef oscillation mode wavelength approximately equal to four times the width of the reef flat.

The interaction between reef structures and low-frequency waves has only briefly been considered to date. It is unclear how these waves are affected by reef systems in general as well as by the reef morphology itself. While the specific reef geometry has been shown to control the resonance on a reef, such resonance has only been demonstrated for a limited number of cases in the field. In addition, high friction has the potential to dissipate shoreward low frequency energy significantly, a process that has not been addressed in these studies.

1.5   Scope and aim of present study

This project was undertaken as a collaborative project between Deltares, Technische Universiteit Delft (TU Delft) and The University of Western Australia who provided the data. This project was an exploratory study that aimed to investigate the influence of bathymetric geometry on the development of resonance induced by the interaction between low-frequency waves and a reef and to compare the results with an analytical expression.

The specific objectives of this research (summarised pictorially in Appendix A) were to:

- identify indicators and measures of low frequency wave resonance in existing field data;
- conduct an analysis to identify if a low-frequency wave resonance is present in the Ningaloo Reef data set;
- determine if the numerical model XBeach has the capability to reproduce resonance in a fringing reef model; and
- investigate the influence of geometric parameters and friction on the generation of low-frequency wave resonance (in a 1D model). The four parameters investigated were:
    - Reef width;
    - Reef depth;
    - Lagoon width; and
    - Lagoon depth.

1.6 Structure of this report

The theoretical basis of resonance is provided in Chapter 2 along with the hypothesised indicators and measures. In Chapter 3, analysis of data obtained at Ningaloo Reef is undertaken to define the hydrodynamic features at the site. An analysis to determine if resonance is present in the data is also undertaken. Chapter 4 describes the development of XBeach and its suitability for use in this study. Chapter 5 tests the hypothesis related to the identification and measurement of resonance in a simple reef and reef-lagoon case. The influence of the lagoon, friction and offshore wave heights are also analysed. A geometric profile sensitivity analysis is summarised in Chapter 6 with the results for a frictionless and friction case discussed. From this analysis, the influence of different parameters is considered and compared with the analytical solution. The conclusions from this study and recommendations are presented in Chapter 7.

Chapter 2

LOW-FREQUENCY WAVE RESONANCE

2.1 Introduction

Low-frequency wave resonance has been intensively studied in relation to harbours where resonant oscillations may cause significant operational damage (eg. Okihiro et al., 1993; Harkins and Briggs, 1995; Hinwood and Luick, 2001; Miles, 1974; Wu and Liu, 1990; Luick and Hinwood, 2008). Resonant oscillations have also been shown to occur on beaches (eg. Karunarathna et al., 2005; Özkan-Haller et al., 2001; Suhayda, 1974) as well as in the laboratory (eg. Kirby et al., 2006). In contrast, only limited research has been undertaken with respect to resonance in a fringing reef environment (primarily confined to Nakaza and Hino, 1991; Nwogu and Demirbilek, 2010; Péquignet et al., 2009). Recently the contribution of such resonance to increased coastal inundation and damage has been suggested (Lugo-Fernández et al., 1998; Péquignet et al., 2009) and near resonant oscillations observed (Péquignet et al., 2009). Such observations are an indication of the importance of this phenomenon and justify further research in this area.

This chapter describes low-frequency wave resonance and its relationship with fringing reefs. The definition of resonance adopted in the present study is defined in Section 2.2 and the concept of a standing wave is reviewed in Section 2.3. The dynamic process that results in resonance is reviewed and the natural resonant frequencies associated with different basin types described in Section 2.4. This section also highlights the connection between these resonant frequencies and standing waves. Finally, Section 2.5 presents the indicators of resonance that were used to identify and measure resonance in data obtained from the field and numerical model components of the present study.

2.2 Definition of resonance

In the present study, resonance is defined as *the state in which shore-normal incident and reflected wave motion within a basin attains a standing wave pattern and increases in amplitude due to the wave motion's possession of a frequency that is near or at the natural resonant frequency of the basin considered*. This definition is consistent with the concepts described in coastal engineering texts (eg. Sorensen, 2006 pp. 128-129). The two interrelated elements that form this definition (standing wave pattern and natural resonance frequency of a basin) are discussed in the sections that follow.

2.3 Standing wave pattern

The concept of a standing wave is discussed in many different coastal engineering manuals and textbooks (eg. Dean and Dalrymple, 1991; Kamphuis, 2010). A review of the essential elements of a standing wave is presented in this section and its relation to low-frequency wave resonance in a reef environment discussed.

2.3.1 Standing wave theory

In the purest sense, a standing wave is generated by superposition of two waves that have the same height and phase but travel in opposite directions. This situation can occur when an incident wave, that travels normal to a boundary, is (perfectly) reflected. The points where the surface oscillates between a maximum and a minimum are defined as 'anti-nodes' while the points at which the surface elevation does not oscillate are defined as 'nodes' (Figure 2-1).
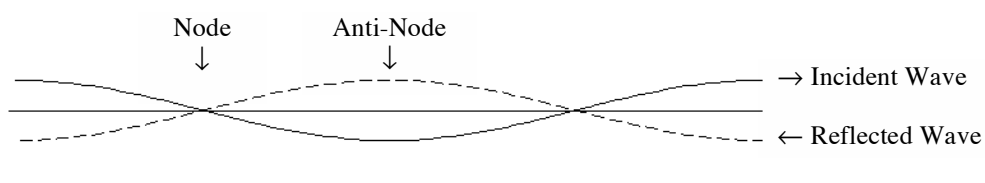
Figure 2-1: Generation of a standing wave by incident and reflected waves

In practice however, waves rarely achieve perfect reflection at a boundary. This is because a portion of the energy is absorbed by or transmitted past the boundary. This loss or dissipation of energy results in a reduction in the height and a slight change in the phase of the reflected wave. In this case, no 'true' node or anti-node will exist but rather a 'quasi' node and anti-node that represents the average node and anti-node location (Figure 2-2). A 'partial' standing wave is said to be generated.
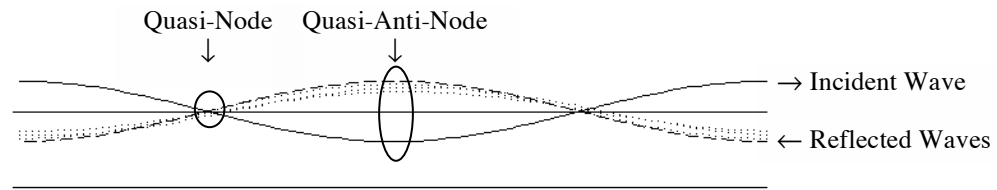
Figure 2-2 : Partial standing wave
Reflected waves of slightly different phase are shown as dotted lines.

In both the pure and partial standing wave cases, the distribution of nodes and anti-nodes are determined from the basin arrangement and the harmonic of the standing wave under consideration (Section 2.4.1).

2.3.2   Low-Frequency standing waves

For a beach, van Dongeren (2007) demonstrated that its slope determines if a low-frequency wave is dissipated (mild slope) or reflected (steep slope). In a fringing reef environment, where a lagoon and a beach typically back a reef, low-frequency waves are expected to reflect or dissipate based upon the same slope criteria. However, the ability for a standing wave pattern to be generated in a reef environment, where the comparatively rough bed surfaces result in higher dissipation, has not been intensively considered. Özkan-Haller et al. (2001) suggests that an incident wave that is subjected to high dissipation will cause resonance to 'detune'. In such a case, the frequency peaks associated with the resonance will not be sharp. The energy is also spread over a range of frequencies by dissipation, which for a reef is highly influenced by bed friction. The 'detuned' waves make the resonance frequencies contained within data indistinguishable.

Lugo-Fernández et al. (1998) observed in a study at Tague Reef that low-frequency standing wave type oscillations occurred in accordance with the open-basin model (Section 2.4). A recent study has also confirmed this model approach (Péquignet et al., 2009). This suggests that a standing wave pattern is indeed possible behind reef structures.

2.4   Natural resonance frequency modes

Natural resonant frequencies associated with basins have been studied for over 100 years. It has been demonstrated that basins possess a fundamental natural resonant frequency and an infinite number of harmonics of this frequency that is related to its geometric shape (Dean and Dalrymple, 1991). If the resonance frequencies are subjected to cyclic excitation force (for example, waves), the response can be amplified. This is demonstrated by the classical figure (Figure 2-3) that can be found in many textbooks on the dynamic responses of systems (eg. Naess, 2007). Nakaza and Hino (1991) produced a similar response curve for a reef under

laboratory conditions, which indicates that a reef may be considered to respond in a manner consistent with a dynamic system.
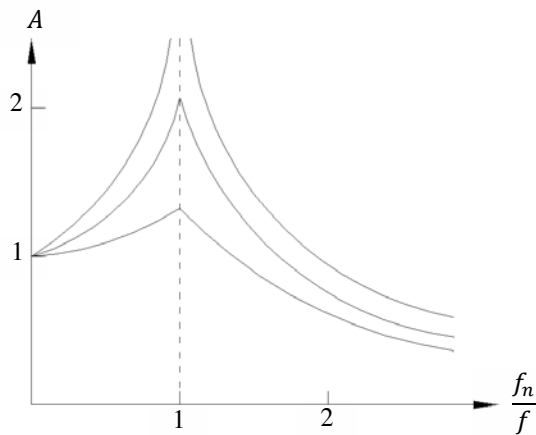
Figure 2-3: Conceptual amplification curve
The amplification factor (A) is located on the vertical axis. The ratio between the basin natural frequency (f_n) and the forced frequency (f) is located on the horizontal axis. The upper curve is the conceptual frictionless case and the lower curves conceptually describe the influence of increased friction.

Such figures illustrate that as the excitation frequency (f) approaches the natural resonant frequency of the system (f_n), amplification (A) of the response occurs. In the theoretical case of no energy dissipation, the system response approaches infinity. In practice however, such amplification is dampened by friction always present in the system. Amplification of the oscillation may continue for a period of time after the cessation of the cyclic force as the effects of frictional dampening return the system to equilibrium.

For excitation frequencies much greater than the natural resonant frequency $\left(\frac{f_n}{f} \to 0\right)$, the amplification of the system is equal to the excitation force while for excitation frequencies smaller than the natural resonant frequency $\left(\frac{f_n}{f} \to \infty\right)$, the amplification reduces.

2.4.1   Natural resonant frequencies for basins

Two idealized geometries (in two dimensions) have consistently been presented in numerous textbooks and are commonly used to estimate the natural resonant frequency of a basin: the closed-basin geometry (Equation 2-1) and the open-based geometry (Equation 2-2). Other idealized geometries have also been derived and many were summarized by Wilson (1966) and reproduced by Dean and Dalrymple (1991).

A closed-basin geometry, often used to described lakes forced by wind shear, has a natural resonance frequency equivalent to a wavelength twice the length of the basin. An antinode is located at each end of the basin and nodes across the centre of the basin. In contrast, the open-

basin geometry (common for harbours and bays) has a natural resonance frequency wavelength four times the length of the basin. As a consequence, it is characterised by a node at the open end of the basin and an antinode at the closed end. This equation is extended in Section 3.8.1 to include the influence of a lee-side lagoon. Figure 2-4 illustrates the two geometries and the first three natural resonant frequency modes. The figure demonstrates that the harmonics of the fundamental resonant frequency occur as fractions of the basin length.

$$T_n = \frac{2L}{(n+1)\sqrt{gh}} \quad (closed\ basin) \tag{2-1}$$

$$T_n = \frac{4L}{(2n+1)\sqrt{gh}} \quad (open\ basin) \tag{2-2}$$

T_n is the standing wave period (in seconds) associated with mode n for a basin of length L and depth h.

OPEN BASIN   CLOSED BASIN
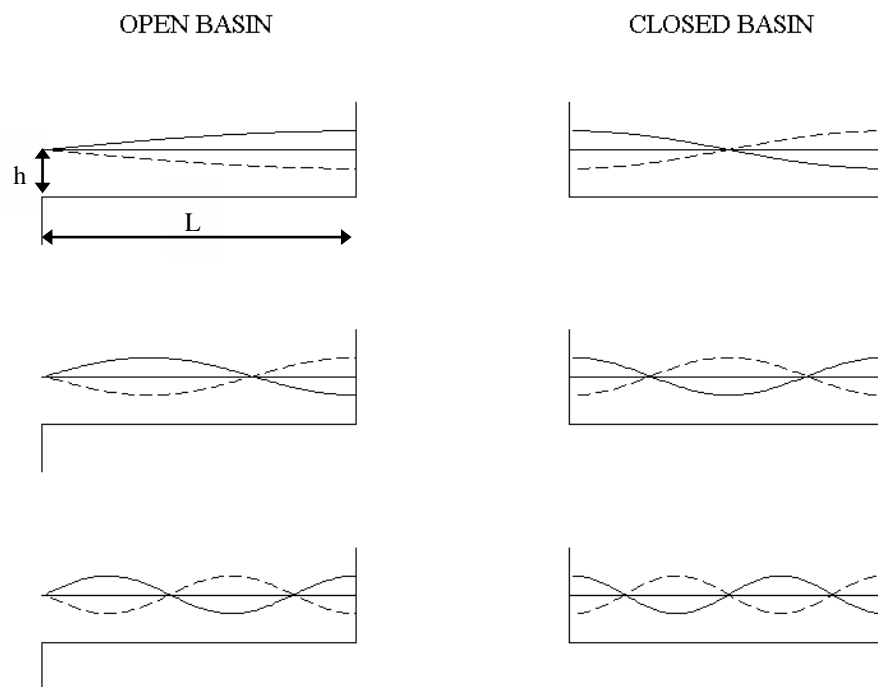
Figure 2-4: Resonance frequencies
The Mode 0, 1 and 2 standing wave forms for an open basin (left) and closed basin (right).

Lugo-Fernández et al. (1998) suggested that an open basin model is a suitable estimation of a reef's natural resonant frequency. Pèquignet et al. (2009) demonstrated that this model corresponded with the approximate natural resonant frequencies of a fringing reef at Guam during tropical storm Man-Yi. Similarly, Nakaza and Hino (1991) have demonstrated that an

open basin model represents the natural resonant frequencies of a reef structure well in the laboratory.

2.4.2 Relationship between (partially) standing waves and natural basin frequencies

A progressive wave at the frequency of a natural basin resonance frequency will cause a momentary amplification in the surface elevation but as this excitation is not cyclic it is unlikely to persist long enough to cause a resonant oscillation. If however, a (partially) standing wave pattern is generated at the fundament natural basin frequency (or one of its harmonics), amplification of the wave height could be expected (resonance). It is therefore important to determine if a (partially) standing wave can form at a fringing reef site and if such a wave can induce resonance - this is a key element of the present study.

2.5 Indicators of resonance and their assessment

The identification of resonance requires an analysis of signal data obtained at two or more spatially lagged locations in the field or within a numerical model domain. While the factors that contribute to the generation of a (partially) standing wave are quite clear, demonstration of such a wave pattern is complicated. This is due to the presence of many other waves at different frequencies. Furthermore, the effects of friction (dampening) may result in excitation of a band of frequencies (as opposed to a particular frequency) or the suppression of natural resonant frequencies at the site. In the present study, three indicators based upon the characteristics of a standing wave (Section 2.3) are hypothesised to be suitable for the determination of resonance present in data obtained at two spatially lagged locations:

1. a highly coherent variance in water surface elevation at a given frequency;
2. a phase relationship between water surface elevations at a given frequency must (closely) correspond to 0° or 180° phase difference; and
3. an amplification of the water surface elevation at a given frequency.

Individually, each indicator is insufficient to demonstrate the existence of resonance within a basin and therefore all must be satisfied in order to demonstrate resonance. While other forms of resonance exist (for example due to edge waves), these were not the focus of this study.

2.5.1 Indicator 1: A highly coherent variation in water surface elevation

The generation of a (partially) standing wave results in highly coherent surface motions across a basin at the approximate standing wave frequency. In this state, the variance in surface elevation at one location is (reasonably) predictable from the surface motion at another location. In Figure 2-5, the motion at Point B would be some function of Point A with the lag being the spatial

difference between the two points. The type of function that relates these points cannot be defined in the current context, only that such a function exists.
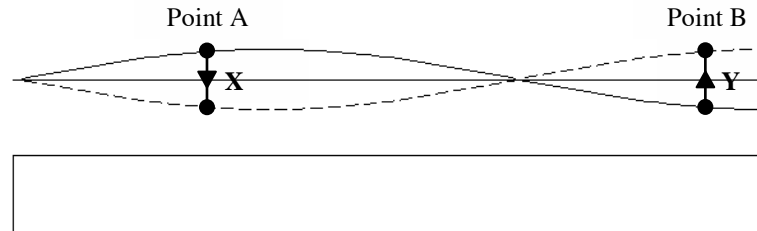
Figure 2-5: Schematic representation of coherence between two spatially lagged signals
X represents the downward motion of the surface at Point A and Y the upward motion at Point B.

In frequency space, the (squared) coherence function (Equation 2-3) can be used to identify and measure the coherence (normalised correlation) between signals obtained at two spatially lagged locations (Appendix C).

$$\gamma_{xy}^2(f) = \frac{\left|G_{xy}(f)\right|^2}{G_{xx}(f)G_{yy}(f)} \tag{2-3}$$

where:

x and y are timeseries obtained at two spatially separated points, $G_{xx}(f)$ and $G_{yy}(f)$ are the auto-spectra of the two data sets while $G_{xy}(f)$ is the cross-spectra of the two data sets (Appendix C).

If the (squared) coherence (γ^2) is one, the signals are said to have a direct relationship (*informally: one signal can be predicted from the other*). In practice, it is not expected that a coherence of one will be achieved due to losses associated with reflection (Section 2.3).

A high coherence at a particular frequency does not in itself indicate the presence of a standing wave in the data. An assessment of the phase relationship between the two signals is therefore required to determine if the wave is standing or progressive in character (Section 2.5.2). If the signals are not coherent (correlated) than the phase relationship determined in Indicator 2 cannot be evaluated.

2.5.2 Indicator 2: Phase difference must (closely) correspond to 0° or 180°

The phase relationship between two signals obtained from spatially separated stations is an indicator of whether the wave is of progressive or standing character. The phase relationship can be determined by analysis of the coincident (co) and quadrature (quad) components of the cross-spectra of the two signals (Appendix C).

The co-spectrum (Equation 2-5) is defined as the 'real' component of the cross-spectrum (Equation 2-4) and is represented by a cosine function. The quad-spectrum (Equation 2-6) is the 'imaginary' component of the cross spectrum and is described by a sine function. Together, in polar coordinates, these spectra define the phase difference (an angle) between the two signals (Equation 2-7). *Informally: the phase difference describes the phase difference between a point on the curve function at the second station in relation to the first station.*

$$\begin{aligned} G_{xy}(\tau) &= 2\int_{-\infty}^{\infty} R_{xy}(\tau)e^{-j2\pi f\tau}df \\ &= C_{xy}(f) - jQ_{xy}(f) \end{aligned}$$

(2-4)

$$C_{xy}(f) = 2\int_{-\infty}^{\infty} R_{xy}(\tau)\cos(2\pi f\tau)\, d\tau$$

(2-5)

$$Q_{xy}(f) = 2\int_{-\infty}^{\infty} R_{xy}(\tau)\sin(2\pi f\tau)\, d\tau$$

(2-6)

$$\theta_{xy}(f) = \tan^{-1}\left[\frac{Q_{xy}(f)}{C_{xy}(f)}\right]$$

(2-7)

$$|G_{xy}(f)| = \sqrt{C_{xy}^2 + Q_{xy}^2}$$

(2-8)

Where:

x and y are timeseries obtained at two spatially separated lagged (τ) points, $G_{xy}(\tau)$ is the cross-spectra of the time-series, which is determined from the cross-correlation function $R_{xy}(\tau)$ of the two timeseries. $C_{xy}(f)$ is the co-spectrum and $Q_{xy}(f)$ is the quad-spectrum. $\theta_{xy}(f)$ is the phase difference between the two timeseries.

In this study, the co-spectrum and quad-spectrum were normalised by the amplitude of the cross-spectrum (Equation 2-8) to enable the phase difference to be clearly established. If the two signals are in-phase $(\theta_{xy} = 0°)$, the (normalised) co-spectrum will indicate a strong positive density (≈ 1) and the (normalised) quad-spectrum will be near zero. Similarly, if the signals are 180° degrees out of phase, the (normalised) co-spectrum will indicate a strong negative density (≈ -1) and the (normalised) quad-spectrum will be near zero. These two cases, along with a high coherence, describe the basin under a standing wave condition (but not necessarily resonant condition).

If the two signals are progressive, the (normalised) co-spectrum and the (normalised) quad-spectrum will both possess density. The distribution of normalised density describes which

instrument will lead the other instrument and by how much. These concepts are illustrated in the form of a modified unit circle (Figure 2-6).

$$+Q_{xy}(f)$$

$$\frac{\pi}{2} \leq Q_{xy}(f) \leq \pi$$

y leads x at frequency f

$$0 \leq Q_{xy}(f) \leq \frac{\pi}{2}$$

y leads x at frequency f

$\sin\theta$

θ $\cos\theta$

$$-C_{xy}(f)$$ $$+C_{xy}(f)$$

$$-\pi \leq Q_{xy}(f) \leq \frac{\pi}{2}$$

x leads y at frequency f

$$\frac{-\pi}{2} \leq Q_{xy}(f) \leq 0$$

x leads y at frequency f

$$-Q_{xy}(f)$$
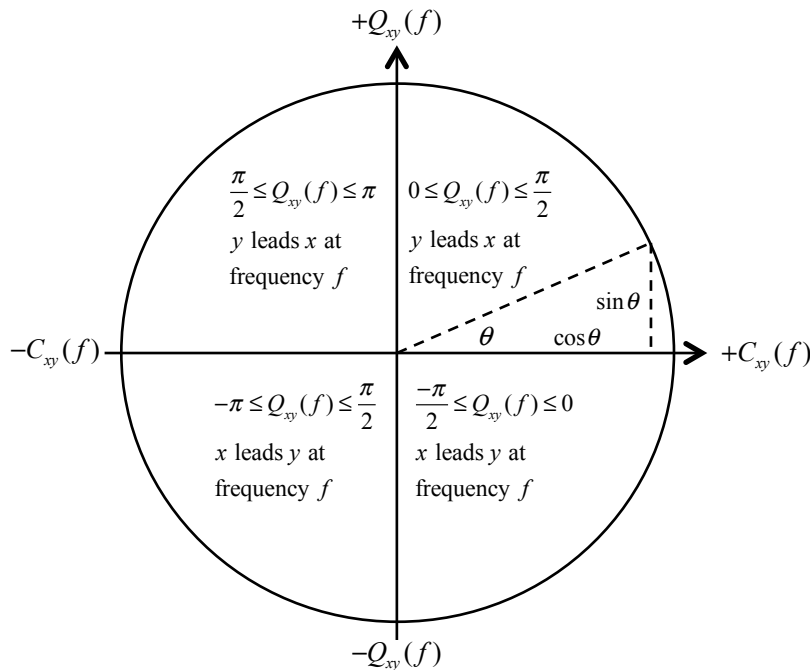
Figure 2-6: Relationship between co-spectrum, quad-spectrum and phase

2.5.3   Importance of instrument location

The position of the instruments, relative to the nodes associated with the standing wave harmonic considered, will determine if the phase between the two signals is 0° or 180° (a co-spectral value of +1 or -1). If the two sampling stations are positioned between two nodes (Point A and Point B in Figure 2-7), the co-spectrum is expected to be unity $\left(\theta_{xy} = 0°\right)$. However, if the two stations are positioned such that a node is located between them (Point A and Point C), the co-spectrum is expected to be minus one because the motion described by the time series are 180° out of phase. This is demonstrated by Figure 2-7 and summarised by Equation 2-9. The location of the instruments in relation to nodal points in the present study is discussed further in Section 3.8.3.

Point A   Point B   Point C
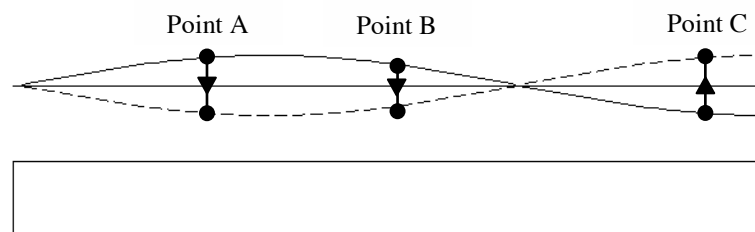
Figure 2-7: Schematic locations of different instruments in relation to nodes in waveform

$$C_{xy}(f) = \begin{cases} 1 \text{ if n nodes} = 0, 2, 4 \dots \\ -1 \text{ if n nodes} = 1, 3, 5 \dots \end{cases} \qquad (2\text{-}9)$$
$$Q_{xy}(f) = 0$$

2.5.4 Indicator 3: Amplification of the wave signal

Indicators 1 and 2 demonstrate that a standing wave form exists in data at a specific frequency however they do not provide any information about the amplitude of this wave at the two locations. For resonance to occur, amplification in the signal must exist between the two points considered. The amplification can be determined by the division of the incident wave height near the shoreline by the incident wave height near the reef crest as indicated by Equation 2-10. Calculation of such amplification across all frequencies of the auto-spectra produces an amplification curve. This curve can be used to identify the resonant frequencies (consistent with Figure 2-3).

$$A = \frac{H_{m0.s}}{H_{m0.c}} = \frac{4\sqrt{m_{0.s}}}{4\sqrt{m_{0.c}}} = \frac{4\sqrt{\int S_{shore} \, df}}{4\sqrt{\int S_{crest} \, df}} \qquad (2\text{-}10)$$

Where:

$H_{m0.s}$ and $H_{m0.c}$ are the H_{m0} wave heights at the shoreline and reef crest, $m_{0.s}$ and $m_{0.c}$ are the zero spectral moments on the shoreline and reef crest derived from the respective auto-spectrum (S_{shore}, S_{crest})

2.6 Conclusion

Resonance in the present study is characterised by a wave signal that enters a standing wave form and is excited by cyclic forcing (the wave climate). An open-basin model has been suggested to conceptually represent a fringing reef and its natural resonant frequencies. Three indicators have been hypothesised to be suitable to identify and measure resonance. The relation between high coherence, phase difference and a standing wave pattern was clarified with the need for a measure of amplification to identify resonance justified. The content of this chapter is important to understand the present study's context and the basis of methodologies adopted.

Chapter 3

NINGALOO REEF DATA ANALYSIS

3.1 Introduction

The Ningaloo Reef (114°E, 22°S) is a fringing coral reef located in Western Australia. The reef extends from the North-West Cape southward for approximately 260 km to 280 km and has been identified as the only example of an extensive coral reef that fringes the west coast of a continent (Taylor and Pearce, 1999).

Associate Professor Ryan Lowe (The University of Western Australia) conducted a three-week field study at Ningaloo Reef (Sandy Bay) in June 2009 to obtain pressure, wave height and current data. An analysis of this data is presented in this section.
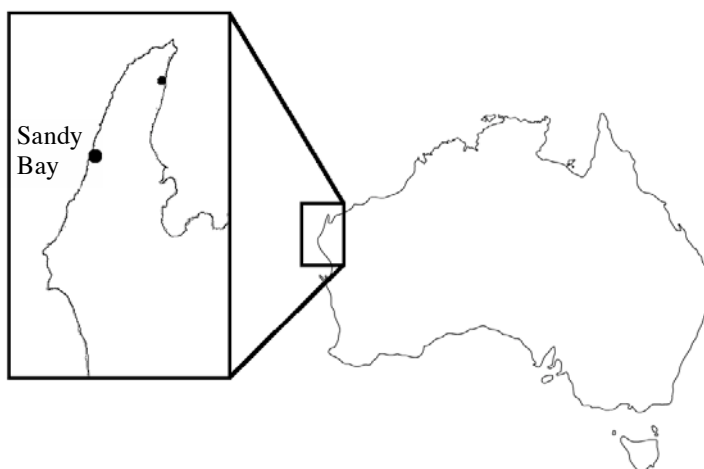
Figure 3-1: Study site location
The inset is the North-West Cape with the regional centre Exmouth represented by the small dot.

The general features of the Ningaloo Reef are summarised in Section 3.2 with the specific features of the study site along with details of the instrumentation summarised in Section 3.3. The wave climate determined from the field study data is discussed in Section 3.4 with the estimated sea surface elevation spectra for each measurement station presented. In Section 3.5, the separation frequency $\left(f_{split}\right)$ between sea-swell waves and low-frequency waves is defined for the Ningaloo Reef study site. The burst averaged wave heights for each measurement station are then determined for sea-swell and low-frequency waves in Section 3.6. To determine if the low-frequency waves are dissipative or reflective, the incident and reflected waves are separated in Section 3.7. Finally in Section 3.8, the natural resonance frequencies at Ningaloo Reef are estimated and the data analysed to determine if a resonance signal is contained within the data obtained from the Ningaloo Reef study site.

3.2   Reef features and structure

The location of the Ningaloo Reef, relative to the shoreline, varies between 200 m and 7 km with an average of 2.5 km (Hearn and Parker, 1988; Taylor and Pearce, 1999). Between the reef and the coastline there is a partially enclosed coastal lagoon that is between 1 m and 2.5 m deep (relative to low spring tide). Other features include a number of steeply shelving underwater canyons along the narrower portion of the shelf (Taylor and Pearce, 1999) and gaps in the reef structure that differ along the reef. Approximately 15 % of the northern portion of the reef length consists of gaps while in other regions a more open and broken topography exists (Hearn and Parker, 1988). A number of studies related to Ningaloo Reef have been undertaken and provide a good analysis of a variety of specific hydrodynamic and biological processes (eg. Lowe et al., 2010a; Lowe et al., 2010b; Trang et al., in prep; Hearn and Parker, 1988; Taebi et al., 2011; Trang, 2010; Hearn, 1999 and many others, particularly in the field of marine biology).

3.3   Study site and data measurement

The site from which the data in this study was obtained was located at Sandy Bay. At the site, the fore-reef slope rises at approximately 1:20 to the reef crest, which is located approximately 1.35 km from the coastline. The shallow reef, of between 1 m and 2 m deep and approximately 500 m in width, is covered in dense coral assemblages. A lagoon (approximately 850 m wide) with an average depth of 2 m to 3 m separates the reef from the coastline. The lagoon is characterised by sand and coral rubble. This profile is typical throughout the study site (approximately 3 km) in which shore-parallel reef sections are periodically broken by channels (Lowe et al., 2010b; Taebi et al., 2011; Lowe, 2011).

The site and areas nearby have previously been used for a number of field studies (eg. Hearn and Parker, 1988; Hearn, 1999; Taebi et al., 2011 and references within). Taebi et al. (2011) describe this site as a generally good representation of the Ningaloo Reef structure.
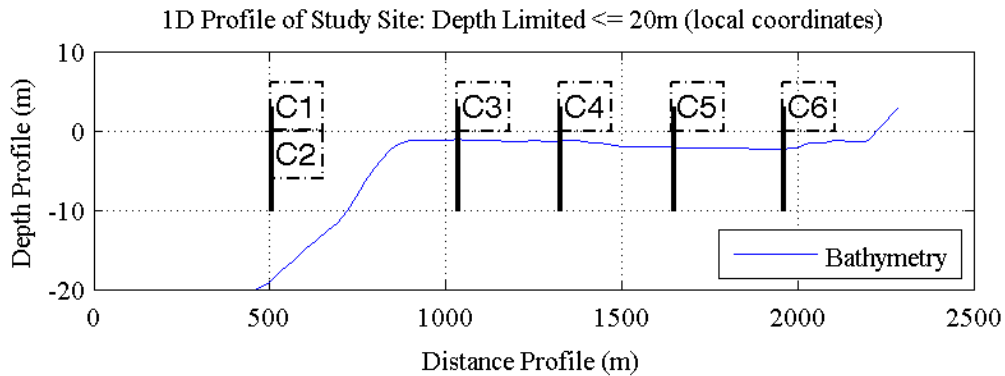
Figure 3-2: Profile of Ningaloo Reef study site transect
Bathymetric profile and the location of six instrument stations at the Ningaloo Reef study site (to local coordinates).

A synchronized array of instruments was deployed along a cross-shore transect that consisted of six measurement stations (Figure 3-2). Two stations were located in front of the reef (C1 and C2), two on the reef flat (C3 and C4) and two in the lagoon behind the reef (C5 and C6). All instruments were deployed between the 9th June 2009 and the 11th June 2009 and were retrieved between 30th June 2009 and 1st July 2009. The instrument and measurement details are summarised in Table 3-1 and Table 3-2.

Table 3-1 - Station instruments

ID	Instrument	Pressure	Current	Easting	Northing
C1	Nortek AWAC	X	X	792022	7540922
C2	Seabird SBE26	X		792022	7540922
C3	Nortek Vector ADV	X	X	792519	7540734
C4	Nortek Vector ADV	X	X	792790	7540624
C5	Nortek Vector ADV	X	X	793100	7540540
C6	Seabird SBE26	X		793389	7540418

Table 3-2 - Measurement details

ID	Current Measurements		Pressure Measurements		
	Height* (m)	Rate#	Height* (m)	Rate#	Offset (m)
C1	10	5 min	0.5	1 Hz 2048 s burst every 3600 s	-
C2	N / A	N / A	0.2	1 Hz 2048 s burst at odd hours	-
C3	0.5	1 Hz	0.1	1 Hz	+ 1.00
C4	0.5	1 Hz	0.1	1 Hz	+ 0.05
C5	0.5	1 Hz	0.1	1 Hz	+ 0.08
C6	N / A	N / A	0.1	1 Hz 2048 s burst at odd hours	+ 0.00
Notes:					
- no instrument offset					
# measured samples were obtained continuously unless otherwise stated					
* measurement height is relative to the seabed					

Station C2 is not considered further in the present study as it was deployed as a backup station in the event that the station C1 failed. Additional instruments were also deployed in an

alongshore array and were not considered in the present study. The reader is referred to Lowe et al. (2010b) for details of the along-shore transect.

3.4 Estimated sea surface elevation spectra

3.4.1 Expectations from literature

A number of studies have investigated the hydrodynamic processes on a reef. Lee and Black (1978) observed at Ala Moana Beach in Hawaii that as sea-swell waves approach a fringing reef and break on the fore-reef, energy is re-distributed to higher and lower frequencies. Similar observations were found at Yonge Reef (Great Barrier Reef, Australia) where the energy redistribution appeared to be related to the processes of wave breaking and frictional dissipation (Young, 1989). It was found at John Brewer Reef (Great Barrier Reef, Australia) that the observed redistribution of energy was governed by the water depth over the reef (Hardy and Young, 1996).

3.4.2 Analysis methodology

The data obtained from the field study at Ningaloo Reef was analysed to identify the sea surface elevation variance associated with different frequencies, and at different locations across the study site.

A sea surface elevation density spectrum was generated for each (hourly) burst of pressure data. The pressure data was corrected for the instrument offset and then transferred into the units of pressure head with a water density (ρ) of 1023.5 kg/m^3 and a gravitational acceleration constant (g) of 9.81 ms^{-2}. Each data burst was assumed to be a stationary signal, which enabled the variation in surface setup, tide and surge to be considered hydrostatic. A linear de-trend function was used to remove these components from the signal.

A one-sided pressure density spectrum $(S_{p,j})$ was assembled for each burst of data by the use of the Welch's averaged modified periodogram method. In this method of spectral estimation Hanning windows with a 50% overlap were used to reduce spectral leakage and to better approximate the spectrum's form. The approach resulted in spectra of approximately 10 equivalent degrees of freedom and a spectral resolution of 0.0011 Hz. The 95% confidence interval is bounded by the lower and upper limits of 2.71 and 0.58. These spectral characteristics were found to offer the best balance between frequency resolution and accuracy.

Each pressure density spectrum was converted (Equation 3.1) to a sea surface elevation wave spectrum $(S_{\eta,j})$ by the use of a linear wave theory transfer function $(T_{p\eta,j})$. This transfer

function accounted for the dynamic effect of the pressure with depth (with the assumption of no current).

$$S_{\eta,j} = \left(T_{p\eta,j}\right)^2 S_{p,j}$$

(3.1)

where:

$$T_{p\eta,j} = \frac{\cosh(k_j h)}{\cosh\left(k_j(h+z)\right)}$$

(3.2)

$$w_j^2 = g k_j \tanh(k_j h)$$

(3.3)

The linear dispersion relation (Equation 3.3) was used to calculate the wave number (k_j) where the angular frequency (w_j) was obtained for each discrete frequency of the pressure density spectra. The vertical distance of the pressure sensor above the seabed is defined by z and h is the water depth at the site.

3.4.3   Observations at Ningaloo Reef

The estimated sea surface elevation density spectra (Figure 3-3) indicated that in front of the reef (C1), the surface elevation variance was dominated by waves at frequencies greater than (approximately) 0.05 Hz. There was very little variation in the sea surface elevation at frequencies below this value with the exception of the period 14th to 19th June 2009. It was identified (Section 3.6) that this period corresponded to a storm that occurred at the site, which was also demonstrated by the arrival of 'faster' low frequency (swell) fore-runners that are clearly visible in the spectra. This result was expected, as this station was located in deep water where very little transfer or dissipation of sea-swell wave energy (due to breaking or friction) is expected to occur.

On the reef edge (C3), the surface elevation variance was dominated by waves at frequencies lower than (approximately) 0.06 Hz. The energy associated with higher frequency surface elevation variance appears to have been transferred to the lower frequencies or dissipated. This is consistent with studies by various authors who document similar observations (eg. Hardy and Young, 1996; Lee and Black, 1978; Young, 1989).

Further along the reef flat (C4), the spectra were dominated by surface elevation variances at frequencies below (approximately) 0.02 Hz. This indicates that further dissipation of energy occurs along the reef flat. Within the lagoon (C5), additional dissipation of energy is observed however this appears to be far less than the dissipation observed on the reef. Close to the
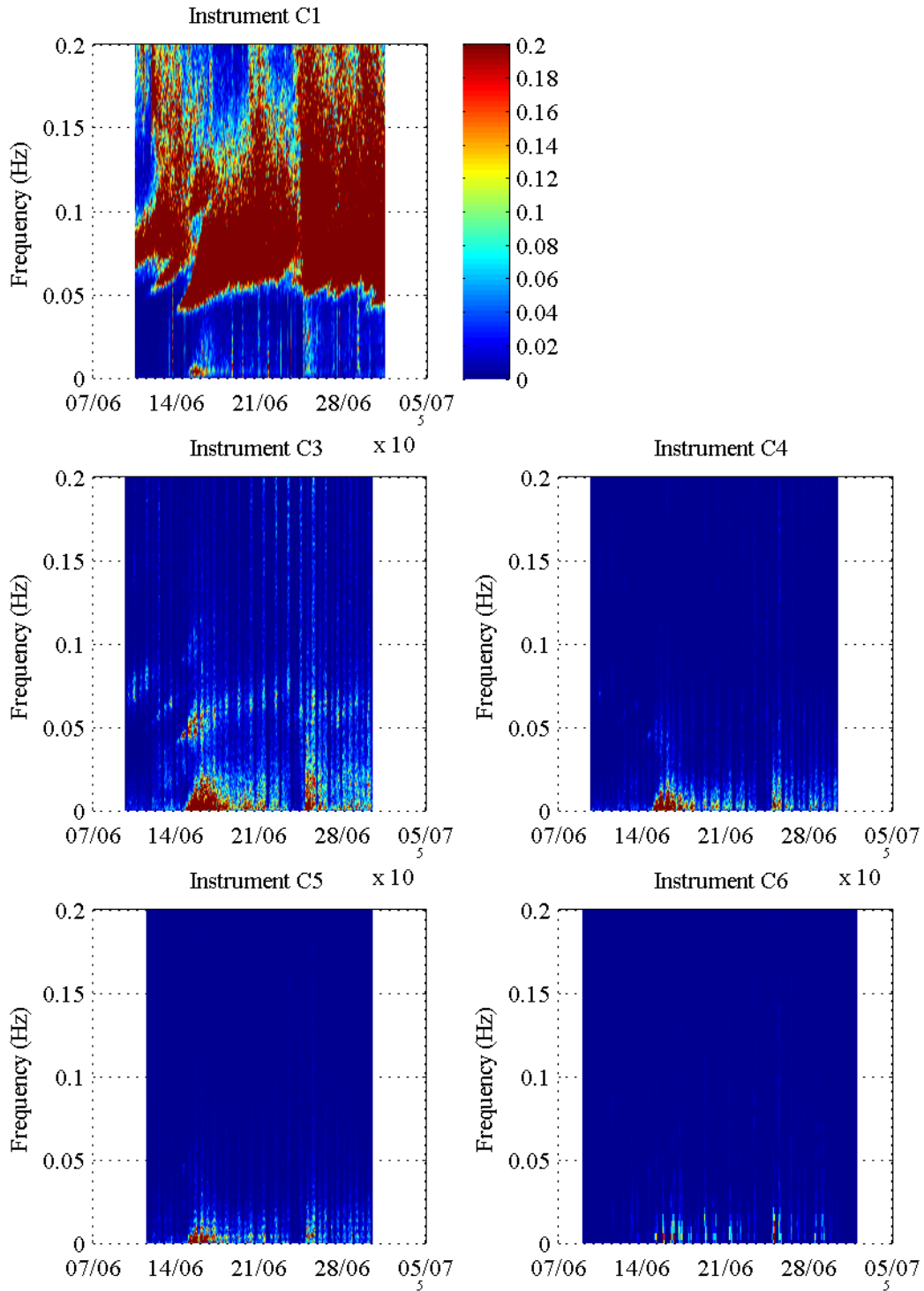
Figure 3-3: Sea surface elevation spectra
Spectral analysis determined by use of the Welch's averaged modified periodogram method, Hanning windows with 50% overlap which resulted in approximately 10 equivalent degrees of freedom and spectral resolution of 0.0011 Hz. The 95% confidence interval was bounded by the lower limit 2.71 and the upper limit 0.58.

shoreline (C6) there also appears to be dissipation of energy however, due to the odd-hour sample regime, it is difficult to compare the sea surface elevation spectra with the spectra at other stations.

This analysis suggests that dissipation processes vary spatially across the study site and appear to consist of (at least) dissipation due to wave breaking as well as due to flow friction. However, it is not possible from this analysis to determine the relative rates attributed to each mechanism.

3.5 Definition of 'Low-Frequency Waves'

3.5.1 Definitions in literature

A number of different frequency bands have been proposed to define sea-swell waves and low-frequency waves (Table 3-3). The majority of these frequency bands have been derived from laboratory experiments or the analysis of different field observations. It is therefore important to recognise that these bands offer general guidance and that the actual frequency that separates the sea-swell waves from the low frequency waves (f_{split}) is affected by the characteristics of the site and the wave climate at a particular instant in time.

Table 3-3: Frequency bands proposed in literature

Sea-Swell Frequency Band	Low-Frequency Band	Reference
0.05 – 0.24 Hz	0.004 – 0.05 Hz	(Sheremet et al., 2002)
0.04 – 0.2 Hz	0.005 – 0.04 Hz	(Péquignet et al., 2009)
0.04 – 0.3 Hz	0.004 – 0.04 Hz	(Elgar et al., 1992)

The upper boundary of the sea-swell waves is consistently defined above approximately 0.2 Hz while the f_{split} varies (0.04 – 0.05 Hz). The lower boundary, that defines the transition from low frequency waves to very low frequency waves, also varies (0.004 – 0.005 Hz). In this study, no distinction is made between low and very low frequency waves. To correctly separate the high and low-frequency waves in the measured data, a site specific f_{split} was calculated for the Ningaloo Reef study site. The calculated frequencies (for each burst of data) were then compared with the proposed frequency bands (Table 3-3) and the sea surface variance spectra. This frequency was then used to separate the data into high and low-frequency subsets.

### 3.5.2 Calculation methodology

The frequency that separates the low-frequency waves and sea-swell waves has been shown by Roelvink and Stive (1989) to be (well) defined as half of the offshore peak frequency (f_{peak}) of the energy spectrum (Equation 3.4).

$$f_{split} = \frac{1}{2} f_{peak}$$

(3.4)

The implicit assumption in the application of this approach is that the variance spectrum estimated for each burst of data represents a stationary signal. Station C1 was selected to determine the f_{split} because it was located in front of the reef (in deep water). The spectra on the reef and within the lagoon behind could not be used as the sea-swell waves undergo transformation over the crest and flat of the reef. This results in distortion of the estimated variance density spectrum by the dissipation and the redistribution of energy from higher frequencies to lower frequencies (Section 1.3).

3.5.3   Calculated f_{split} signal between low-frequency waves and sea-swell waves

The f_{split} signal (Figure 3-4) has three distinct features: a spike on 11 June 2009 at 22:00 (burst 70), a drop on 14 June 2009 at 10:00 (burst 131) that linearly recovers until the 18 June 2009 at 14:00 (burst 231) and a spiked signal over the period 24 June 2009 04:00 to 11:00 (bursts 365 to 372).
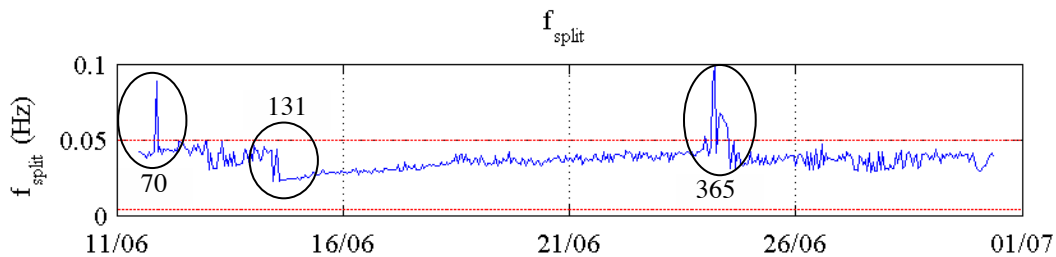
Figure 3-4: f_{split} for each burst of data
The f_{split} for each burst of data was calculated for each burst of data (blue). The domain of the low-frequency band typically cited in studies (red).

The spectrum of the first spike (burst 70) indicates that the second spectral peak is larger than the first peak a result that differs when compared to the spectra before and after (burst 69 and 71). This spectral feature distorts the calculation of the f_{split} (Figure 3-9).
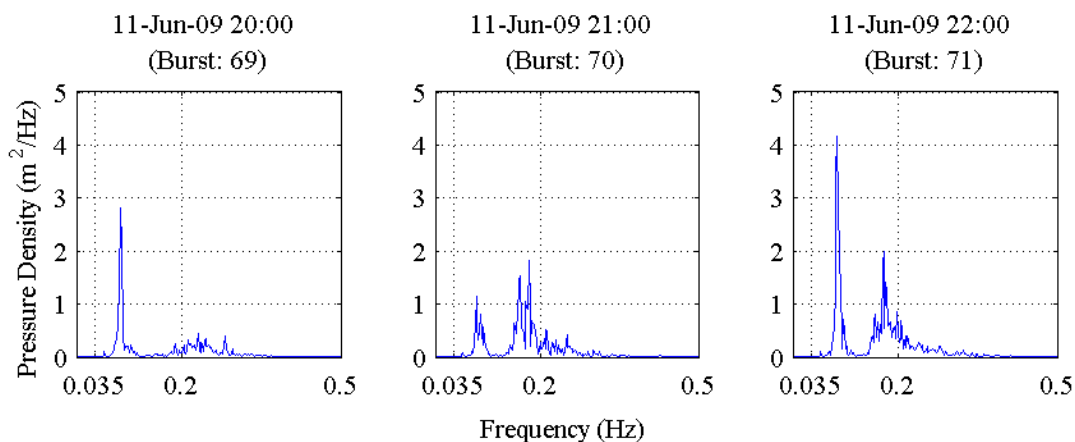
Figure 3-5: Pressure density spectra on either side of first f_{split} feature

32

The drop in the f_{split} (burst 131) appears to indicate the commencement of a storm at the site. Inspection of the spectrum (Figure 3-6) at this and subsequent bursts indicates an increase in low-frequency density when compared with a spectrum of a burst from some hours prior (burst 122). This is suggests the approach of a storm generated far from the site. The low-frequency domination of the spectrum is consistent with wave dispersion theory in which the lower frequency (and faster celerity) swell waves ("fore-runners") arrive ahead of the storm induced sea-waves. This is also demonstrated in the wave height time-series (Figure 3-9).
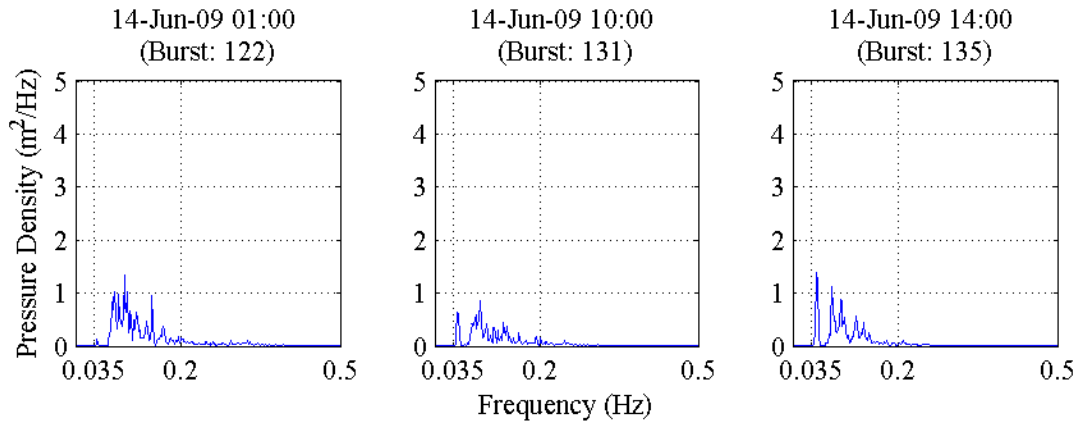
Figure 3-6: Pressure density spectra on either side of second f_{split} feature

The third feature (burst 365 to 372) indicates a concentration of energy between the frequencies of 0.05 Hz and 0.2 Hz. The spectrum is of spiked form and is distributed over a wide frequency range. This period coincides with the third storm observed at the site (Figure 3-9).
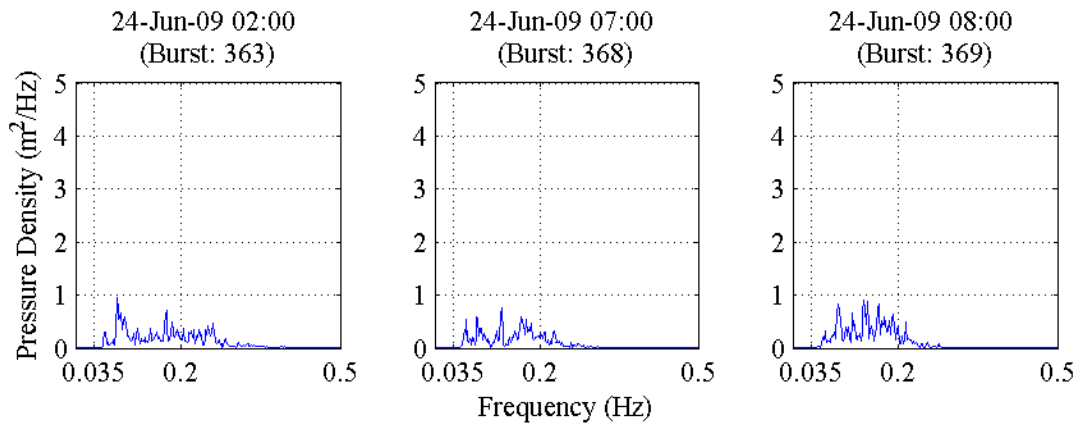
Figure 3-7: Pressure density spectra on either side of the third f_{split} feature

3.5.4 Definition of f_{split} adopted for Ningaloo Reef

The calculated f_{split} agrees well with the strong transition that can be visually observed in the surface elevation variance spectra (Figure 3-8). After removal of the two spikes, the calculated

f_{split} ($\mu = 0.0362\,Hz, \sigma = 0.0055\,Hz$, range: $0.0225\,Hz$ – $0.0576\,Hz$ where μ defines the mean of the signal and σ the standard deviation) was lower than the frequencies proposed in the literature (Section 3.5.1). At this Ningaloo Reef study site, the upper boundary of the frequency band proposed in literature is not suitable as it allows higher frequency energy to leak into the lower frequency band. However, the calculated mean f_{split} value provides a good separation of the higher frequency variance from the lower frequency variance (Figure 3-8) throughout the data in this study. As a consequence, the f_{split} value adopted in the present study was 0.035 Hz.
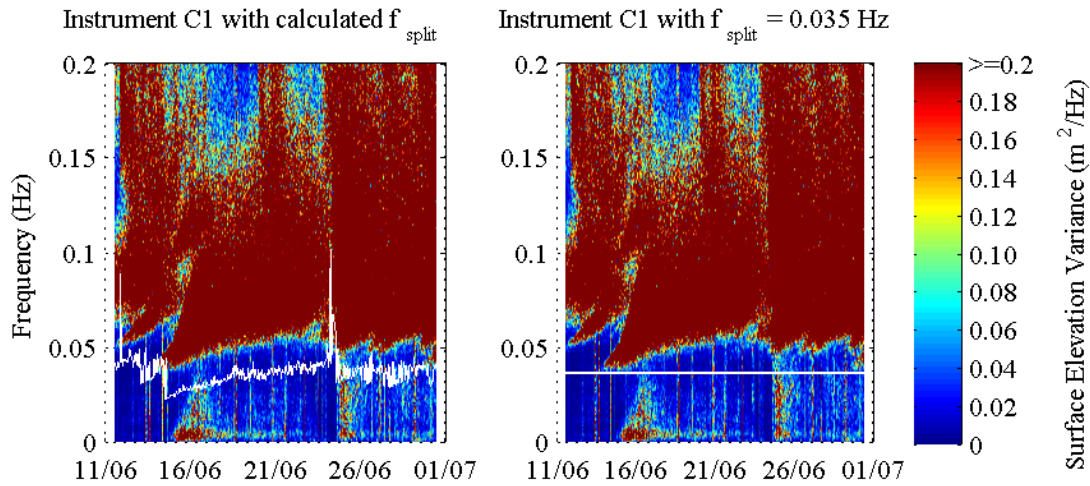
Figure 3-8 – f_{split} plotted with the sea surface elevation spectra
(Left) Surface elevation variance with calculated f_{split} value for each burst of data (Right) Surface elevation variance with the mean f_{split} value (0.0363 Hz).

3.6 Burst averaged wave height (H_{mo})

3.6.1 Determination of sea-swell and low-frequency wave height signal

The burst averaged low-frequency wave height ($H_{mo.lo}$) and high frequency (sea-swell) wave height ($H_{mo.hi}$) was calculated for each burst of data from the estimated sea-surface elevation spectra (Section 3.4). Implicit in this approach is the assumption that a one hour burst of data is stationary which enables stationary random data statistics to be performed.

The wave heights were calculated from the zero moment (m_0) of the wave spectra (Equation 3.5) over the low and high frequency bands. The spectral resolution was reduced in this analysis to 0.0022 Hz (for the pressure measurements) and 0.0044 Hz (for the AWAC in deep water) to enable the accuracy of the amplitude to be increased with a new equivalent degrees of freedom of approximately 21 and confidence limits of 0.64 and 1.81. The low-frequency band was defined as $f_{lo} \leq f \leq f_{split}$ and the high frequency band as $f_{split} < f \leq f_{hi}$.

$$H_{mo} = 4\sqrt{m_0} \tag{3.5}$$

where:

$$m_{0.lo} = \sum_{f=f_{lo}}^{f=f_{split}} S_{\eta,f}\Delta f_b \quad \text{and} \quad m_{0.hi} = \sum_{f=f_{split}}^{f=f_{hi}} S_{\eta,f}\Delta f_b$$

$f_{lo} = 0.0022\ Hz$ or $f_{lo} = 0.0044\ Hz$; $f_{hi} = 0.02\ Hz$; $f_{split} = 0.035$ Hz

The f_{hi} value was selected to be consistent with the upper boundary for sea-swell waves defined in literature (Section 3.5.1) and f_{split} on the basis defined in Section 3.5.4. The lower boundary of the low-frequency domain was defined by the frequency resolution of the spectral estimation methodology. The burst averaged wave heights for each of the instruments in the cross-shore array are illustrated in Figure 3-9.

3.6.2 Observed features of $(H_{mo.lo})$ and $(H_{mo.hi})$

In front of the reef (C1), sea-swell waves are shown to dominate the wave height time-series ($\mu = 140\ cm$, $\sigma = 42\ cm$, range $= 58\ cm – 281\ cm$) while the low-frequency waves exhibit significantly smaller amplitudes ($\mu = 9.0\ cm$, $\sigma = 5.5\ cm$, range $= 1.7\ cm – 48.2\ cm$).

On the reef flat (C3), the low-frequency burst averaged wave height increases in amplitude ($\mu = 16.1\ cm$, $\sigma = 8.6\ cm$, range $= 0.8\ cm – 47.1\ cm$)by a factor of approximately two. At the same location there is a substantial reduction in sea-swell wave height ($\mu = 17.4\ cm$, $\sigma = 9.4\ cm$, range $= 0.8\ cm – 47.5\ cm$). As a consequence, the sea-swell waves are of same order of magnitude in height as the low-frequency waves. It is unclear if the increase in low frequency wave height is due to a transfer of energy from the sea-swell waves (Section 3.4.1) or due to shoaling of the incident low frequency waves.

As the waves progress across the reef flat and the lagoon (C4 to C5), the low-frequency and sea-swell burst averaged wave heights continue to decay until they reach an amplitude of approximately 0.1 m. This indicates that energy is dissipated as the waves progress. Thereafter no further reduction in wave height is observed.

This analysis suggests that both wave breaking and flow friction are important sinks of energy, a suggestion consistent with observations in other studies (Section 1.3). The rapid reduction in sea-swell wave height on the reef crest suggests wave breaking occurs while additional wave breaking along with flow friction appear to dissipate energy on the reef flat. The prolonged

decay in wave height across the lagoon suggests flow friction cannot be ignored behind the reef. From this analysis however, the relative importance of these processes cannot be distinguished.
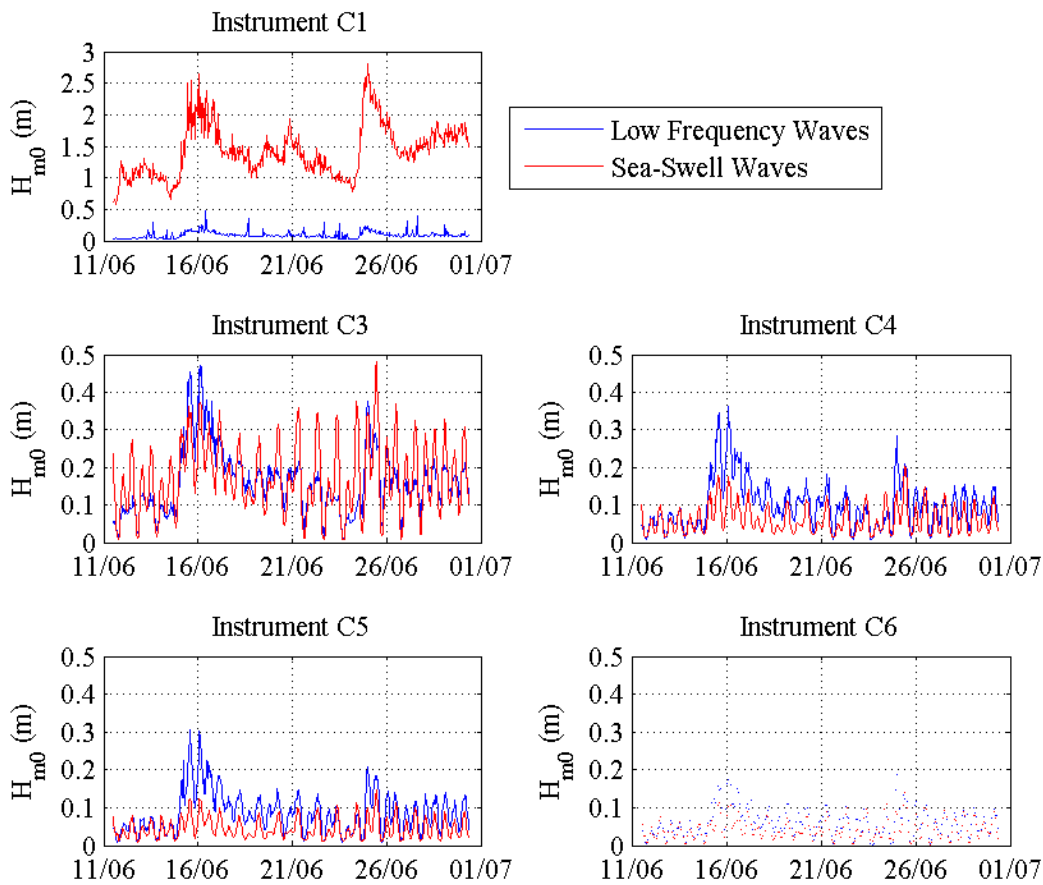
Figure 3-9 – Burst averaged wave height for high and low-frequency bands

3.7 Low-Frequency wave reflection

3.7.1 Determination of dissipative or reflective character

The presence of low-frequency waves at the coastline behind Ningaloo Reef confirms the passage of waves across the site. To determine if these waves are reflected or dissipated at the coastline, the ratio of incident and reflected low-frequency waves at each station was quantified. The method used followed the approach of Guza et al. (1984) and Sheremet et al. (2002), in which these waves were estimated by the decomposition of the low-frequency energy flux.

In this approach, the incident and reflected energy was derived from the substitution of the sea surface elevation equation (Equation 3-6) into the linear wave theory equation for energy (Equation 3-7). The resultant expression (Equation 3-8) evaluates collocated, time synchronised, pressure and cross-shore velocity data in frequency space under the assumptions of shallow water and cross-shore propagation of waves.

$$\eta^\pm = \frac{1}{2}\left(p \pm u\sqrt{\frac{h}{g}}\right)$$ (3-6)

$$E^\pm = \frac{1}{2}\rho g a^2$$ (3-7)

$$E^\pm(f,x) = \frac{1}{4}\left[S_{pp}(f,x) + \left(\frac{h}{g}\right)S_{uu}(f,x) \pm \left(2\sqrt{\frac{h}{g}}\right)S_{pu}(f,x)\right]$$ (3-8)

Where:

S_{pp} is the auto-spectrum of the pressure data, S_{uu} is the auto-spectrum of the velocity data and S_{pu} is the cross-spectrum of the pressure and velocity data. Refer to Appendix C for a detailed discussion on the auto- and cross- spectrum theory.

The spectra used in the analysis were estimated by the use of the Welch's averaged modified periodogram method. For this analysis, Hanning windows with a 50% overlap were used to reduce spectral leakage and resulted in spectra of approximately 20 equivalent degrees of freedom with a spectral resolution of 0.0022 Hz. The confidence limits were 0.64 and 1.84.

The low-frequency energy flux (Equation 3-9) was determined based upon the assumption that the incident and reflected waves travel with the celerity of a free wave. This assumption is reasonable, as it has been demonstrated (Section 1.3) that (most) short waves break on the reef crest and release the bound waves associated with the incident wave group.

$$\mathcal{F}^\pm = E^\pm(f,x)\sqrt{gh}$$ (3-9)

The bulk low-frequency energy flux (Equation 3-10) and the bulk low-frequency reflection coefficient (Equation 3-11) were then calculated for each burst of data.

$$F^\pm(x) = \int_{f=0.0022}^{f=f_{split}} \mathcal{F}^\pm(f,x)df$$ (3-10)

$$R^2(x) = \frac{F^-(x)}{F^+(x)}$$ (3-11)

3.7.2 Reflected waves derived from site data

The bulk low-frequency flux reflection coefficient (R^2) indicates that the incident flux is substantially higher than the reflected flux at stations C3 and C4 (Figure 3-10). This is further demonstrated by the incident and reflected flux time series. Across the basin, the incident flux is

shown to decrease while the reflected flux remains consistent in signal form and amplitude (C3: $\mu = 0.1588, \sigma = 0.0570$, range $= 0.0378 - 0.4804$) and (C4: $\mu = 0.2386, \sigma = 0.0864$, range $= 0.0161 - 0.5422$)

At station C5, the reflected flux coefficient is higher ($\mu = 0.4194, \sigma = 0.1631$, range $= 0.0170 - 0.7761$) than for the previous two stations. This indicates that a larger proportion of the incident wave flux is reflected at the coastline. Spectral analysis of each burst of reflected flux signal (Figure 3-11) indicates that the signal is generated from components with very low frequencies. The higher reflection coefficient is consistent with observations by van Dongeren et al. (2007) in which it was demonstrated that for steep slopes or low frequencies, the value of the reflection coefficient is higher.

The assessment of the incident and reflected flux indicates that the waves at Ningaloo Reef are highly dissipative as little reflection was observed across the basin except at very low frequencies. This suggests that resonance is possible but only at such frequencies.
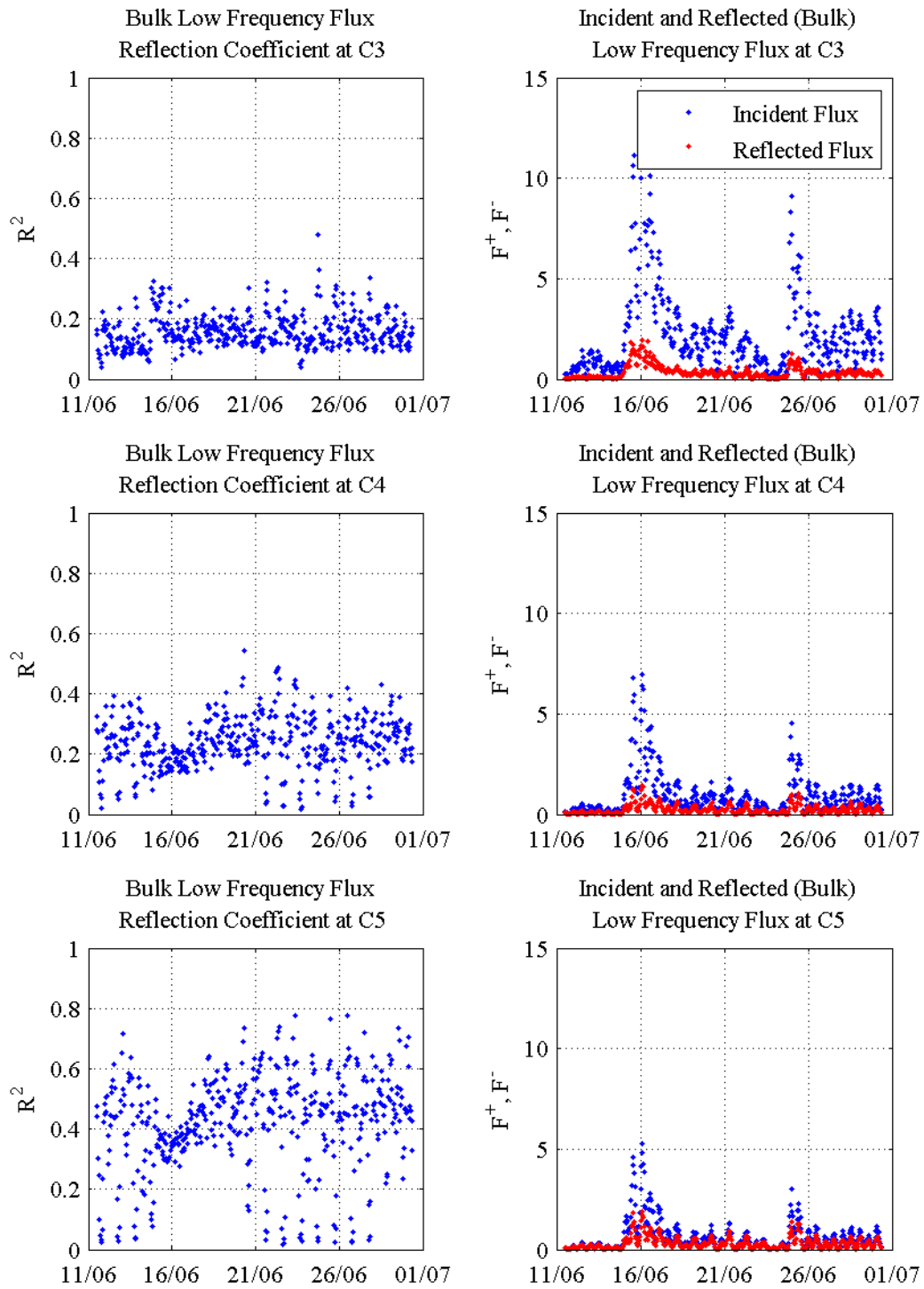
Figure 3-10: Bulk low-frequency incident and reflected flux
(Left) bulk reflection coefficient (Right) bulk incident and reflected flux. A delta factor ($\delta = 0.1$) was introduced in the analysis of both plots to suppress division by small numbers.
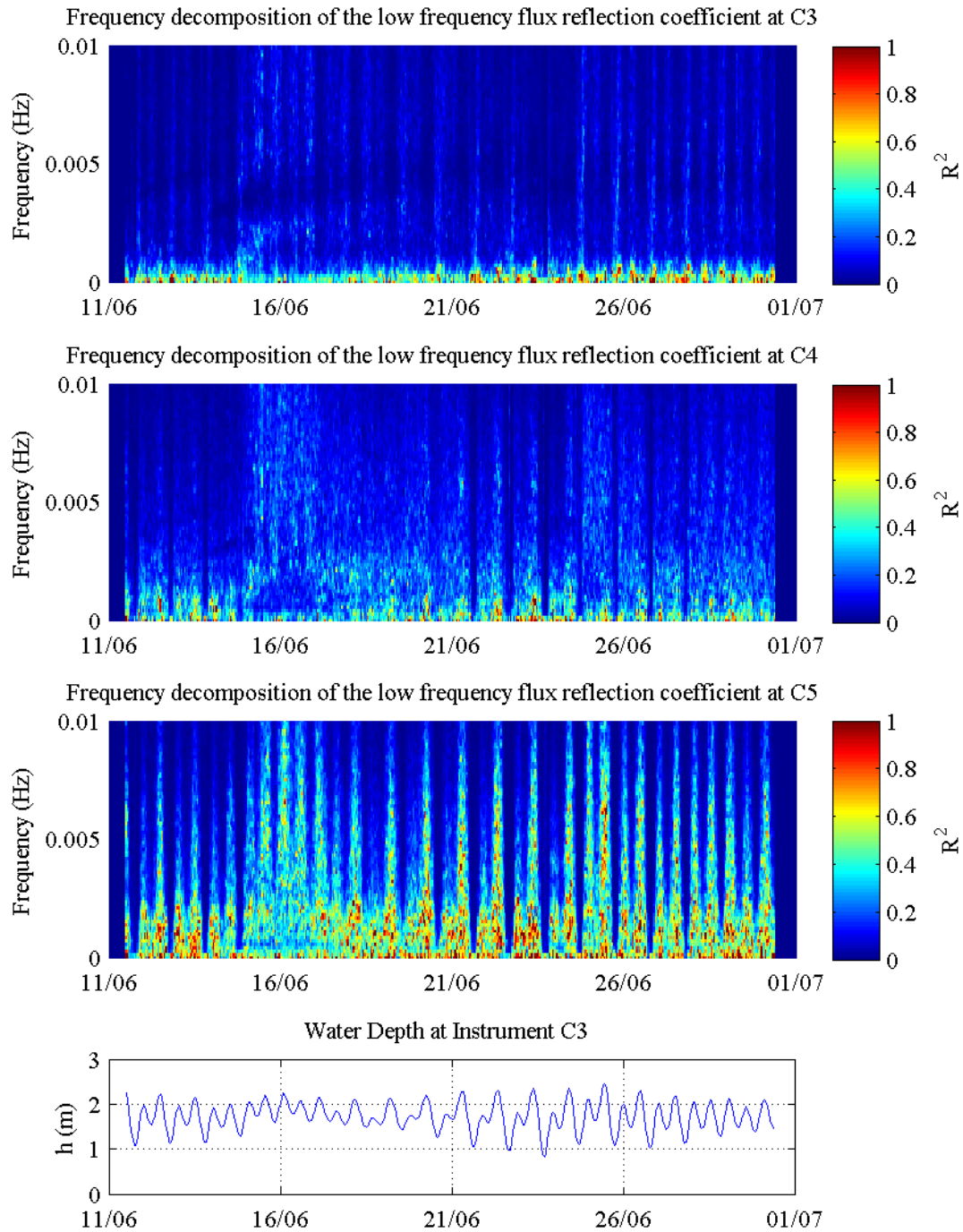
Figure 3-11: Frequency decomposition of the low-frequency flux reflection coefficient
The bulk reflection coefficient was very low (< 0.2) for frequencies greater than 0.1 Hz. To prevent bursts of data that were characterised by low incident and reflected flux from producing a very high reflection coefficient (due to the division of two small numbers in Equation 3-11), a delta factor was introduced ($\delta = 0.005$) in this analysis.

3.8 Resonance at Ningaloo Reef

3.8.1 Estimation of natural resonance frequencies

The first three natural resonant frequencies were estimated to determine the frequencies that would promote a standing wave to form. These were estimated for the Ningaloo Reef study site with an extended idealised open basin model (Equation 3-12), which was derived from Equation 2-2. This approach was consistent with similar studies (eg. Péquignet et al., 2009; Lugo-Fernández et al., 1998). The rationale for the determination of these three frequencies and the use of an open basin model is discussed further in Section 2.4.1.

$$f_n = \frac{(2n+1)}{4}\left(\frac{w_r}{\sqrt{gh_r}} + \frac{w_l}{\sqrt{gh_l}}\right)^{-1} \quad \begin{array}{l} n = \text{oscillation mode } (0,1,2,3\ldots) \\ \text{where: } h_r, h_l = \text{water depth on reef, lagoon} \\ w_r, w_l = \text{length of reef, lagoon} \end{array} \quad (3\text{-}12)$$

The length parameters were calculated from bathymetry data provided by The University of Western Australia. The depth of the water at the site varied with time due to the effects of various components of set-up (tide and surge). Each burst of data was assumed to be stationary and the depth of water was calculated by subtraction of the de-trended signal from the original signal at stations C3 and C4 (for each burst of data).

The first three estimated resonance frequencies are presented in Figure 3-12 and summarised in Table 3-4. The first two modes of resonance are at very low frequencies (< 0.004 Hz) while the mean of the third mode of resonance is at the lower end of the low-frequency wave band. As expected, the amplitude of the resonance frequency increases with each sub-harmonic of the fundamental oscillation due to the amplification effect imposed by $(2n+1)$ in Equation 3-12. Despite the low resonant frequencies, the modes of resonance are higher than tidal oscillations and may be forced by low-frequency waves.
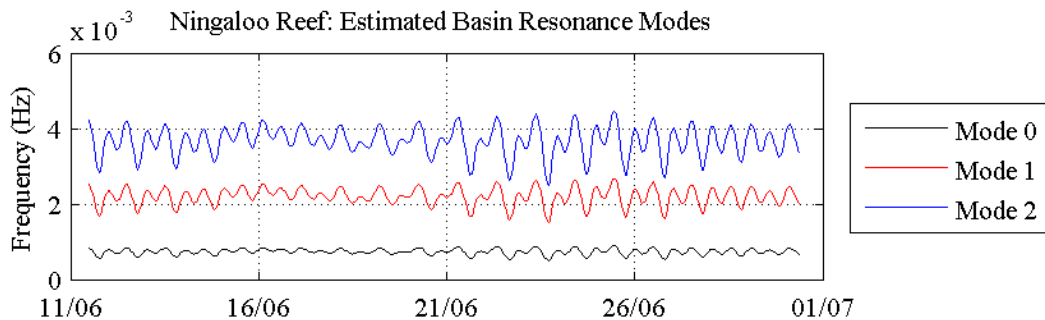

Figure 3-12: Basin resonance modes

Table 3-4: Ningaloo Reef resonance modes

Mode	μ (m)	σ (m)	Range (m)
0	7.34×10^{-4}	7.46×10^{-5}	$4.97 \times 10^{-4} - 8.91 \times 10^{-4}$
1	0.0022	2.24×10^{-4}	0.0015 – 0.0027
2	0.0037	3.73×10^{-4}	0.0025 - 0.0045
3	0.0051	5.22×10^{-4}	0.0035 – 0.0062

3.8.2 Identification of resonance at Ningaloo Reef

A statistical analysis was undertaken (based upon the hypothesised indicators described in Section 2.5 and tested in Section 5.3.3) to identify if a resonance signal was present in the data obtained at Ningaloo Reef. A Welch averaged modified periodogram with 50% window overlap was used to estimate the auto- and cross-spectra for each station and their combinations. This spectral analysis was conducted on a three hour burst (that moved across the sample set) to obtain sufficient spectral resolution. The features of these spectra are summarised in Table 3-5.

Table 3-5: Spectral features

Auto-spectral analysis						
Instruments	**Window**			**Spectrum**		
	Type	**Duration (s)**	**Samples (-)**	**D.O.F.***	**Resolution (Hz)**	**Confidence Limits#**
C3	Hanning	10800	2048	14	0.00049	2.13, 0.59
C4	Hanning	10800	2048	14	0.00049	2.13, 0.59
C5	Hanning	10800	2048	14	0.00049	2.13, 0.59
Cross-Spectral Analysis						
C3 and C4	Hanning	10800	2048	14	0.00049	2.13, 0.59
C3 and C5	Hanning	10800	2048	14	0.00049	2.13, 0.59
C4 and C5	Hanning	10800	2048	14	0.00049	2.13, 0.59
* Effective degrees of freedom						
# Based upon a 95% χ^2 distribution						

The coherence, co-spectrum and quad-spectrum were then calculated for each pair of instruments to determine if a standing wave was present in the data in accordance with the criteria specified in Section 2.5.

3.8.3 Results of analysis: Stations C3 and C5

The analysis focused on the results obtained from the stations C3 and C5. The higher sample resolution of C5 was the basis for the selection of this station in preference to C6, which did not sample at a sufficient rate to spectrally resolve the low frequencies of interest. These stations were selected as the primary focus because their locations represent the near extremities of the basin. Based upon the open-basin assumption, the locations of these stations are hypothesised to demonstrate a 0 ° phase difference (co-spectrum = +1) for even resonance modes and 180 ° phase difference (co-spectrum = -1) for odd resonance modes (Section 2.5.3).

The analysis indicates (Figure 3-13) that throughout most of the data obtained at the study site, the coherence measure of the pressure variance between these stations was very low (< 0.4).

Coherence was however found to be higher (0.5 – 0.8) within the period 14 June 2009 to 19 June 2009. This period corresponds to a storm at the site.

The peak of the storm corresponds to the highest coherence, which was at frequencies 0.007 Hz to 0.008 Hz. The phase plot suggests that the low-frequency waves contained in the data are progressive in nature due to the continuous variation in phase across different frequencies – a feature of progressive waves. This is further supported by the results of the normalised co- and quad-spectra (Equation 2-5, Equation 2-8).

The co-spectrum clearly alternates between +1 and −1. This indicates a phase shift from approximately 0 ° to 180 ° and is a feature of a standing wave pattern. However, inspection of the quad-spectrum indicates that at these co-spectral peaks, the spectrum is not (close to) zero. Rather, this spectrum also possesses strong normalised density. These two spectra together indicate that the waves are progressive (Section 2.5.2). For a standing wave, it would be expected that the co-spectrum would alternate between +1 and -1 (red and blue) with the quad-spectrum near zero (green). An analysis of stations C3 and C4 as well as C4 and C5 was also undertaken and the results are presented in Appendix B.

3.8.4   Conclusion: Is there resonance at Ningaloo Reef?

The analysis of instruments C3 and C5 indicated that that although the variation in pressure demonstrated high coherence at the time of the storm, the co- and quad-spectra defined phase difference between the signals implied that the generation of a standing wave pattern did not occur.

3.9   Conclusions from Ningaloo Reef site data

Analysis of the data obtained from the Ningaloo Reef study site by the University of Western Australia was consistent with observations made by other authors (eg. Lowe et al., 2010b; Taebi et al., 2011). It was observed that offshore, the sea surface elevation spectrum was dominated by high frequency waves. On the reef crest these waves appeared to demonstrate a transfer of some energy to lower frequency waves while a large proportion of the energy was dissipated. Across the reef and lagoon, further high and some low-frequency dissipation was observed. Similar features were observed in the high and low-frequency wave height.

The waves were shown to be highly dissipative with reflected flux only observed at low frequencies for all measurement stations. This indicated that any resonance would be at low frequencies. Coherence, co-spectral and quad-spectral analysis of the data indicated that although high coherence was observed between instruments C3 and C5 during the storm event,

the phase between the instruments was found to be progressive and did not characterise a standing wave pattern.
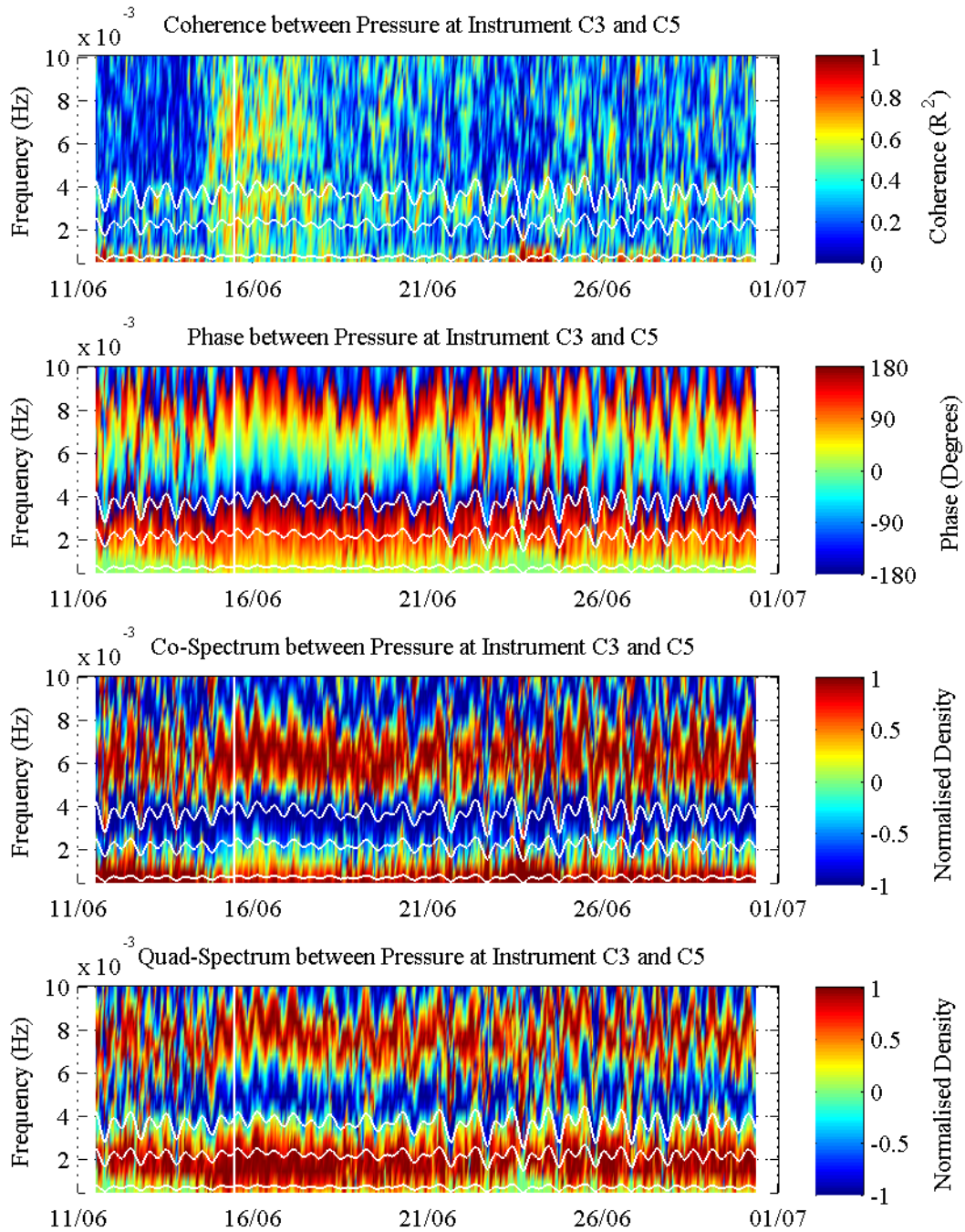
Figure 3-13: Coherence, phase, co- and quad-spectra between instruments C3 and C5
Frequencies higher than 0.01 Hz have been omitted for clarity. The vertical (white) line represents the peak storm observed at the site. The first three modes of natural resonance frequencies are also plotted.

Chapter 4

ASSESSMENT OF XBEACH MODEL SUITABILITY

4.1 Introduction

The processes that govern the interaction between waves and reefs are complex. Various studies have focused on the development of different models to describe specific processes related to reefs (Gourlay, 1994; Gourlay, 1996b; Gourlay, 1996a; Lee and Black, 1978; Lowe et al., 2005; Massel and Gourlay, 2000) while few have assembled models to describe the holistic system of interaction (eg. Gerritsen, 1980; Symonds et al., 1995; Nwogu and Demirbilek, 2010; Lowe et al., 2009b). In the present study, the numerical model XBeach was used to model low-frequency motion across a reef and into a lagoon. Calibration and use of the model demonstrated that the process-based model XBeach could describe the dominant hydrodynamic processes within these complex morphological environments.

Section 4.2 provides a brief summary of the development and numerical structure of XBeach. The case to justify the suitability of the model for the present study is then presented in Section 4.3 with connections made between the current knowledge related to wave-reef interaction and the model. Section 0 describes the setup and calibration of the Ningaloo Reef model in XBeach along with an analysis of the calibration results. In addition, an idealised model is demonstrated to be suitable for the purposes of the present study as part of this calibration effort.

4.2 Model development history

The development of XBeach was initiated by the USACE-ERDC in response to the effects of hurricanes on low-lying sandy coasts in the United States of America. Parallel to this, the Dutch Dune Safety Assessment programme identified a need for more advanced models to assess the

protection provided by dunes against flooding of the hinterland. In particular, advanced models suitable for situations where empirical model assumptions no longer hold were required. This led to the rapid development and validation of XBeach, an open source process-based model that is freely available under GNU Lesser General Public Licence and under continuous development by a partnership between UNESCO | IHE, Deltares and the University of Miami (Roelvink et al., 2009).

The model consists of Fortran 90/95 routines that simulate time-dependent 2D-horizontal (depth averaged) processes and has been verified against a number of analytical, laboratory and field tests (Roelvink et al., 2009).

4.2.1   Model structure

The XBeach model (schematically) consists of two boundary condition modules (waves and flow) and four calculation modules (wave propagation, flow, morphology and sediment transport). The key elements of each module, the output it generates and the relationship with other modules are illustrated in Figure 4-1. In the present study, the hydrodynamics associated with the propagation and transformations of waves that interact with a reef were the focus of the analysis. Consequently, the wave propagation and flow modules were activated with the remainder of the modules de-activated. The numerical basis behind these models is briefly summarised in Appendix D as well as in Roelvink et al. (2009).
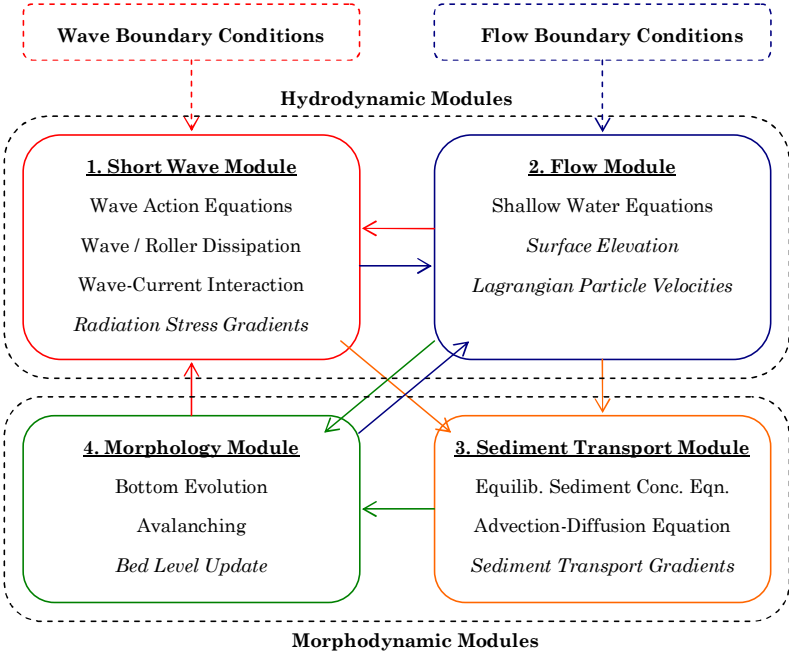

Figure 4-1: XBeach Model Structure from (Daly, 2009).

46

4.3 Suitability of model

Roelvink et al. (2009) along with Daly (2009) have undertaken a verification of the low-frequency component of the XBeach model with high resolution laboratory data and found that XBeach, in general, described the observed processes well. Trang (2010) further investigated the ability to use the numerical model XBeach to investigate the interaction between reefs and low-frequency waves. The model was analysed against the linear model proposed by Symonds et al. (1995) in one dimension and also compared to field data recently obtained by Lowe et al. (2010b) at Ningaloo Reef. This study is important as it demonstrates that the numerical model XBeach appears to have the capability to investigate the complex interaction between reefs and low-frequency waves. While these studies indicate that the model is applicable, a review of the numerical expressions within XBeach and their relation to literature is required to obtain confidence that this is the case.

Four key processes are consistently cited in literature and need to be included in XBeach in order to ensure that the numerical equations behind the model are consistent with the results of studies related to coral reef hydrodynamics. These processes are:

- Long wave generation and release;
- Wave induced setup on a reef;
- The wave breaking process; and
- Dissipation by bottom friction (from wave breaking and mean flow).

These processes will each be considered to demonstrate that XBeach is a suitable tool to model coral reef hydrodynamics. Appendix D provides a summarised description of the XBeach model and its numerical equations. The reader is referred to this section prior to reading the following section, which has been prepared based upon the assumption that the reader has an understanding of the XBeach model structure.

4.3.1 Long wave generation and release

The generation and release of long waves is fundamental for the present study. Currently three mechanisms have been proposed to explain the generation of long waves: the bound long wave concept (Longuet-Higgins and Stewart, 1962), the breakpoint generation mechanism (Symonds et al., 1982) and the integrated bound and free wave concept (Schaeffer, 1993).

To understand how long waves are generated in XBeach, one must first understand the timescale of this model. In this model, waves are resolved on the wave group time scale based upon a parameterised wave scale boundary condition. Two equations are the basis of this

approach, the wave action equation and the shallow water equation. These equations are coupled via the force term related to the concepts of radiation stress (Longuet-Higgins and Stewart, 1962). The variation in groupiness of the short waves (described by the wave action equation) generates this force term that is then used as an input into the shallow water equation from which a shallow water wave (the long wave) is generated. In deep water, this wave is bound to the wave groups by this short wave forcing but as these short waves transform (via shoaling and breaking), the group structure is destroyed along with the forcing it generates. The bound wave is 'freed' and is then subjected to the processes associated with free waves such as reflection and transformation. In addition, as the waves break on a slope in the model, the groupiness also disappears and results in a shifting breakpoint consistent with the mechanisms by Symonds et al. (1982) and Schaeffer (1993). It is clear from this summary of the XBeach wave structure that the model addresses the three forms of long wave generation described in literature.

4.3.2 Water level variations on a reef

Many authors have investigated the generation of wave-induced set-up on a reef and its importance to different processes on a reef. However, this is only one form of water level variation that may occur on a reef. More broadly, water level variations consist of tides, wave-induced setup and wind-induced set-up. All three water level variation types are modelled in XBeach, of which only the second type applied to the present study.

The surface elevation signal generated in XBeach (Section 4.3.1) can be decomposed into a mean and a dynamic component (Roelvink et al., 2009; Daly, 2009). The dynamic component is the long waves while the mean component is the wave-induced setup. This decomposition demonstrates that the physical process of setup is captured well in the XBeach model through conservation concepts and radiation stress.

4.3.3 Wave breaking

The process of wave breaking is complex and highly non-linear. As a consequence, semi-empirical formulae have been developed to describe this process with the most commonly referred formulations by Battjes and Janssen (1978) and Thornton and Guza (1983). XBeach adopts (by default) the Roelvink (1993) model that incorporates elements of these two formulations and improves the structure of the formulation for easy application on the timescale of wave groups (Equation 4-1).

$$D_{wave} = 2\alpha f_{rep} E_{waves} Q_{break} \tag{4-1}$$

Where:

$$E_{waves} = \frac{1}{8}\rho g H_{rms}^2$$

$\alpha \approx 1, f_{rep}$ is the representative frequency, Q_{break} is a probability function and H_{rms} is the root mean squared wave height.

In addition to this breaking formula, a roller equation is also implemented to capture the process of roller formation and propagation (Equation 4-2), a process that has not been explicitly captured in other studies cited in relation to coral reefs.

$$Dr = \frac{2g\beta E_r}{c} \tag{4-2}$$

Where:

β is the wave surface slope angle, E_r is the roller energy and c is the wave celerity

4.3.4 Wave and flow friction

The roughness of a coral reef is perhaps one of the most important elements to capture in a numerical model. This roughness (which is imposed in the form of bed friction) is commonly separated into two processes, friction by wave breaking and friction on flow.

Gerritsen (1980) evaluated the expression for wave breaking bed friction (Equation 4-3) to wave friction dissipation on reefs. This formulation is also the basis for the analysis conducted in XBeach.

$$\varepsilon_f = \frac{2}{3} f_w \frac{\rho}{\pi} \left(\frac{\pi H_{rms}}{T_{rep}\sinh kh} \right)^3 \tag{4-3}$$

Where:

f_w is the wave breaking bed friction parameter, H_{rms} is the root mean squared wave height and T_{rep} is the representative wave period.

The calculation of the flow friction in XBeach (Equation 4-4) follows the approach by Ruessink et al. (2001). Other models have been developed and could be equally valid.

$$\tau = C_f \rho u_e \sqrt{(1.16 u_{rms})^2 + \bar{v}^2} \tag{4-4}$$

Where:

τ is the bed stress, u_e is the local Eulerian orbital velocity, u_{rms} is the local orbital velocity derived from H_{rms} and $\bar{v}$ is viscosity.

4.4 Model setup and calibration

4.4.1 Previous calibrations

A detailed XBeach calibration study, with field data obtained at the Ningaloo Reef study site has previously been undertaken (Trang, 2010). It was identified that the model calibration was influenced by the flow friction dissipation parameter (C_f) and wave friction dissipation parameter (f_w). The analysis concluded that the best agreement between XBeach and measured data was achieved with $C_f = 0.1$ and $f_w = 0.6$.

4.4.2 Aim of the present calibration

Since the previous Ningaloo Reef calibration study was undertaken, XBeach has evolved and new releases of the model have become available. Furthermore, additional tools (primarily MATLAB functions) have been developed to assist in the setup of the model and the analysis of its results. In this study a model grid generation function and a new one-dimensional command was used extensively.

The aim of the present calibration effort was to confirm the calibration of the XBeach Ningaloo Reef parameters previously proposed by Trang (2010) remain valid in the current model environment.

4.4.3 Model profile

The cross-shore transect of the study site was extracted from a three-dimensional bathymetric profile of the Ningaloo Reef that was supplied by The University of Western Australia (Figure 4-2a). The one-dimensional profile (Figure 4-2b) of the project transect was defined, with a deep-water limit of −20 m, and used to calibrate XBeach with data obtained at the site. A comparative calibration was also undertaken to assess the influence of an idealised profile on the agreement between the XBeach results and the data observed at the site.
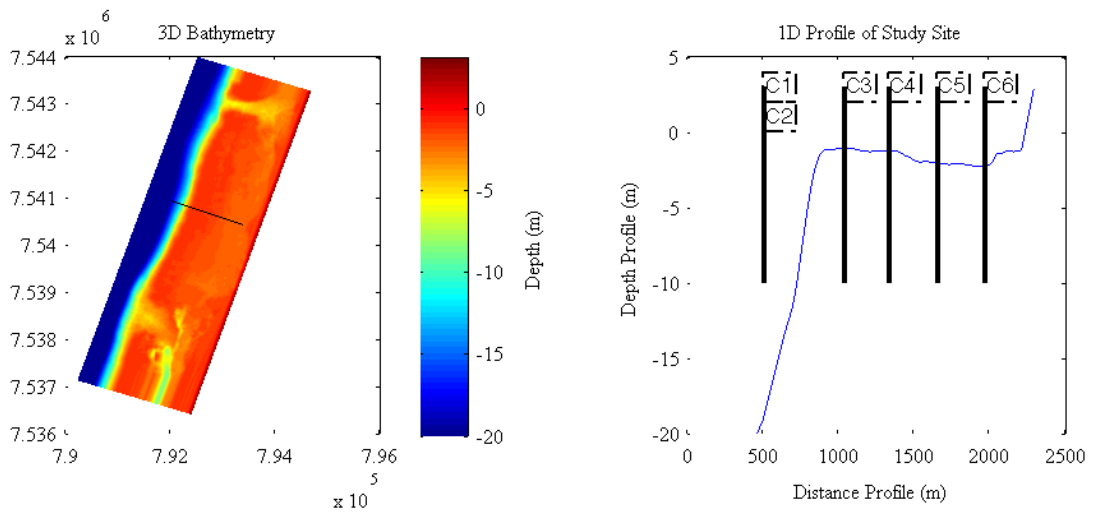
Figure 4-2: Ningaloo Reef bathymetry and transect profile
(a) 3D bathymetry of the portion of the Ningaloo Reef within which the site was located. The instrument transect of the field study is denoted by the black line on the bathymetry (b) the transect site profile along with the location of the field study instruments.

4.4.4 Wave boundary conditions

The peak of a storm observed in the data (Section 3.6) was used as the wave boundary condition for the calibration of the model. The presence of a large low-frequency signal in the response of this particular storm (Section 3.4.3) justified this calibration approach with the previous calibration also conducted on the same basis (Trang, 2010). Spectral analysis of this peak storm identified that a zero-moment wave height (H_{m0}) of 2.80 m and peak frequency (T_p) of 18.96 s represented the wave conditions for this event. The spectral analysis was conducted by use of the Welch's averaged modified periodogram method in which Hanning windows with a 50% overlap resulted in a spectrum of approximately 10 equivalent degrees of freedom and a spectral resolution of 0.0056 Hz. The lower and upper confidence intervals were 2.71 and 0.58.

The spectrum of the peak storm was fitted to a JONSWAP spectrum. While other forms of wave boundaries can be specified in XBeach, the application of a JONSWAP spectrum was found to be the most reliable and flexible for the present study. A JONSWAP-type spectrum was found to fit the peak storm well with $\gamma = 15$ (rather than $\gamma = 3.3$ which calibrated well with the JONSWAP project data from the North Sea) (Figure 4-3). The variations in the spectrum fit near 0.045 Hz and 0.065 Hz are attributed to non-linear effects. A small peak of variance above 0.1 Hz that was also not captured in the JONSWAP-type fit. The adopted spectral parameters for the wave boundary condition are summarised in Table 4-1.
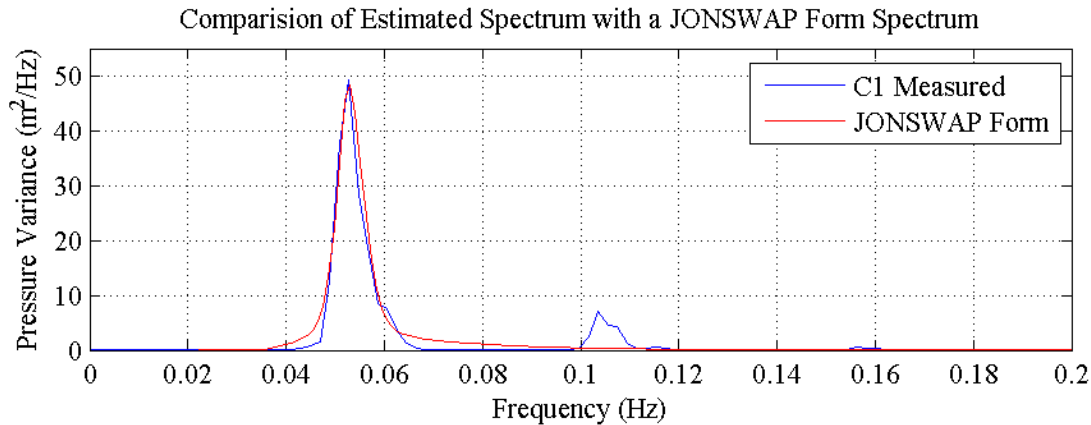
Figure 4-3: JONSWAP-type spectrum fitted to the wave conditions observed at the site
The spectral analysis of the observed data was calculated with 10 equivalent degrees of freedom and spectral resolution of 0.0056 Hz. The JONSWAP type spectrum was defined with $\gamma = 15$, $H_{m0} = 2.606$ m and $T_p = 18.96$ s.

Table 4-1: Adopted JONSWAP and wave boundary condition parameters for model calibration

Parameter		Value	Selection Basis
Dir0	[°]	250	Defined for the Ningaloo Reef model structure
Gamma	[-]	15	Best fit to the peak of the storm at Ningaloo Reef
Spreading	[-]	20	Defined in previous calibration study (Trang, 2010)
T	[s]	21600	Sufficient to provide spectral resolution for analysis
Tstep	[s]	0.1	Recommended value (Roelvink et al., 2010)
Hm0	[m]	2.606	Peak storm wave height
Tp	[s]	18.96	Peak storm wave period

4.4.5 Flow boundary conditions

The flow boundary conditions adopted in this calibration were consistent with an open 'flume type' model (Table 4-2).

Table 4-2: Flow boundary conditions for model calibration

Boundary	Value	Boundary Condition
Front	1	1D Absorbing Generation Boundary Condition
Back	0	Wall
Left	0	Wall
Right	0	Wall

4.4.6 Tide

The data obtained from the Ningaloo Reef study site included a tidal signal as well as setup. A tidal analysis for the period of the field study was undertaken and a time series of the tide for the site generated (Lowe, 2011). The tidal component was identified for the peak storm and included as a fixed increase in water level for the duration of the model calibration. The setup was generated in the model. In this analysis, the peak storm conditions were considered stationary throughout the simulation time and on this basis the use of a fixed tidal contribution

was justified. The tidal contribution for the calibration case was zs0 = 0.0364 m. This enabled direct comparison of XBeach with the data obtained at the site.

4.4.7 Calibration simulations and analysis methodology

Calibration of the XBeach model involved 14 simulations (Table 4-3 and Table 4-4) that were grouped into two simulation sets:

1. 1D calibration and sensitivity analysis (with site profile);
2. 1D calibration analysis (with idealised profile).

Initially, a purely one-dimensional (1D) model was calibrated (by use of the XBeach command 'superfast'). This model differed from the model in the previous calibration in which a 1D model was estimated by the use of a three cell (2D-like) model (Trang, 2010). In this definition, three grid-cells were used in the y-direction rather than one grid-cell. This was not expected to produce a significantly different result because the gradients in the y-direction $\left(\frac{d}{dy}\right)$ were forced to be zero by alongshore uniformity in the model. Such a model was calibrated in the present study and was compared with the purely 1D model developed in the present study (Appendix F). A sensitivity analysis was undertaken for the proposed C_f and f_w values and the optimal combinations identified. Different profile idealisations were simulated in the second simulation set to determine the influence the simplifications had on the calibration.

Table 4-3: 1D calibration simulations conducted

1D model simulations with site profile		
ID	C_f	f_w
C1D-S1	0.05	0.55
C1D-S2	0.05	0.60
C1D-S3	0.05	0.65
C1D-S4	0.10	0.55
C1D-S5	0.10	0.60
C1D-S6	0.10	0.65
C1D-S7	0.15	0.55
C1D-S8	0.15	0.60
C1D-S9	0.15	0.65

Table 4-4: Idealised model analysis

Idealised model analysis					
ID	**mf**	**ml**	**mb**	C_f	f_w	**Notes**
C1D-I1	0.0458	0.0048	0.0500	0.1	0.6	Simplified bathymetry model
C1D-I2	0.0458	0	0.0500	0.1	0.6	Step into lagoon
C1D-I3	0	0	0.0500	0.1	0.6	Step onto reef and into lagoon
C1D-I4	0.0458	0	0	0.1	0.6	Step into lagoon and end wall
C1D-I5	0	0	0	0.1	0.6	All transitions vertical

Four statistical measures, consistent with the calibration study undertaken by Trang (2010), were used to evaluate the calibration results in relation to the measured data:

- Mean Squared Error (Equation 4-5);
- Root Mean Squared Error (Equation 4-6);
- Normalised Root Mean Squared Error (Equation 4-7); and
- Bias (Equation 4-8).

These statistical measures enabled the agreement between the XBeach generated results (for the whole model) and the measured data to be quantified. The accuracy of individual station was assessed spatially with line plots.

$$MSE = \frac{\sum_i^n \left(X_{XBeach,i} - X_{measured,i} \right)^2}{n} \tag{4-5}$$

$$RMSE = \sqrt{MSE} \tag{4-6}$$

$$Norm.RMSE = \frac{RMSE}{X_{measured}} \times 100 \tag{4-7}$$

$$BIAS = \overline{X_{XBeach}} - \overline{X_{measured}} \tag{4-8}$$

Where:

$X_{XBeach,i}$ is the variable output from XBeach under consideration, $X_{measured,i}$ is the variable measured at the Ningaloo Reef study site, $\overline{X_{measured}}$ is the mean of the measured variable at the Ningaloo Reef study site and n is the number of data.

4.4.8   1D model calibration results (Site Profile)

The statistical analysis of the 1D calibration results is summarised in Figure 4-5 with the spatial distribution of the best-fit results illustrated in Figure 4-6. Plots of the spatial distribution for the other simulations are attached in Appendix E.

The computed sea-swell wave heights under predicted the observations (RMSE: 13.6 cm – 16.5 cm, BIAS: -54.8cm – - 3.5 cm) for all combinations of C_f and f_w. Inspection of the spatial distribution indicates that this underestimation occurs in deep water. On the reef and within the lagoon, good agreement was observed between the model and measured results.

A high level of agreement was determined between the XBeach low-frequency wave results and the measured low-frequency wave heights (RMSE: 0.0276 – 0.0848 m, BIAS: 0.0520 – 0.0711 m). A distinct combination of parameters resulted in the best calibration $\left(C_f = \right.$

0.1 and $f_w = 0.6$). Spatially, the low-frequency waves were underestimated offshore and overestimated near the reef crest however on the inner reef edge and within the lagoon, the wave heights estimated by the model are found to agree well with the measured values. Near the shoreline, the low-frequency wave heights were slightly overestimated when compared with the field results.

Statistically, similar results were observed for the tidal and setup component (RMSE: 0.0364 – 0.0830 m, BIAS: -0.0639 – - 0.0699 m) however the spatial distribution of the best-fit results was consistently underestimated.

Overall, the XBeach model demonstrated a (approximately) consistent Normalised-RMS of 20 – 25%. The low-frequency waves were found to achieve the best calibration when $C_f = 0.1$ and $f_w = 0.6$ as also determined by Trang (2010).

4.4.9 Adopted values for C_f and f_w

Based upon the current calibration results, the C_f and f_w values previously identified by Trang (2010) $(C_f = 0.1$ and $f_w = 0.6)$ were found to calibrate the present model with the data observed at the site and were adopted for the present study.

To assist in the visualisation of how these frictional parameters relate to the field, typical bottom roughness is illustrated in Figure 4-4 from a visit to the site attended by the author from 14 – 16 May 2011.

Figure 4-4: Typical coral on bed of study site
Photographs: Roelvink (2011)

4.4.10 Influence of an idealised profile on the 1D model calibration

The Ningaloo Reef profile was replaced in the model with an idealised profile of the reef to assess the influence of this idealisation on the model's calibration. No appreciable difference was observed in the model results when compared with the best-fit model statistically or spatially (Figure 4-7 and Figure 4-8).

The analysis was extended to assess idealisations of the profile transitions. It was observed that substitution of the sloped transition from the reef into the lagoon did not significantly affect the calibration of the model with a slight improvement in calibration observed. A similar result was observed for the beach slope transition.

Implementation of a vertical transition at the fore-reef edge resulted in an overestimation of the low frequency waves and the tide and wave setup components while the short waves were well represented (but slightly overestimated).

This analysis indicated that the reef profile could be idealised with a vertical transition into the lagoon and at the shoreline but that the foreshore slope had to be retained to maintain calibration with the data obtained at the site.

4.5 Conclusions

Review of the XBeach model demonstrates that the model's structure and numerical basis is suitable for the analysis of reefs. In particular, the advantage of decoupled dissipation terms (C_f and f_w) enabled the calibration of the model to be achieved under conditions that are different from sandy coasts.

A 1D XBeach model was calibrated against data obtained from the study site at a peak storm for which low-frequency energy was observed in the data. The calibration of the dissipation parameters was found to agree with the previous calibration study undertaken (Trang, 2010), with $C_f = 0.1$ and $f_w = 0.6$ adopted for these parameters.

The use of an idealised profile was not found to significantly affect the model calibration. Implementation of vertical step transitions on the reef-lagoon transition and at the beach was also not found to affect the calibration of the model while substitution of the fore-reef slope with a vertical transition was found to overestimate the low frequency waves and tide and wave setup.
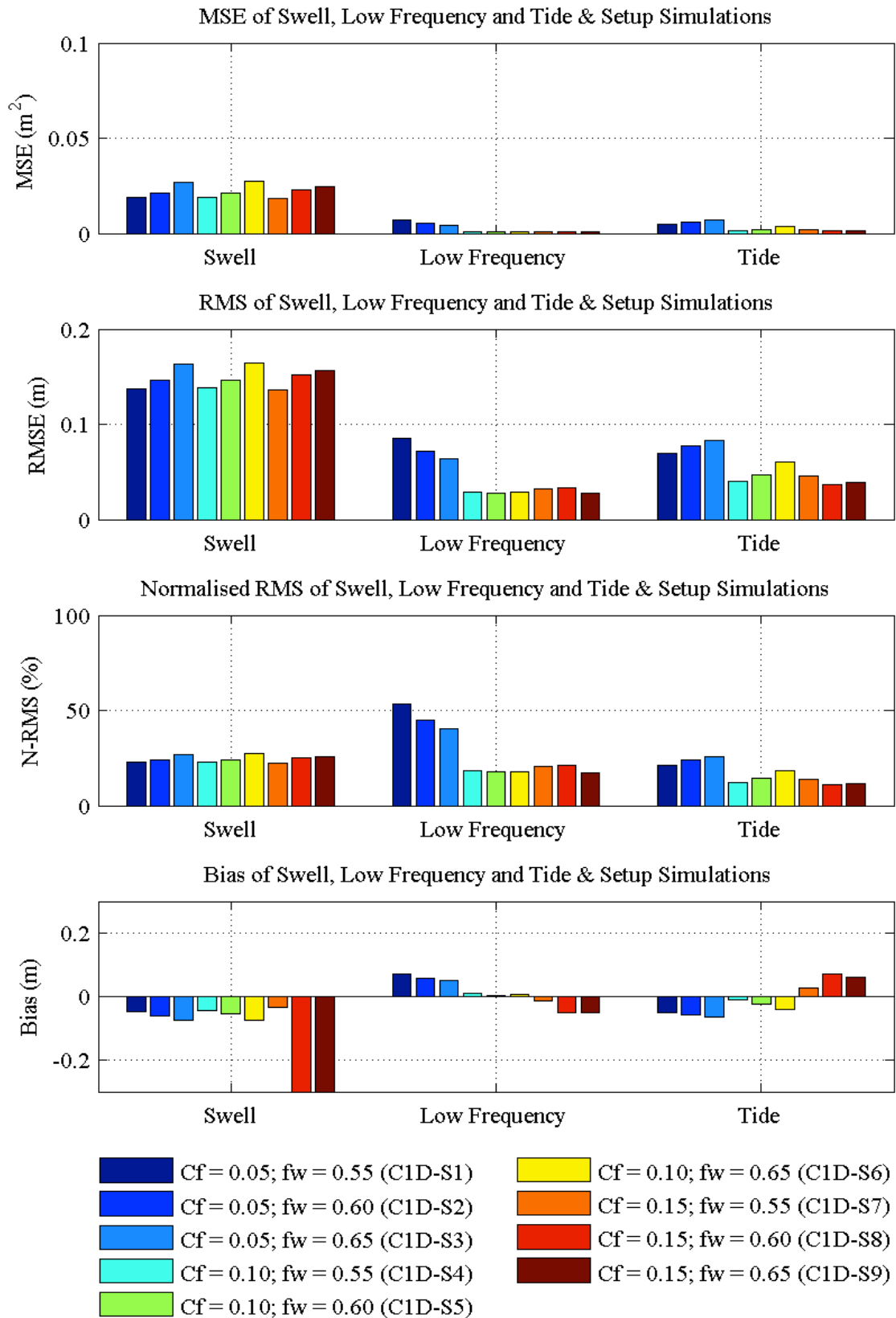
Figure 4-5: Statistical results of 1D model calibration
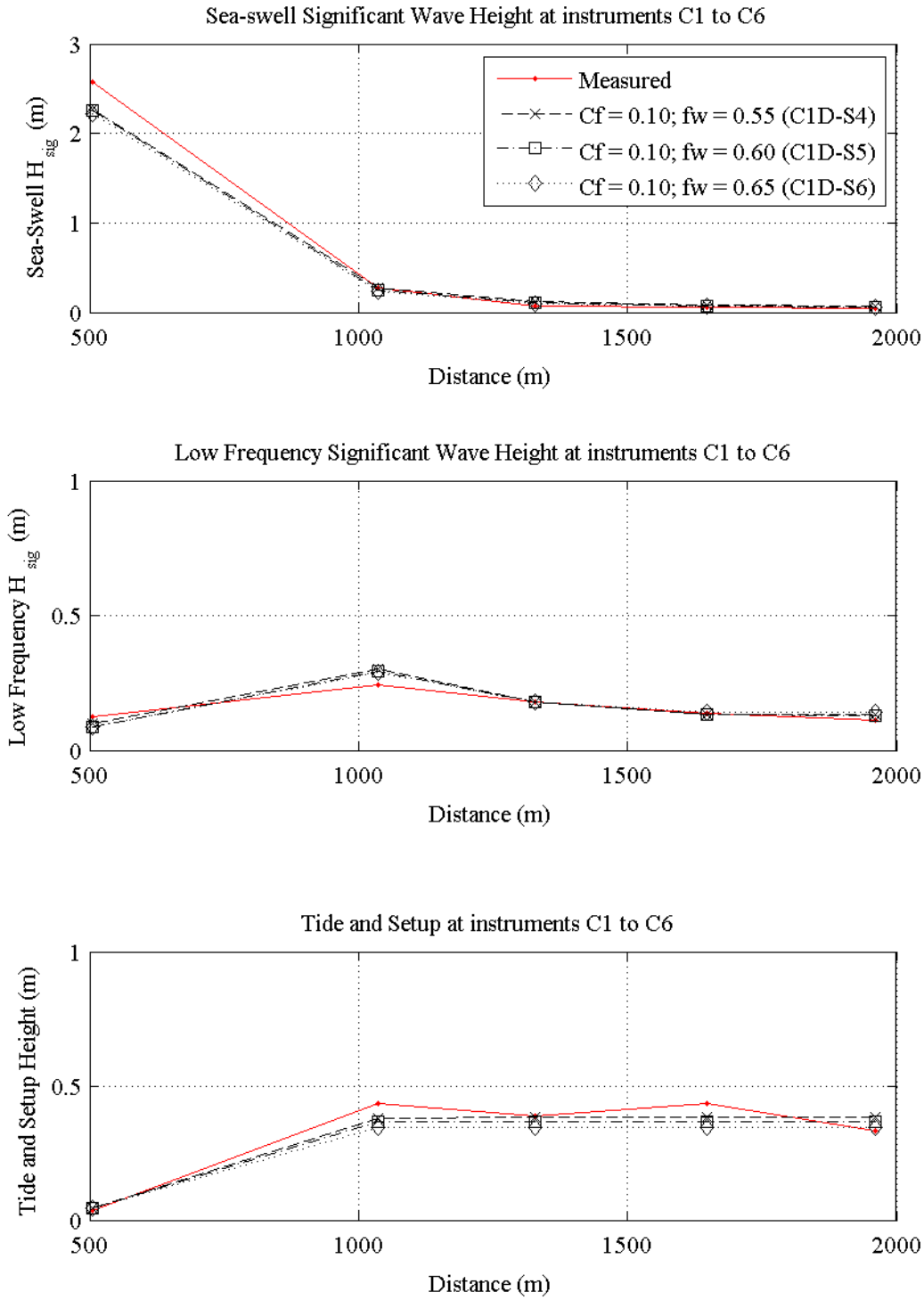
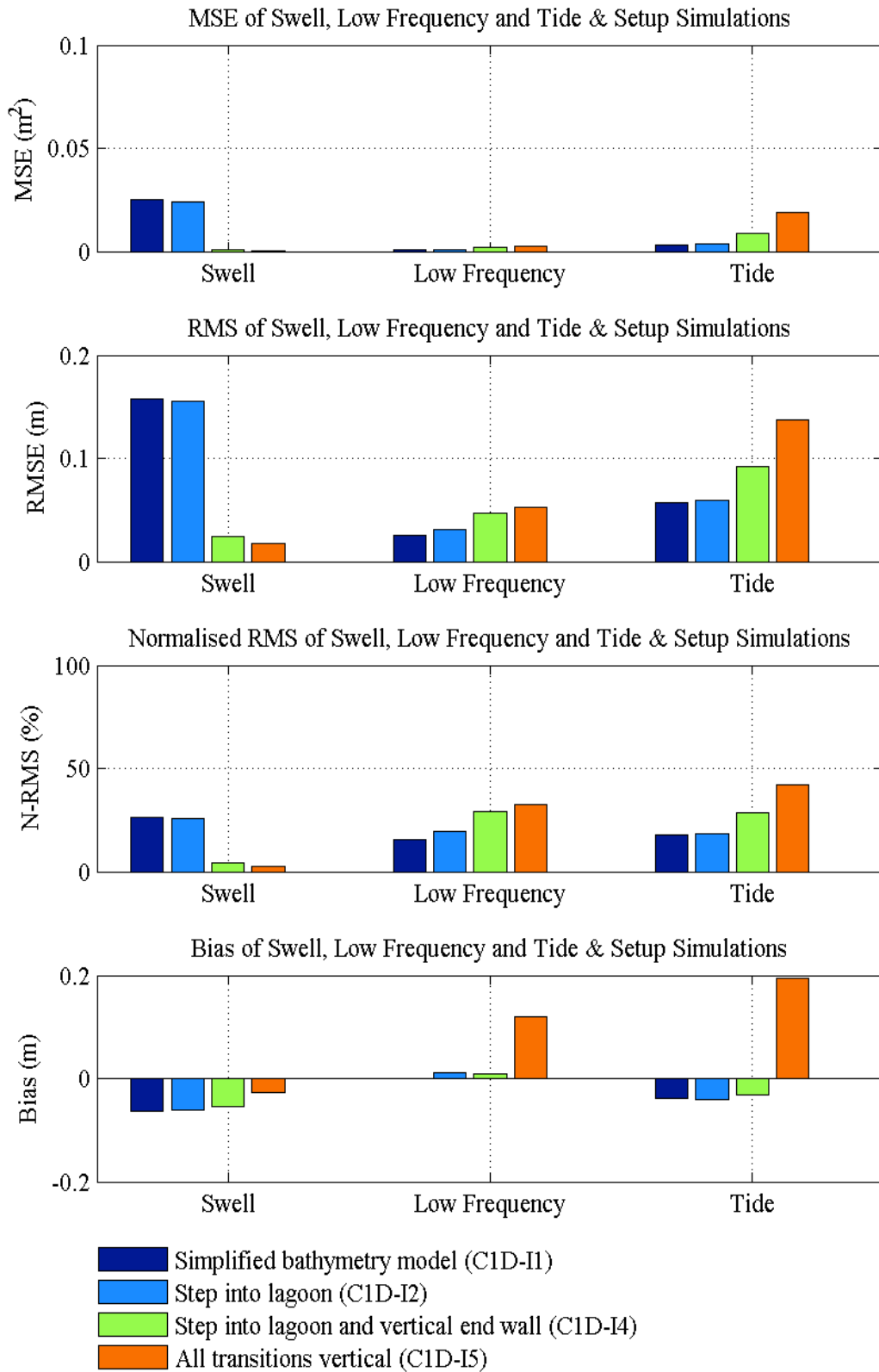**Figure 4-6: Spatial distribution of the 'best-fit' 1D model calibration results**

Figure 4-7: Statistical analysis results of 1D profile idealisations
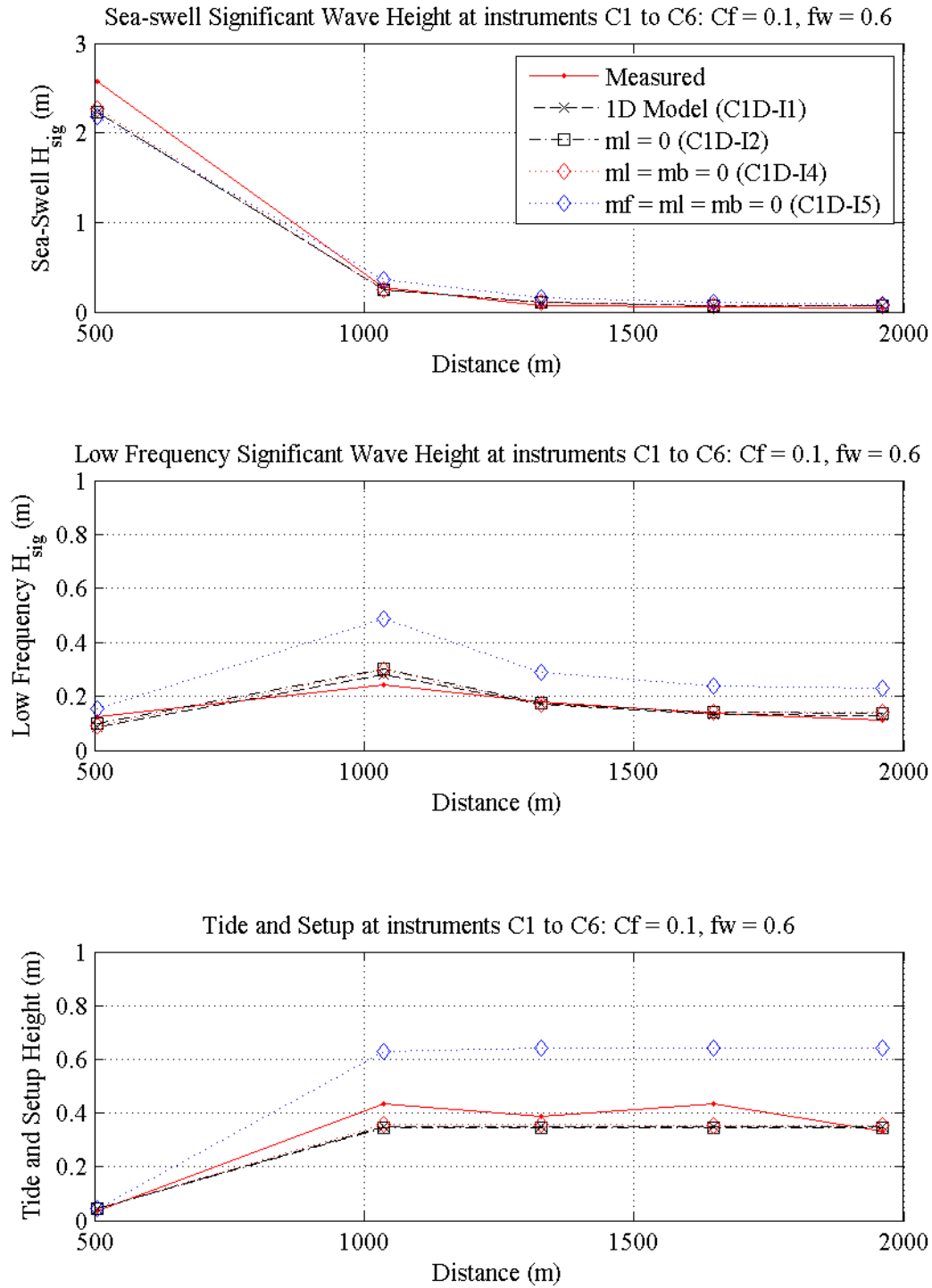
Figure 4-8: Spatial distribution of 1D profile idealisations

Chapter 5

ANALYSIS OF THE ANALYTICAL SOLUTION WITH XBEACH

5.1 Introduction

Indicators and measures were hypothesised to identify and quantify resonance on a reef in Section 2.5. To demonstrate the suitability of these measures along with the capability of XBeach to reproduce standing waves and resonance, two test cases were established: a simple reef model and a reef-lagoon model.

Section 5.2 describes the model development and simulations conducted. Section 5.3 presents the results of the simple reef analysis and discusses the observed processes, the suitability of the proposed indicators and provides a comparison of the XBeach results against the analytical expression. Section 5.4 considers the influence of a lagoon while the influence of friction and offshore wave height on the generation of resonance is considered in Section 5.5.

5.2 Simple reef and reef-lagoon XBeach models
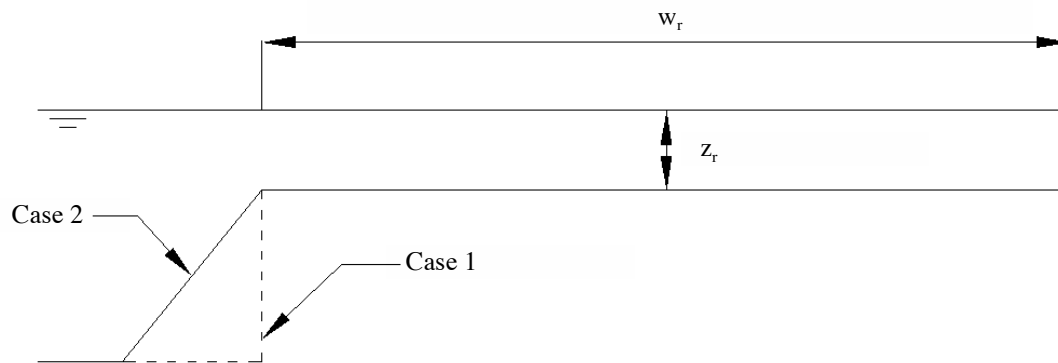
5.2.1 Model profiles

A simple one-dimensional reef model, with an idealised profile based upon the reef geometry at Guam was constructed and analysed with XBeach. The justification for the use of the Guam profile as the basis for the model structure was:

1. the structure of this reef is consistent with the idealised open basin model (Figure 2-4 and Equation 2-2); and

2. Péquignet et al. (2009) documented near resonant conditions at this site, which suggests that under ideal conditions, the generation of resonance may be possible with this reef geometry.

The model (Figure 5-1) was characterised by a transition from deep water to the reef crest and a horizontal reef flat, which extended from the crest to a vertical wall that represents the shoreline (and promoted maximum wave reflection). Two transition types from deep water were analysed: a vertical step and a slope with a gradient 1-in-20 (typical for reefs).

Figure 5-1: Simple Reef XBeach model profile

To investigate the influence of a lagoon on standing wave (resonance) hydrodynamics, the simple reef model was modified to form a reef-lagoon model with vertical steps at all transitions to avoid co-variation of parameters (Figure 5-2).
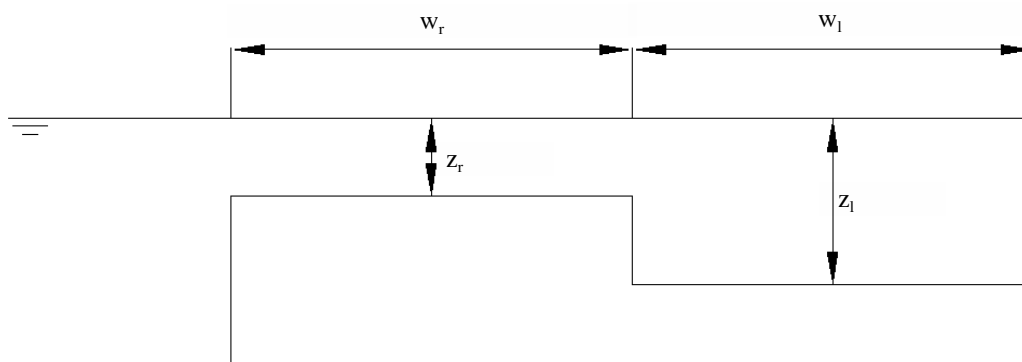
Figure 5-2: Reef-Lagoon XBeach model profile

5.2.2 Boundary conditions

The wave boundary was forced with a Pierson-Moskowitz (PM) spectrum (Table 5-1). The rationale for the use of this type of spectral input at the boundary was that by application of a broad frequency spectrum (considered noise), the natural resonance frequencies of the basin would be activated, become energised, and form peaks in the spectral output.

The flow boundaries were defined to be consistent with the definition of a one-dimensional 'flume type' analysis (Table 5-2).

Table 5-1: Wave boundary conditions

Parameter		Value	Selection Basis
Dir0	[°]	249.8693	Defined by the Ningaloo Reef model structure
Gamma	[-]	1	Generates a PM spectrum
Spreading	[-]	20	Recommended Value (Roelvink et al., 2010)
T	[s]	21600	Duration to provide spectral resolution for the analysis
Tstep	[s]	0.1	Recommended Value (Roelvink et al., 2010)
Hm0	[m]	1, 2, 5	Varied in accordance with simulation under consideration
fp	[Hz]	0.1	Typical swell period (10 seconds)

Table 5-2: Flow boundary conditions

Parameter	Value	Definition	Selection Basis
front	1	1D absorbing generating	
back	0	wall	Boundary conditions consistent with a 'flume type' model
left	0	wall	
right	0	wall	

5.2.3 Simulations conducted

Eleven simulations were conducted (Table 5-3) to investigate the processes that affect the development of a standing wave pattern and lead to the generation of resonance. The results from these simulations are the basis for the discussion in the sections that follow.

Table 5-3: Model simulations

ID	z_r [m]	w_r [m]	z_l [m]	w_l [m]	H_{m0} [m]	C_f [-]	f_w [-]	Fore Reef[#]	Selection Basis
SB-S1	0.5	400	-	-	1.0	0	0	V	Analysis base case
SB-S2	0.5	400	-	-	2.0	0	0	V	Influence of increased wave height
SB-S3	0.5	400	-	-	5.0	0	0	V	
SB-S4	0.5	400	-	-	1.0	0.01	0.6	V	Influence of friction
SB-S5	0.5	400	-	-	1.0	0.05	0.6	V	
SB-S6	0.5	400	-	-	2.0	0.01	0.6	V	Influence of increased wave height and friction
SB-S7	0.5	400	-	-	5.0	0.01	0.6	V	
SB-S8	0.5	400	-	-	1.0	0.1	0.6	V	Influence of friction at typical reef values
SB-S9	0.5	400	-	-	1.0	0	0	S	Influence of sloping fore-reef on waveform
SL-S10	0.5	400	-	-	1.0	0.1	0.6	S	Influence of friction on simple reef with a slope
SL-S11	0.5	200	1	200	2.0	0	0	V	Reef-Lagoon Case
Notes: # V = Vertical step transition at fore-reef (Case 1); S = Slope transition at fore-reef (Case 2) - indicates that this variable did not apply to this simulation									

5.3 Analysis of simple reef simulation results

5.3.1 Identification of natural resonant frequencies, nodal locations and waveform

Auto-spectral analysis of the sea surface elevation at two points (near the reef crest and near the shoreline) identified prominent peaks (Figure 5-3) at specific frequencies in the frictionless vertical transition model (SB-S1). The first three near crest and near shore auto-spectral peaks were located at the frequencies 0.0014 Hz, 0.0047 Hz and 0.0078 Hz. Near the crest, the density ranged from 0.59 m^2/Hz to 0.34 m^2/Hz while near the shoreline the range was from 3.8 m^2/Hz to 0.47 m^2/Hz. This demonstrates that the wave signal associated with these frequencies is more energetic near the shore than near the reef crest.
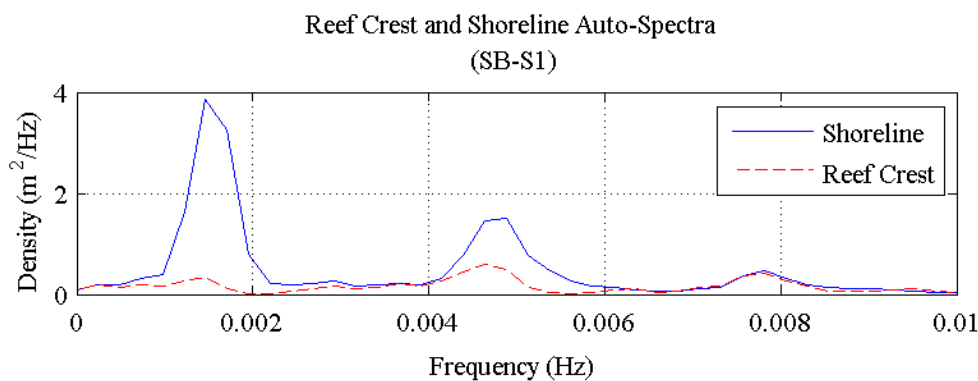
Figure 5-3: Auto-spectra of the surface elevation in the frictionless mode (SB-S1)
Hanning windows with an overlap of 50% were used to obtain 14 degrees of freedom and spectral resolution of 0.00065 Hz. The 95% confidence limits were 0.59 and 2.13.

The non-frictional slope transition model (SB-S9) produced less defined peaks (Figure 5-4) with energy distributed across a wider band of frequencies than the non-friction vertical transition model (SB-S1). The first three auto-spectral speaks at the shoreline were located at the frequencies 0.0015 Hz, 0.0046 Hz and 0.0076 Hz. The density range was from 2.60 m^2/Hz at the first peak to 0.34 m^2/Hz at the third peak. These results demonstrate that the introduction of a slope transition from deep water causes a decrease in the frequency associated with each of the peaks, a result that becomes more prominent at higher modes. This decrease in frequency is attributed to an effective extension of the basin length that results from the introduction of a slope and a subsequent shift in breakpoint offshore.
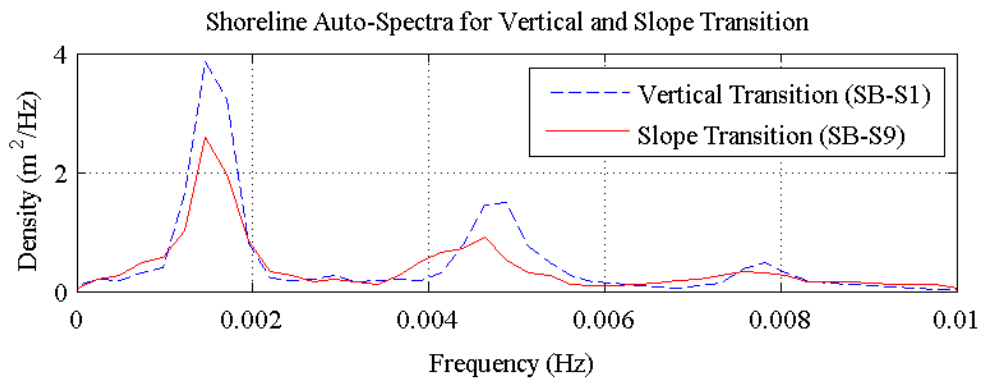
Figure 5-4: Influence of the fore-reef transition type
Hanning windows with an overlap of 50% were used to obtain 14 degrees of freedom and spectral resolution of 0.00065 Hz. The 95% confidence limits were 0.59 and 2.13.

The sea surface elevation signal components associated with each of the peak frequencies (for both transition cases) were extracted from the total sea surface elevation signal by the use of a band filter. Visualisation of these signal components produced waveforms consistent with the first three standing wave (resonance) modes (Figure 5-5). The waveforms have larger amplitudes at the shoreline than near the reef crest. The seaward node for both transition types is located (approximately) at the edge of the reef. The node location is more defined for the vertical transition than for the sloping transition, a result that is consistent with the breaking of waves over a slope in which the larger waves break further offshore than the smaller waves. This may also account for the wider frequency distribution observed. The location of this node is consistent with the assumed node location in the analytical mode.

On the basis of the clearly defined auto-spectral peaks, along with visualisations of the waveform associated with each of these peaks, it is proposed that these peaks represent standing waves. This result was affirmed by comparison with the analytical solution (Section 5.3.2).

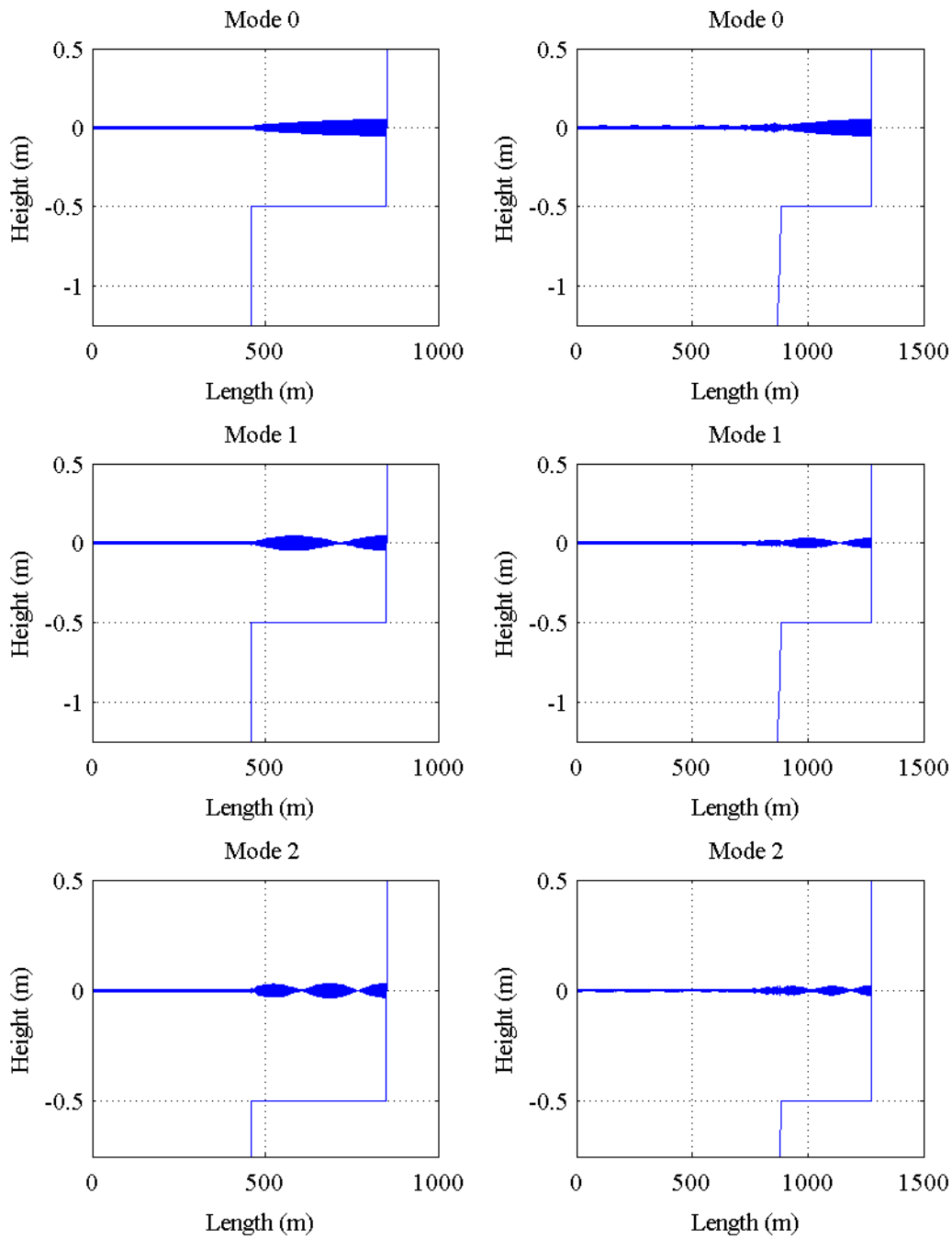**Figure 5-5: Band-passed waveforms of non-frictional simple reef with vertical and sloping fore-reef transitions**

5.3.2   Comparison with analytical solution

Estimation of the frequencies associated with the first three standing wave modes were calculated with the analytical solution (Equation 3-12) and compared with the frequencies identified from clearly defined peaks in the auto-spectral analysis (Section 5.3.1). In this

analysis, the length variable (L) was defined as the length from the reef crest to the shoreline and the water depth (h) as the sum of the still water depth and the wave induced setup generated by the XBeach model (Equation 5-1).

$$h_x = zs_x - \overline{zs} \qquad (5\text{-}1)$$

Two methods were used to evaluate the setup from the XBeach model data: a simplified approach and an integral approach. The simplified approach defined the setup as the mean of the near constant setup observed across the basin (Figure 5-6). The integral approach acknowledged that the seaward node was located near the reef edge and that the setup across the basin varies, particularly on the seaward edge of the reef. To account for this variation this approach integrates the analytical solution across the basin length (Equation 5-2). The results from each estimate along with the frequencies of the auto-spectral peaks are summarised in Table 5-4. An estimate that excluded the effect of setup was also determined for comparison.
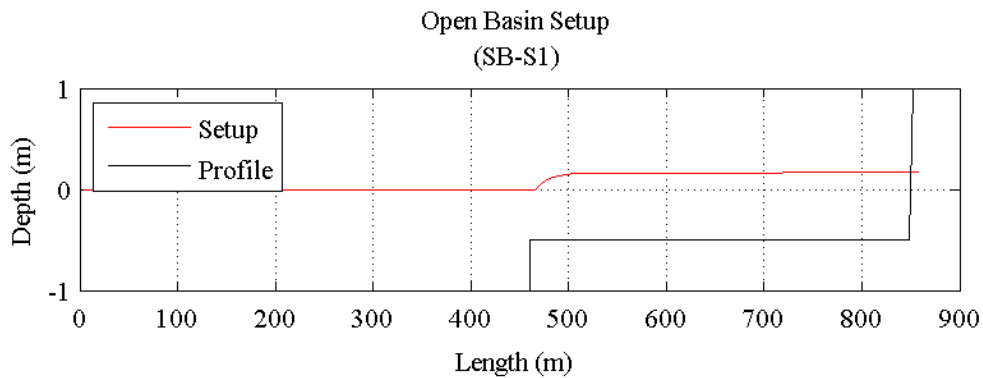
Figure 5-6: Setup calculated in the simple reef model

$$f_m = \frac{2m + 1}{4} \int_{crest}^{shoreline} \frac{\sqrt{gh_x}}{x} dx \qquad (5\text{-}2)$$

Table 5-4: Modelled and estimated standing wave frequencies

Mode	Frequency (Hz)			
	XBeach	No Setup Estimate	Simplified Estimate	Integral Estimate
0	0.0015	0.0014	0.0016	0.0016
1	0.0047	0.0042	0.0048	0.0049
2	0.0078	0.0069	0.0081	0.0082

The frequencies estimated by the analytical solution without the inclusion of setup were consistently lower than that results estimated from the defined peaks obtained from the XBeach auto-spectral analysis. Application of the simplified estimate (setup of 0.18 m) demonstrated stronger agreement with the model results with a slight overestimate determined when the integral estimate was used.

The analysis of the defined XBeach auto-spectral peaks, their associated waveforms and the analytical expression together demonstrate good agreement and indicate that the peaks represent standing waves.

5.3.3 Analysis of the suitability of the resonance indictors

In Section 2.5, three indicators were hypothesised to be suitable for the determination of resonance. The suitability of each of these indicators is evaluated in this section.

Indicator 1: A highly coherent variance in water surface elevation at a given frequency

The first indicator hypothesised that the variation in water surface elevation at the standing wave frequency must be highly coherent. The (squared) coherence was proposed as a suitable statistical function to identify and measure this coherence (Section 2.5.1).

The (squared) coherence between the near reef crest and the near shoreline exhibits (Figure 5-7) clearly defined bands of near unity. These bands represent frequencies at which the response between the two spatially lagged signals are correlated. The peak frequencies of the auto-spectral density consistently contained within but at the upper bound of the bands of high coherence.
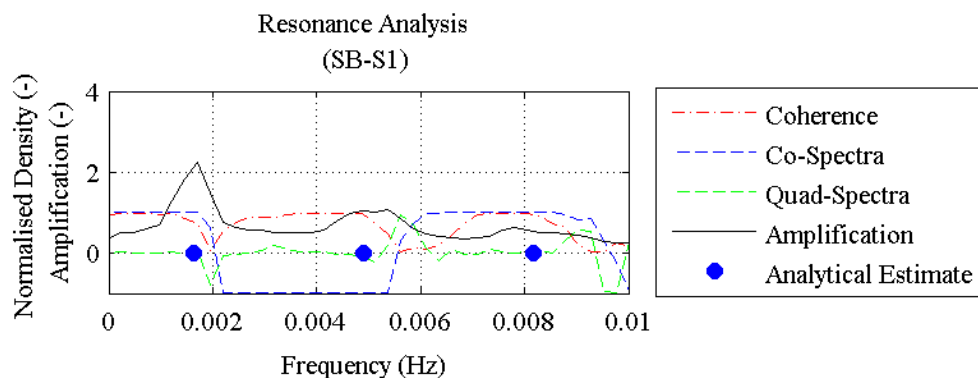
Figure 5-7: Simple reef model indicator analysis
Hanning windows with an overlap of 50% were used to obtain 14 degrees of freedom and spectral resolution of 0.00065 Hz. The 95% confidence limits were 0.59 and 2.13.

Indicator 2: Phase relationship must (closely) correspond to 0° or 180° phase difference

The second indicator hypothesised that a phase relationship that corresponds to a phase difference of (near) 0° and 180° must exist between the frequency of a wave signal obtained near the reef crest and near the shoreline. The co-spectrum and quad-spectrum were suggested to quantify this relationship from two spatially lagged signals (Section 2.5.2).

Consistent with the coherence, the co- and quad-spectrum in this analysis spanned a band of frequencies with the peak auto-spectral frequency contained within this band (Figure 5-7). The

co-spectrum is found to be near unity at the zero-mode, near negative unity at the first-mode and near unity at the second-mode. The quad-spectrum is shown to be near zero at each peak frequency and gains normalised density at the co-spectral transition from positive to negative unity (or vice versa) consistent with a phase transition process. The two spectrum combined (Section 2.5.2) were consistent with an alteration in phase difference of 0° and 180°.

Indicator 3: The low-frequency wave at a resonant frequency must be amplified

Indicators 1 and 2 demonstrated that in this model the auto-spectral peaks in surface elevation varied coherently across the basin and possessed a phase relationship that was consistent with the presence of standing waves (this waveform was also demonstrated in Figure 5-5). Indicator 3 determined if the standing waves were amplified and therefore in a state of resonance.

A frequency-by-frequency evaluation of the auto-spectra near the crest of the reef and near the shoreline (Equation 5-3) produced an amplification curve (transfer function) between the zero moment wave heights at the two locations (Figure 5-7). This curve was consistent in form to amplification curves observed in other forms of dynamic analysis (eg. mechanics) however unlike the theoretical amplification curves often cited, a feature of this specific non-frictional curve is that the peaks did not increase to infinity. The reason for this is that unlike a 'pure' resonance case, energy was lost from this system by the propagation of the reflected free waves out of the model domain at the seaward boundary. The result of this loss was that an upper amplification limit was imposed.

The largest amplification occurred at the zero standing-wave mode (the zero-mode of resonance). The first mode of resonance also demonstrated positive amplification while the second mode of resonance was subjected to dampened amplification. This damped amplification results in the loss of the distinct presence of the standing wave amongst the progressive waves.

Suitability of indicators

This analysis demonstrated that the indicators hypothesised in Section 2.5 are suitable for the identification and measurement of resonance, the frequencies of which were found in this model to agree well with the estimated frequencies from the analytical expression. This analysis also demonstrated that all indicators are required to be satisfied in order to demonstrate resonance (Figure 5-7). The coherence determined if the signal at a specific frequency was related between two spatially lagged locations while the phase relationship for a particular frequency described if the waveform was standing or progressive. These two indicators together demonstrated the

presence of a standing wave however these two indicators alone do not clearly define resonance. Therefore only when the amplification curve was considered was it known for which frequencies a state of resonance occurs.

5.4 Analysis of reef-lagoon simulation results

The Simple Reef model was extended to include a lagoon and a comparison was undertaken between the two models to investigate the influence of the lagoon on the generation of standing waves and resonance. The model profile and boundary conditions are described in Section 5.2.1.

5.4.1 Standing wave frequencies, nodal locations and waveform

The zero mode auto-spectral peak for the reef-lagoon model (Figure 5-8) considered in this analysis was located at (approximately) the same frequency (0.0017 Hz) as the equivalent peak in the simple reef model (0.0015 Hz). However, for higher modes the reef-lagoon peaks were located at higher frequencies (0.0056 Hz and 0.0093 Hz) compared to the equivalent peaks in the simple reef model (0.0048 Hz and 0.0078 Hz).
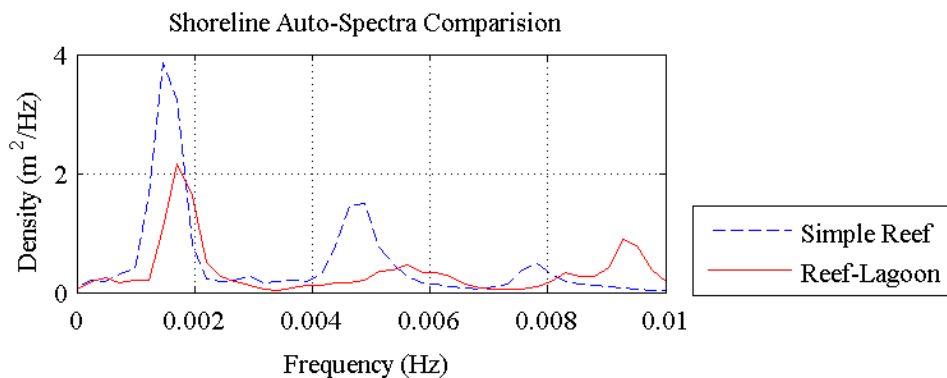
Figure 5-8: Comparison of Auto-spectral peaks and analytical solutions for simple reef and reef-lagoon models

In this model the total length variable was consistent ($L = 400\,m$) with the simple reef model, which indicated that the variation in frequency is directly related to water depth. The difference in setup generated in the lagoon-reef model was negligible when compared to the simple reef model (Figure 5-9), which further refined the variation in peak frequency to the introduction of a lagoon into the model. This result was consistent with the structure of the analytical solution (which is a function of wave celerity and the basin length). Integration of this expression over the basin length indicates that as the wave enters the deeper water of the lagoon, the wave 'speeds up'. This results in a reduction in travel time from the reef crest to the shoreline and back – a higher frequency of standing-wave form.

70
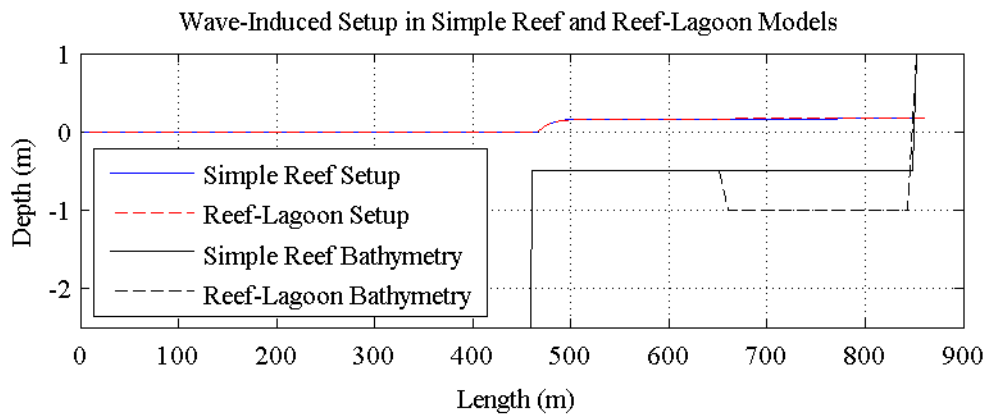
Figure 5-9: Setup generated in simple reef and reef-lagoon XBeach models

The waveform associated with the peaks of the reef-lagoon spectra (extracted by a band filter) were consistent with the waveforms demonstrated by the simple reef model. The auto-spectral peaks represented waveforms consistent with the first three standing wave modes with the seaward node located near the reef crest (Figure 5-12).

5.4.2   Comparison of indicator results

The amplification of the signals on the simple reef and the reef-lagoon model differ. Both models produce a similar zero mode amplification however the first mode was amplified more for the simple reef model while the second mode was amplified more for the reef-lagoon model (Figure 5-11). The zero mode frequency was approximately equal for both models while the first and second mode frequency of the peaks were greater for the reef-lagoon model than for the equivalent simple reef model. The coherence, co- and quad-spectral analyses are presented (Figure 5-12) for the simple reef model and the reef-lagoon model. In this analysis, the amplification peaks for both models were located on the upper boundary of the band of frequencies that consisted of near positive (negative) unity in the co-spectra, near zero in the quad-spectra and high coherence.
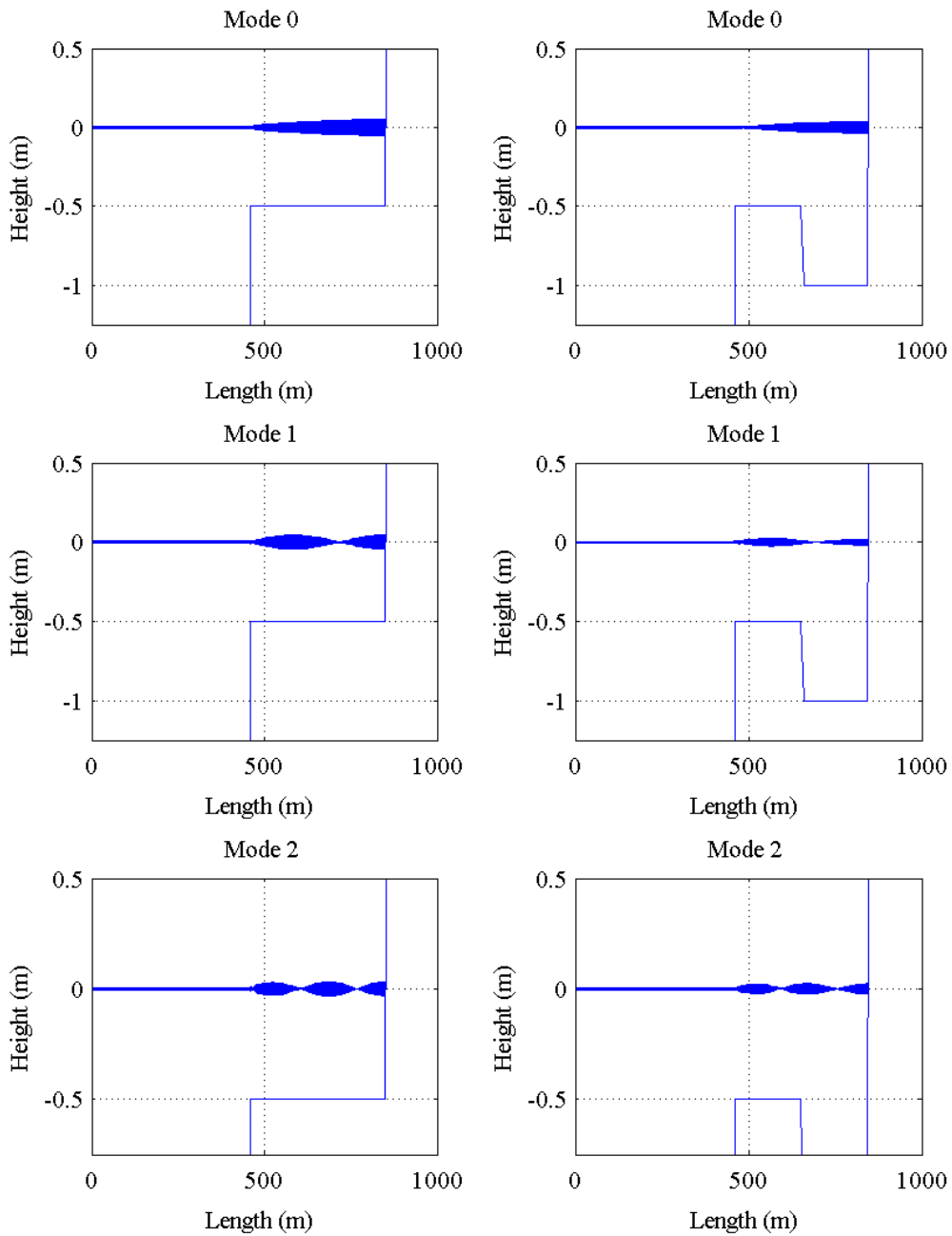
Figure 5-10: Nodal patterns for a simple reef (left) and reef-lagoon model (right)
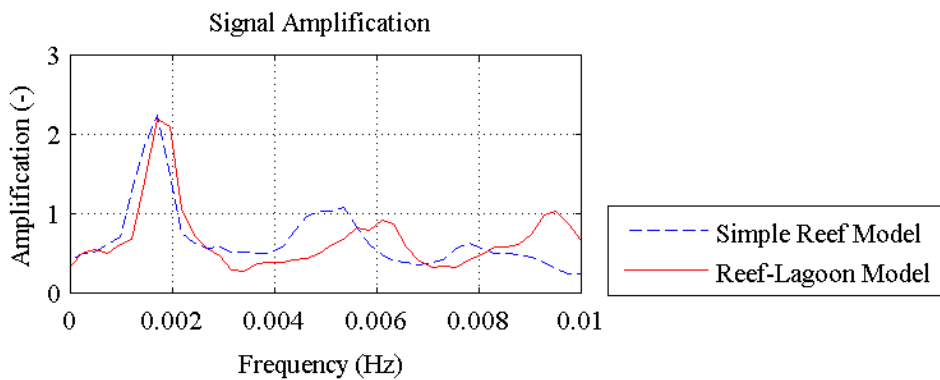
Figure 5-11: Comparison of simple reef and reef-lagoon amplification
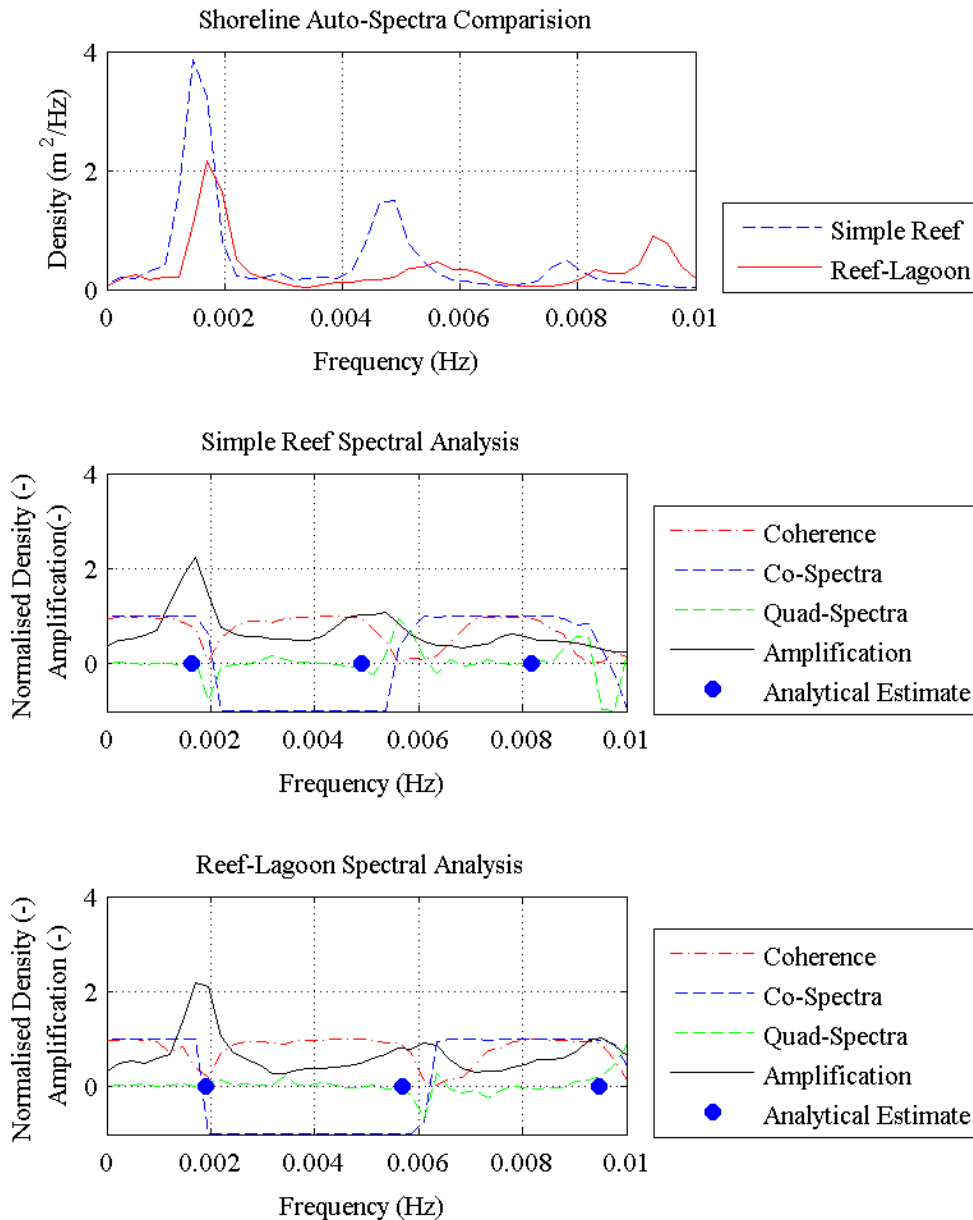
Figure 5-12: Comparison of spectral and resonance analysis results for the simple reef and reef-lagoon models (Top) Comparison of amplification (middle) Results of simple reef spectral and resonance analysis (bottom) Results of reef-lagoon spectral and resonance analysis.

5.5 Influence of friction and offshore wave height

5.5.1 Influence of friction on resonance

The introduction of friction into the simple reef model resulted in changes to the resonance response (Figure 5-13). A (approximately) linear increase in setup was observed at the shoreline that resulted in a shift in the peak natural resonance frequency from a lower frequency to a higher frequency. In addition to this frequency shift, the magnitude of the amplification at each peak frequency was reduced. At high frictional values ($C_f = 0.05 - 0.1$) the amplification peaks are 'flattened out' and become approximately equal in density to the progressive

frequencies. This observation suggests that as the friction increases the ability of this waveform to be amplified is reduced due to dissipation of energy.
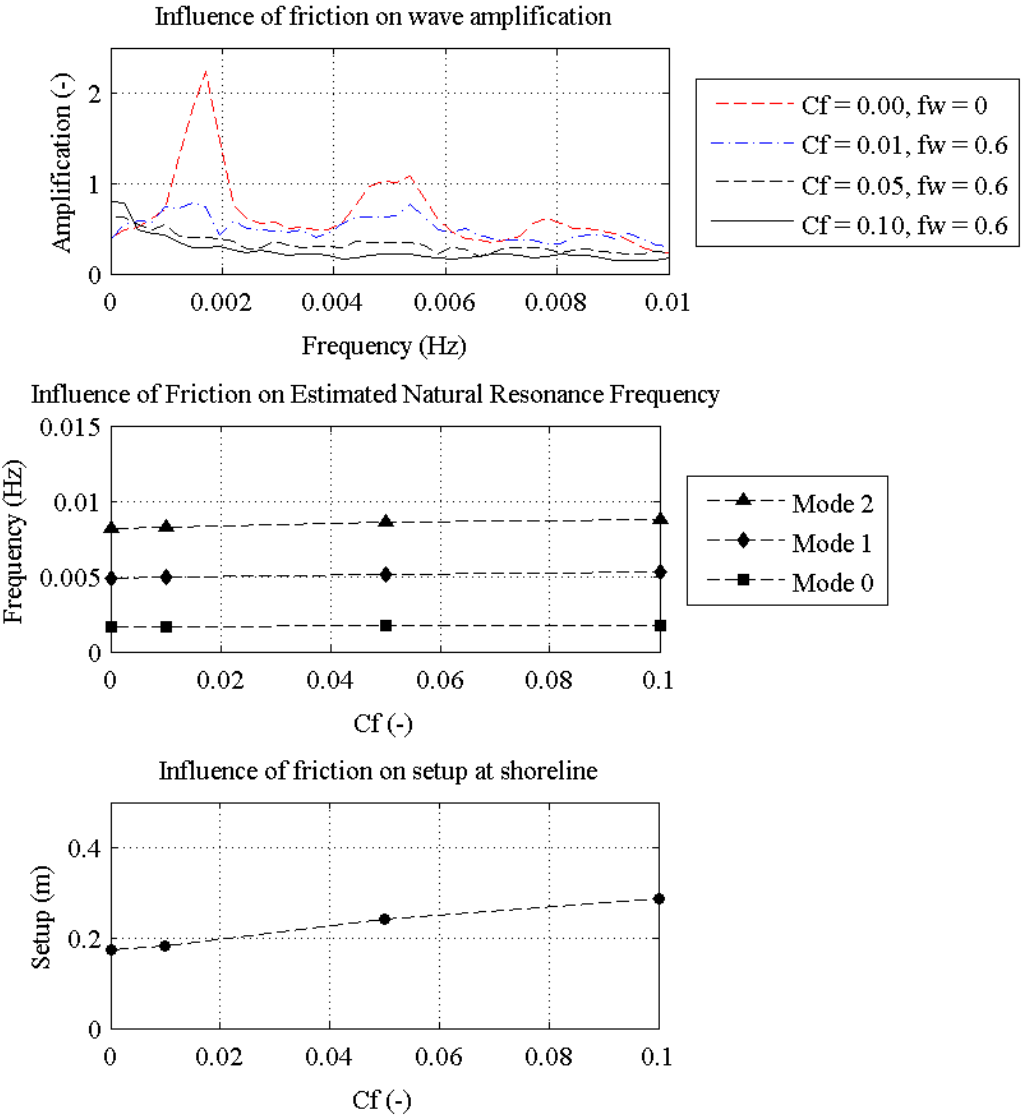
Figure 5-13: Influence of friction on simple reef model

5.5.2   Influence of offshore wave height

The influence of the offshore wave height on the resonance response was analysed by the simulation of three offshore wave heights (1 m, 2 m and 5 m) in the simple reef model. The results from these simulations are presented in Figure 5-14.

An increase in the offshore wave height was shown to increase the setup approximately linearly from 0.18 m to 0.5 m. As expected, the frequencies associated with the first three standing wave modes shift to higher frequencies. Despite these shifts, the form of the amplification curve was

not significantly altered with the exception of the peak of the amplification, which was found to increase with the offshore wave height.

Introduction of friction into the model along with the variation in offshore wave height resulted in a further increase in the setup and consequently the frequency of the first three modes of standing waves (Figure 5-15). Furthermore, the peak of the amplification curve is reduced significantly with the resonance case only occurring for the 5 m offshore wave height case.
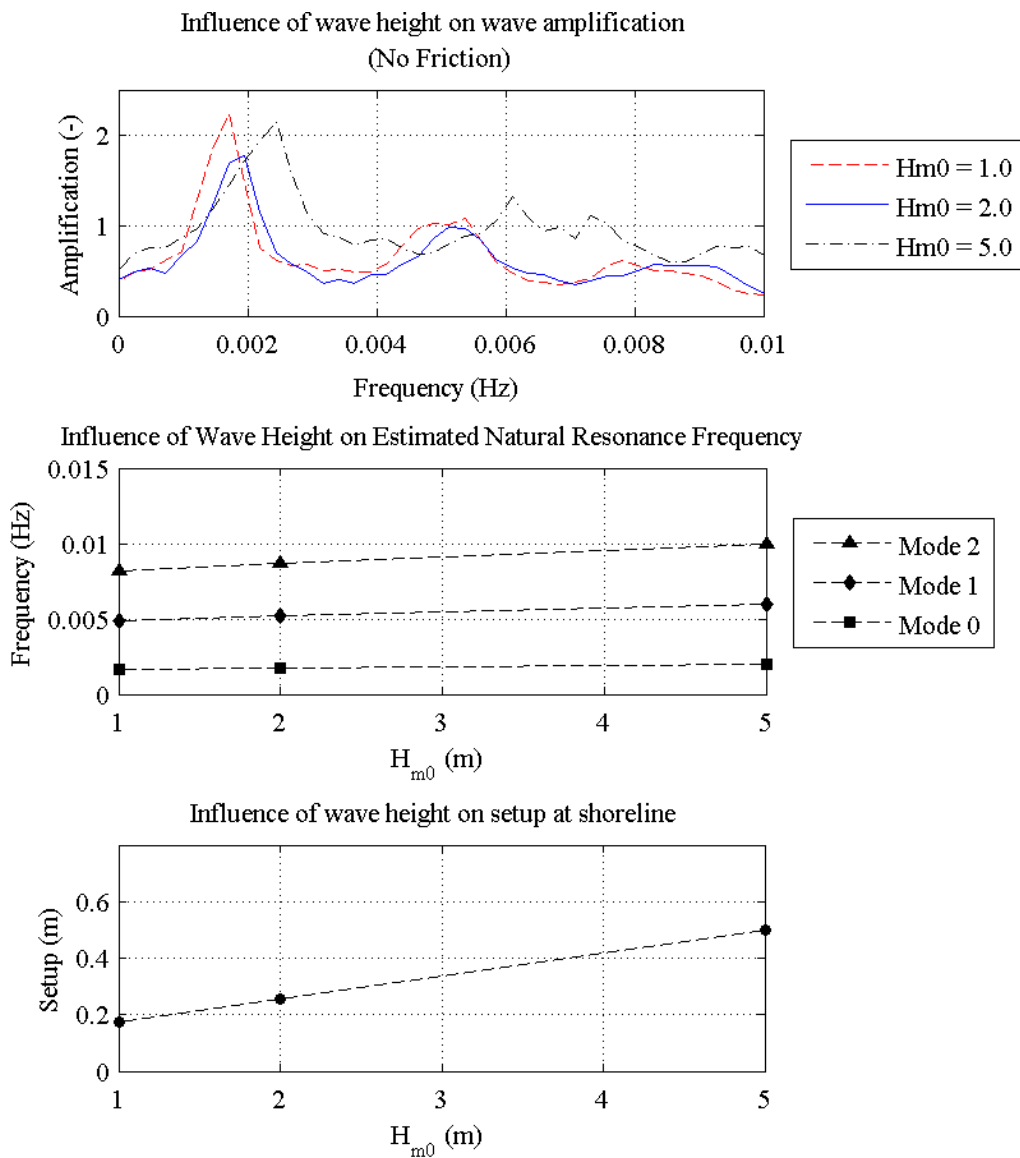
Figure 5-14: Influence of offshore wave height on simple reef model
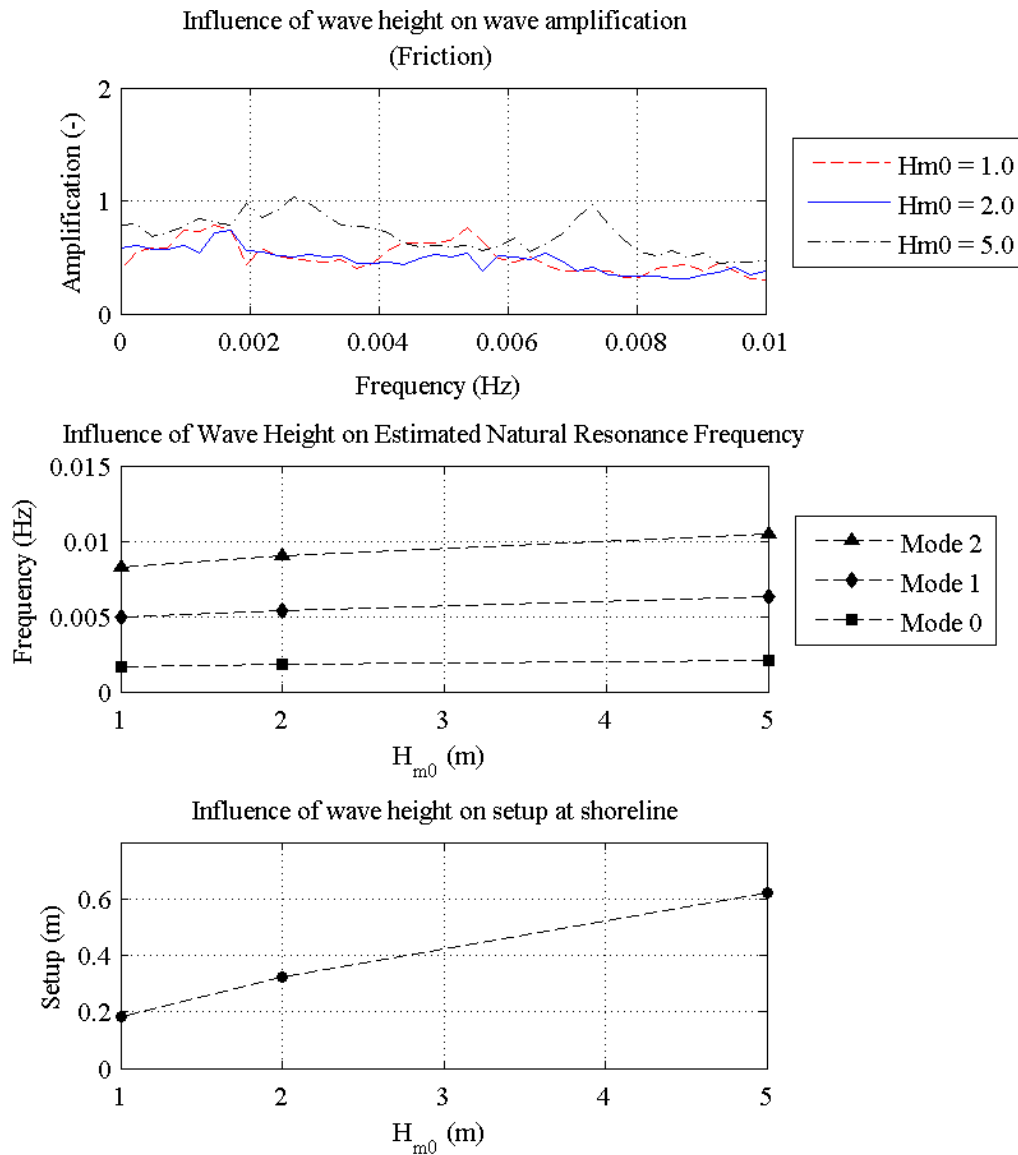
Figure 5-15: Influence of friction and offshore wave height on simple reef model.

5.6 Conclusions

The study of a simple reef and reef-lagoon model demonstrates that in order to define the presence of resonance, three distinct aspects need to be assessed: coherence, frequency and amplitude. While analysis of the signals at either end of the reef using coherence, co-spectral and quad-spectral analysis are good indicators of a standing wave form and the general band of frequencies for which it occurs, the specific basin peak frequency was found to best be identified from the direct comparison of the auto spectra either individually or in the form of an amplitude (transfer) function. This demonstrates that although the analysis of coherence and phase identify a band of standing wave frequencies, only for a narrow band of frequencies are the waves 'tuned' and in a resonant state.

Furthermore, the simple reef and reef-lagoon model demonstrate that the presence of a vertical step in the simple model resulted in a distinct node point near the reef edge while for a slope transition the node was less defined. The presence of a lagoon increased the resonance frequency, and resulted in higher amplifications. Friction dampened the resonant frequencies with the energy density near the energy of the progressive waves for friction associated with reefs. An increase in offshore wave height resulted in an increase in the amplification as well as an increase in the frequency of resonance.

Chapter 6

SENSITIVITY OF RESONANCE TO GEOMETRIC PARAMETERS

6.1 Introduction

A sensitivity analysis of the fundamental geometric parameters that form a reef was conducted with XBeach with a series of 1D models. The models were assembled from four parameters: the reef width (w_r), reef depth (h_r), lagoon width (w_l) and the lagoon depth (h_l). A binary friction case was also considered (friction on and friction off). The purpose of this analysis was to investigate the influence of different geometric parameters on the generation of a standing wave and the promotion of resonance. The scope of the sensitivity analysis was defined by a review of typical reef geometries cited in literature and summarised in Section 6.2. The methodology used to undertake this analysis is then described in Section 6.3. The results and an analysis are presented for the non-frictional model in Section 6.4 and for the frictional model in Section 6.5.

6.2 Typical reef geometric parameters

A review was undertaken to identify typical values of fringing reef geometric parameters cited in literature. The results of this review are summarised in Table 6-1. The review indicates that the width of a reef can vary significantly (80 m – 1500 m) however the depth of a reef is, on average, approximately 2 m. For a fringing reef, the lagoon may or may not be present and was found to vary considerably in width (150 m – 2000 m) and depth (2 m – 12 m). For the present study, the range of values simulated in the XBeach sensitivity model are summarised in Table 6-2 and has been defined to capture the variety of reef geometries cited. In addition to these parameters, two conditions were tested: friction on (C_f = 0.1 and f_w = 0.6) and friction off ($C_f = f_w = 0$).

Table 6-1: Geometric dimensions of fringing reef cited in literature

Site	w_r	z_r	w_l	z_l	Cited
Heron Island (Australia)	700	2			(Gourlay and Colleter, 2005)
Kaneohe Bay (Hawaii)*	1500	2	2000	12	(Lowe et al., 2005) (Lowe et al., 2009a) (Hearn, 1999)
Ningaloo Reef (Australia)	500	1	855	2	(Hearn, 1999) (Taebi et al., 2011)
Haymond Island (Australia)	800	2 - 4	-	-	(Gourlay, 1994) (Massel and Gourlay, 2000)
Guam	Crest	2	150	5	(Seelig, 1983)
Ala Moana Reef (Hawaii)	230	1.5 – 4			(Gerritsen, 1980)
Ipan (Guam, Hawaii)	450	0.5	-	-	(Péquignet et al., 2011; Péquignet et al., 2009)
Tague Reef	80	1.2	520	5	(Lugo-Fernández et al., 1998)

Other reefs were cited in literature but were not applicable to this study due to their form (for example barrier reef, atolls) or sufficient information could not be obtained include:
- John Brewer Reef, Australia (Hardy and Young, 1996)
- Majuro Atoll (Kraines et al., 1999)
- Yonge Reef, Australia (Young, 1989)
- Okinawa Islands, Japan (Nakaza and Hino, 1991)

* It may be argued that Kaneohe Bay possesses the characteristics of a barrier reef.

Table 6-2: Geometric parameter sensitivity range

Reef Width (w_r)	Reef Depth (z_r)	Lagoon Width (w_l)	Lagoon Depth (z_l)
100	-0.50	150	-1.00
200	-0.75	300	-2.00
300	-1.00	450	-3.00
400	-1.25	600	-4.00
500	-1.50	750	-5.00
600	-1.75	850	-10.0
700	-2.00		
800			

6.3   Sensitivity analysis methodology

The reference case for the sensitivity analysis was the calibrated reef model with an idealised profile (Figure 6-1). Each dimension of this reference case was sequentially varied (Table 6-2) and a simulation of the reef hydrodynamics conducted for a 12 hour period. This produced a stationary time series of data suitable in duration to obtain the frequency resolution required for analysis of the low-frequency waves. Consistent with the proposed resonance indicators, the amplification, coherence, co-spectrum and quad-spectrum were evaluated for each simulation. The spectral components of the analysis were assessed by use of the Welch's averaged modified periodogram method. Hanning windows with a 50% overlap were used to produce spectra of 14 equivalent degrees of freedom, spectra resolution of 0.00033 Hz. The 95% confidence limits were 0.59 and 2.13. The result of this analysis was an indication of the frequencies associated with a standing wave form for each simulation. An analysis of the amplitude (Equation 5-3) was then undertaken for each simulation to identify the frequencies for which resonance occurred.

The analytical expression was evaluated for each simulation case by use of the integral approach (Equation 5-2). Upper and lower limits for the estimate were defined by evaluation of the expression for the standard deviation of the setup determined from the XBeach model results. The calculated frequencies were then compared with the model results.
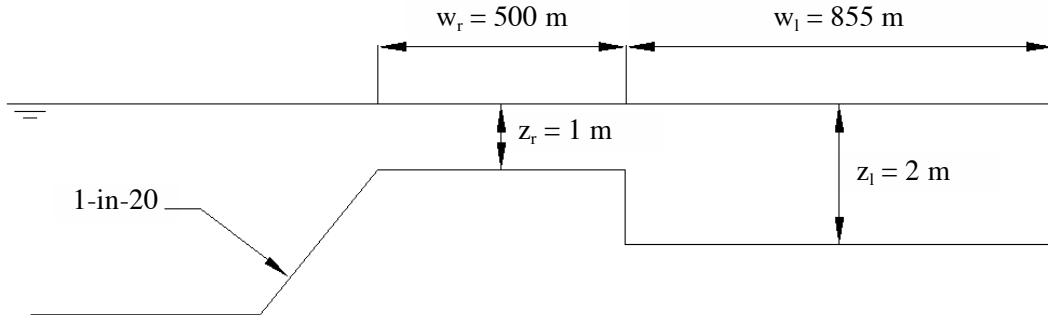
Figure 6-1: Idealised reef reference case

6.4 Results and analysis of frictionless model simulations

6.4.1 Analysis of indicator results

The amplification analysis (Figure 6-2) indicated that the strongest amplification occurs for the zero mode of resonance. For some simulations, the first mode of resonance was also strongly defined. Higher modes did not possess a strong amplification and were typically dominated by a damped amplification. To confirm the amplification is associated with resonant standing waves, a coherence and phase analysis were conducted.

Distinct bands of high coherence were identified throughout the analysis (Figure 6-3) with an increase in the coherence observed for deeper reef and lagoon water depths. It is unclear why the coherence increased however it is hypothesised that this may be due to less noise in the signal that results from less bed dissipation. These bands were well defined for the first three modes, however for higher modes the coherence decreased.

The co-spectral analysis (Figure 6-4) demonstrated distinct alternation between positive unity and negative unity with the transition between these two limits defined by a narrow band of intermediate values. The zero and first mode were clearly defined while higher modes had less defined boundaries.

The quad-spectral analysis (Figure 6-5) possessed less defined bands, however near zero normalised densities are prevalent at frequencies that correspond to near positive and negative unity in the co-spectra. Consideration of these results together indicates that a standing wave form may be expected within these phase regions. The conclusion drawn from the four analyses

is that the bands of strong amplification are resonant standing waves. These results were compared to the frequencies estimated by the analytical expression.

### 6.4.2   Analytical solution comparison

The analytical expression, inclusive of the upper and lower standard deviations, fits the data well. The upper and lower estimates were determined from the wave-induced setup in which the standard deviation of the setup was determined. The water depth used in the analytical solution was then taken as the sum of the water depth and setup plus/minus the standard deviation. The estimated frequencies agreed with the zero and first resonant amplification results associated with the sensitivity analysis on the reef. A strong agreement was also observed for the zero-mode in the lagoon sensitivity analysis but the analytical solution under-estimated the frequency for higher modes of resonance.

The coherence analysis was highly agreeable with the estimated resonant frequencies for all simulation cases. The estimated frequency was observed to be typically located at the upper boundary of the band of coherence, a result consistent with observations from the simple reef case (Section 5.3). Similar agreement was also observed for the coincident spectrum. The quadrature spectrum illustrated near zero results for the first and second mode but a higher density for the zero-mode. A slight over-estimation of the resonant frequency was observed at this mode however the reason for this over-estimation is unknown.

6.4.3   Influence of geometric parameters

The analysis demonstrates that the width of the reef and the lagoon have a greater influence on the resonant frequency than the water depth. This result is consistent with the analytical expression in which the influence of depth is $h^{\frac{-1}{2}}$ while the influence of length is L. Furthermore, the effect of the scale of these parameters is important. In this analysis, the sensitivity range was fitted to geometric observations cited in literature. It was observed that the length parameter can vary significantly (in the order of hundreds of meters) while the depth parameter on the reef varies very little (in the order of centimetres) and similarly, the lagoon (in the order of meters). The result of this analysis is that the evaluation of the reef frequencies is more sensitive to the length parameters than the depth parameters. A full four-variable analysis was not conducted due to computational and time constraints and forms a recommendation to fully understand the influences of the combined effects of these parameters on the resonant frequency.
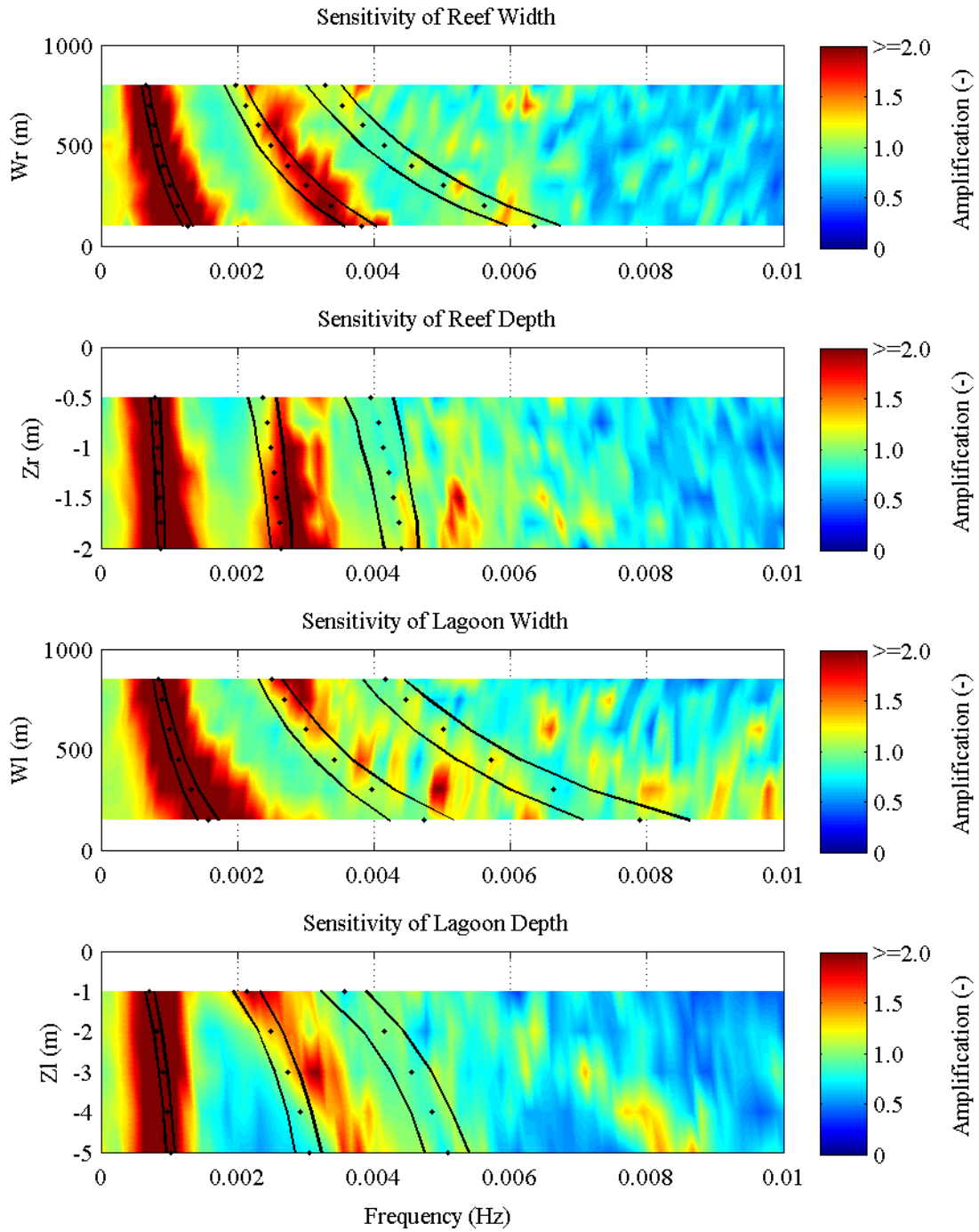
Figure 6-2: Amplification analysis of non-frictional sensitivity analysis
Hanning windows with an overlap of 50% were used to obtain 14 equivalent degrees of freedom, spectral resolution of 0.00033 Hz and 95% confidence limits of 0.59 and 2.13. The analytical estimate is indicated along with the upper and lower standard deviations.

83

REEF GEOMETRY SENSITIVITY ANALYSIS: (SQUARED) COHERENCE
Vertical Lagoon and Beach Slopes with Cf = 0 and fw = 0
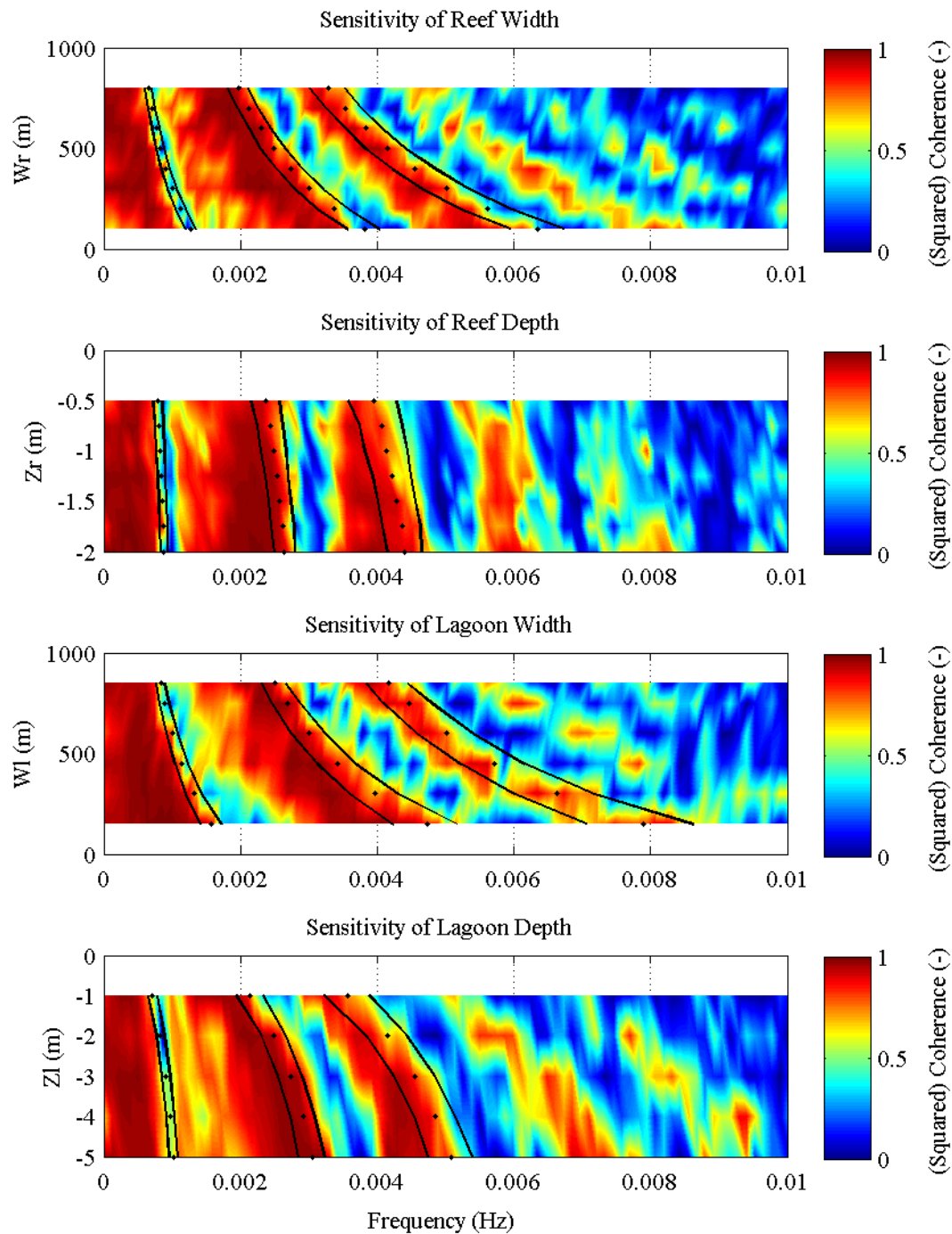
Figure 6-3: Coherence of non-frictional sensitivity analysis
Hanning windows with an overlap of 50% were used to obtain 14 equivalent degrees of freedom, spectral resolution of 0.00033 Hz and 95% confidence limits of 0.59 and 2.13. The analytical estimate is indicated along with the upper and lower standard deviations.

REEF GEOMETRY SENSITIVITY ANALYSIS: COINCIDENT SPECTRA
Vertical Lagoon and Beach Slopes with Cf = 0 and fw = 0
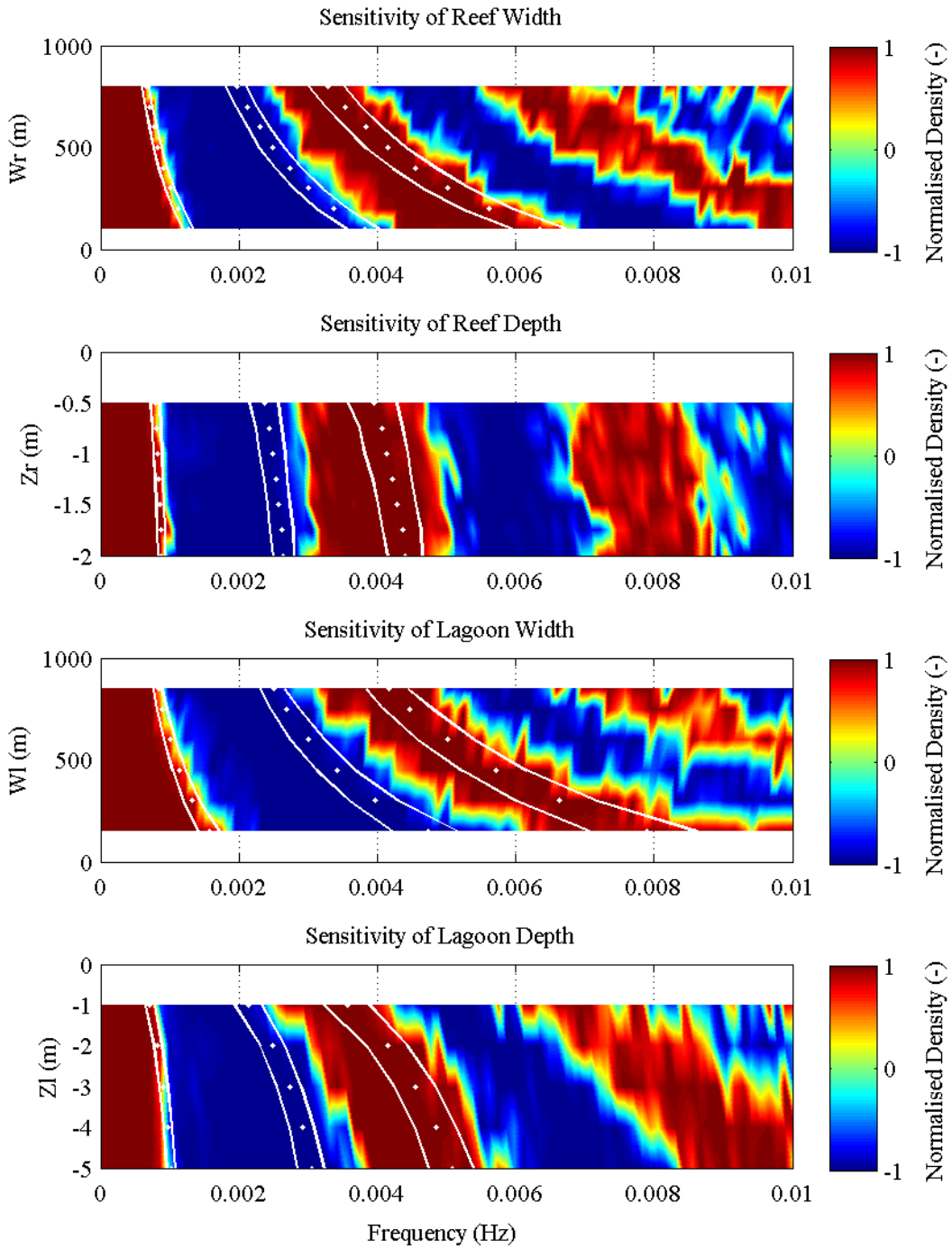
Figure 6-4: Co-spectral analysis of non-frictional sensitivity analysis
Hanning windows with an overlap of 50% were used to obtain 14 equivalent degrees of freedom, spectral resolution of 0.00033 Hz and 95% confidence limits of 0.59 and 2.13. The analytical estimate is indicated along with the upper and lower standard deviations.

REEF GEOMETRY SENSITIVITY ANALYSIS: QUADRATURE SPECTRA
Vertical Lagoon and Beach Slopes with Cf = 0 and fw = 0

Figure 6-5: Quad-spectral analysis of non-frictional sensitivity analysis

Hanning windows with an overlap of 50% were used to obtain 14 equivalent degrees of freedom, spectral resolution of 0.00033 Hz and 95% confidence limits of 0.59 and 2.13. The analytical estimate is indicated along with the upper and lower standard deviations.

6.5   Results of model simulations including friction

Analysis of the same geometric sensitivity with the influence of friction included in the model produced a significantly different result. The frictional parameters used in the analysis were adopted from the calibration of the model against the Ningaloo Reef data ($C_f = 0.1$ and $f_w = 0.6$).

Inspection of the amplification indicates that for all simulation cases, the signal amplification was negative. This indicates that the introduction of friction into the system results in a large dissipation of energy across the reef and lagoon and prevents the generation of resonance. The failure of this indicator enables the direct conclusion to be made that resonance is not generated at a coral reef when the friction, forcing and geometric properties are consistent with the simulation cases tested.

For completeness, analysis of the coherence, coincident and quadrature spectra were conducted. The coherence was found to be high across all frequencies examined. This result suggests that significant dissipation occurs across the reef and lagoon and very small wave amplitudes remain at the shoreline that result in the determination of high coherence. The high coherence was confined to the low frequencies. The higher frequencies were not found to be coherent.

Distinct bands in the coincident and quadrature spectra were found to occur however these spectra did not possess the necessary characteristics to demonstrate a standing wave form at the frequencies considered, they were progressive waves. The waveforms generated by these spectra were not investigated and will form a recommendation from this study.

Figure 6-6: Amplification of frictional sensitivity analysis
Hanning windows with an overlap of 50% were used to obtain 14 equivalent degrees of freedom, spectral resolution of 0.00033 Hz and 95% confidence limits of 0.59 and 2.13. The analytical estimate is indicated along with the upper and lower standard deviations.
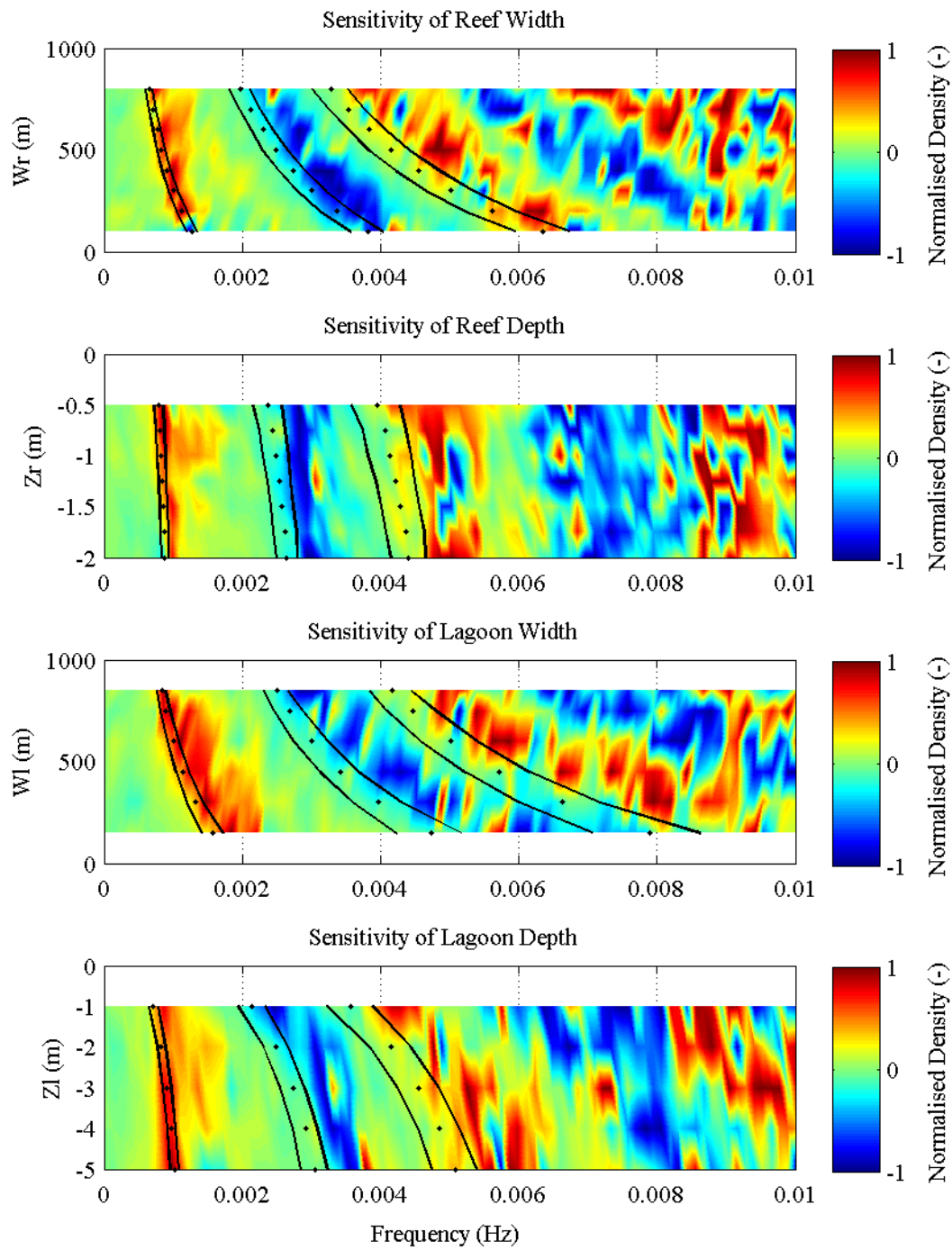
Figure 6-7: Coherence of frictional sensitivity analysis
Hanning windows with an overlap of 50% were used to obtain 14 equivalent degrees of freedom, spectral resolution of 0.00033 Hz and 95% confidence limits of 0.59 and 2.13. The analytical estimate is indicated along with the upper and lower standard deviations.

REEF GEOMETRY SENSITIVITY ANALYSIS: COINCIDENT SPECTRA
Vertical Lagoon and Beach Slopes with Cf = 0.1 and fw = 0.6

Figure 6-8: Co-Spectra of frictional sensitivity analysis
Hanning windows with an overlap of 50% were used to obtain 14 equivalent degrees of freedom, spectral resolution of 0.00033 Hz and 95% confidence limits of 0.59 and 2.13. The analytical estimate is indicated along with the upper and lower standard deviations.
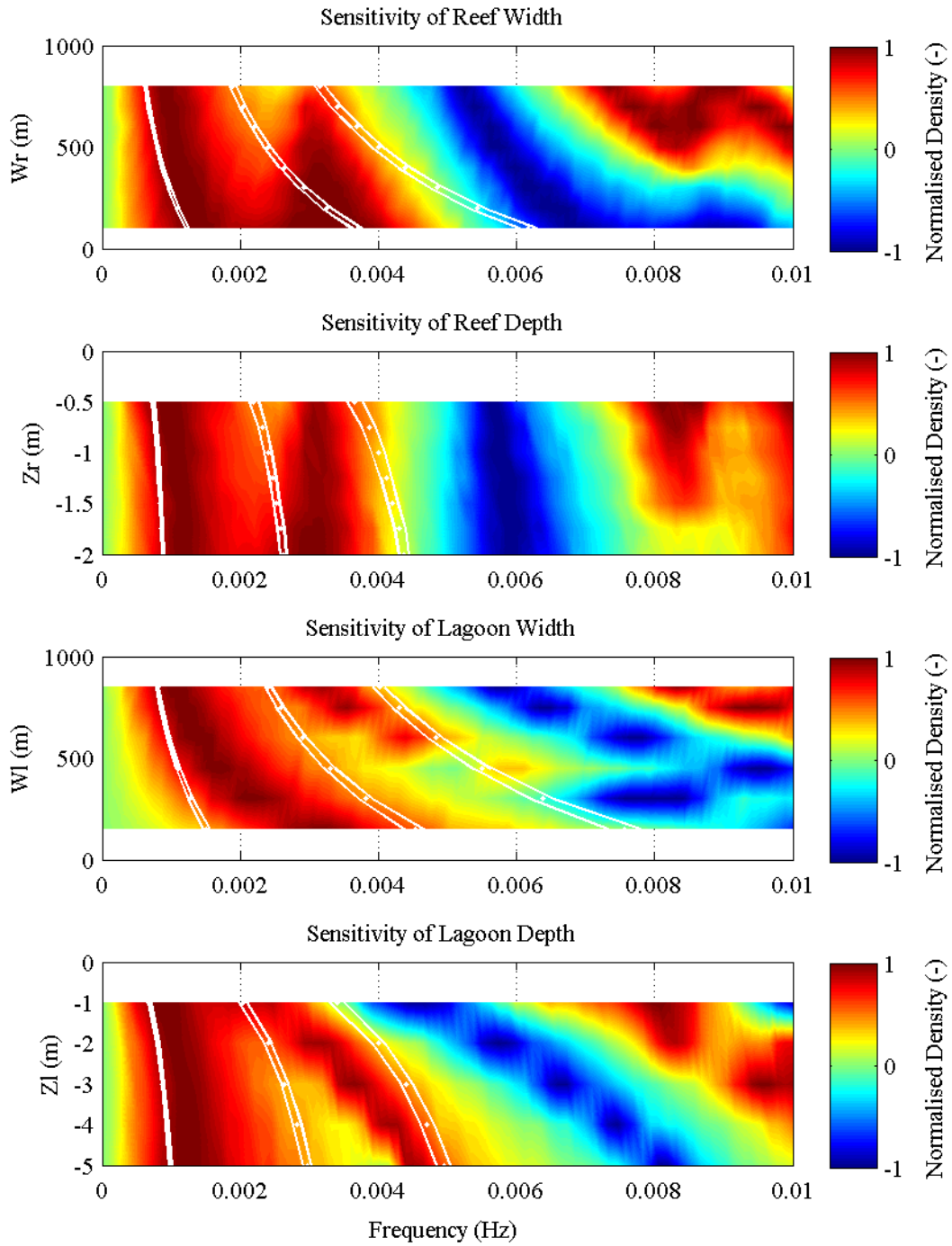
Figure 6-9: Quad-spectra of frictional sensitivity analysis
Hanning windows with an overlap of 50% were used to obtain 14 equivalent degrees of freedom, spectral resolution of 0.00033 Hz and 95% confidence limits of 0.59 and 2.13. The analytical estimate is indicated along with the upper and lower standard deviations.

6.6   Conclusions

The sensitivity analysis was found to agree well with the frequencies estimated by the analytical expression in the non-frictional model. A strong coherence signal for the first three standing wave modes with the co- and quad-spectral phase components consistent with these modes and demonstrate that these frequencies of high amplification are associated with resonant standing waves. Amplification was the greatest for the zero-mode with a decrease in amplification at higher modes observed.

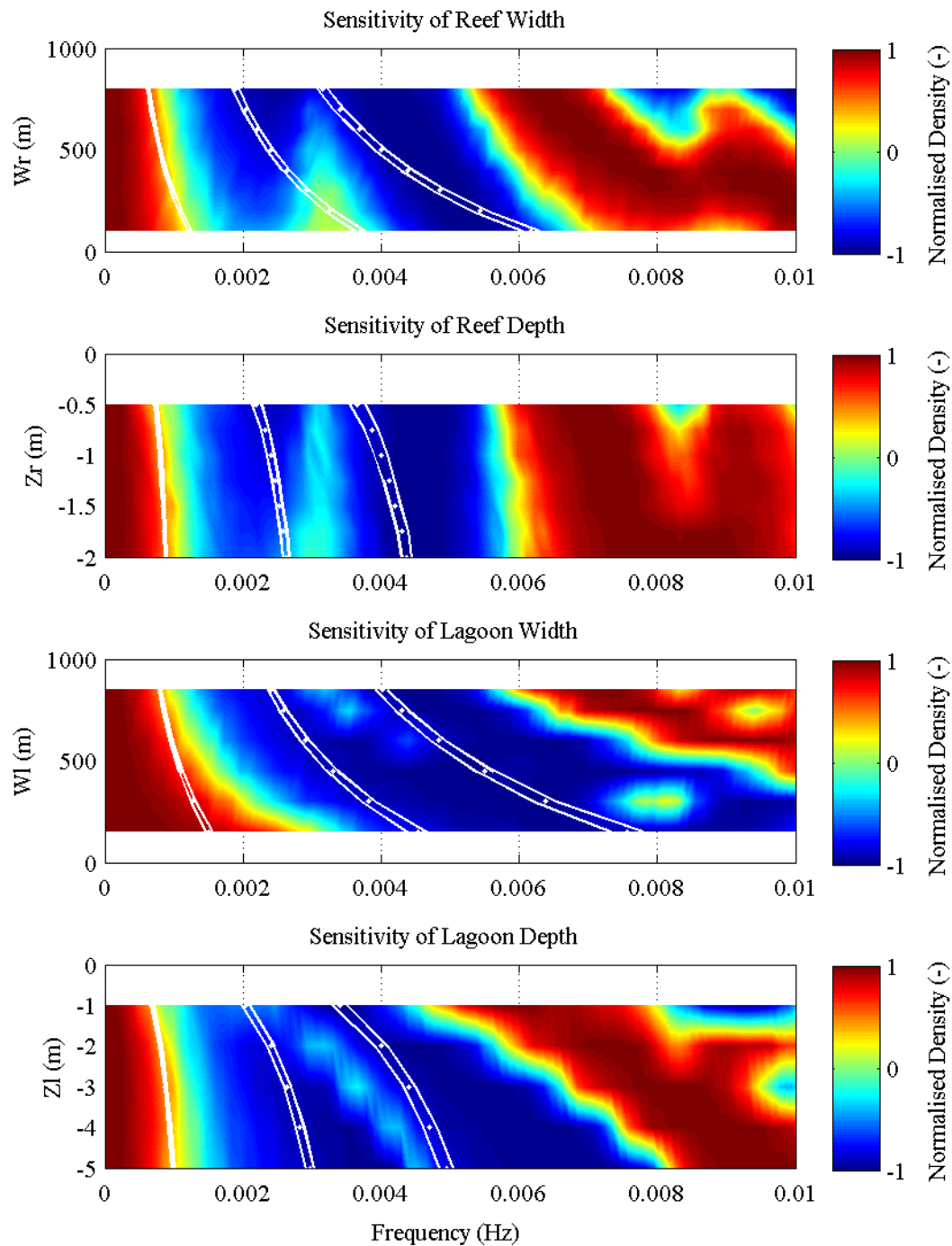The frictional model demonstrated very different results with a damped amplification observed throughout the simulation cases. High coherence results were observed across all frequencies considered along with defined bands of normalised co- and quad-spectral density. The phase relationship described by these results was found to be strongly progressive. The analytical estimate was not found to agree with the model phase relationship, which further demonstrates the progressive nature of the waves in this environment.

Perhaps the most important observation in this study was that for a coral reef, the influence of friction on the state of resonance is very significant. The large roughness of the reef surface results in high dissipation of the incident and reflected wave energy such that amplification could not occur for the simulations undertaken in this study. The result of this analysis did not agree with the results obtained by Péquignet et al. (2009) in which near resonance conditions were observed at Guam. It is hypothesised that this is due to a higher water depth at Guam than for the similar geometric condition in the sensitivity analysis – this would result in an increase in the resonance frequency and a reduction in the frictional effects. In addition, the wave boundary conditions that occurred at Guam consisted of a higher wave height and a shorter wave period – a result that may also contribute the difference in the results. Finally, the frictional parameters have been calibrated against the Ningaloo Reef, which may possess different frictional characteristics than Guam.

Chapter 7

CONCLUSIONS AND RECOMMENDATIONS

7.1 Introduction

This study investigated resonance on a reef, its identification and measurement and the influence of friction and geometry on its generation. A comparison was undertaken with an analytical model, which was also extended to analyse a reef-lagoon geometry. The numerical model XBeach was used to conduct the analysis and was calibrated with high-resolution data obtained at Ningaloo Reef (Western Australia). The analysis indicated good agreement between the analytical model and the model results for the non-friction case. In contract, the introduction of friction (calibrated against the field data) into the model resulted in no generation amplification and illustrated the importance of friction in relation to resonance.

7.2 Conclusions

Ningaloo Reef hydrodynamics

Analysis of data obtained at Ningaloo Reef (Sandy Bay) indicates that the hydrodynamic conditions at the site can be characterised by offshore sea-swell wave heights that vary from 0.58 m to 2.80 m and low-frequency wave heights of 0.02 m to 0.48 m. On the reef flat, the sea-swell waves dissipate with a portion of the energy transferred to the low-frequency wave band that was defined for this site as waves with a frequency less than 0.035 Hz. Shoreward of the reef crest the low-frequency waves dominated the spectra across the site. These waves were found to be highly progressive with little reflected flux calculated. At the shoreline a high reflection coefficient was observed consistent with limited low-frequency wave reflection.

Calibration of XBeach model

Consistent with Trang (2010), the calibration of the XBeach model with data obtained from the Ningaloo Reef was sensitive to the de-coupled wave breaking bed friction parameter (f_w) and the flow bed friction parameter (C_f) . The best calibration was achieved with $f_w = 0.6$ and $C_f = 0.1$.

Identification and measurement of resonance

Three indicators were hypothesised for the identification and measurement of resonance in spatially lagged data:

1. A highly coherent surface elevation signal at the resonant frequencies;
2. A phase relationship that corresponds with a standing wave form; and
3. Amplification at the resonant frequencies across the basin.

These indicators were found to be necessary but individually insufficient to fully describe the presence of resonance in data obtained in the field, laboratory or from numerical models. The coherence was found to identify if there is a relationship between the spatially obtained data but does not define the phase associated with this relationship. Analysis of the phase relationship for the data by the coincident and quadrature spectrum (or the combined polar phase angle) identifies if the coherent data is in a standing wave or progressive form. The analysis indicated that these two indicators alone were insufficient to determine the presence of resonance due to a wide frequency band for which this criterion is satisfactory. Analysis of the amplification demonstrated specific frequencies for which tuning of the incident and reflective waves was optimal and a state of resonance generated. This was identified by the positive amplification of the signal across the spatially lagged data. The amplification was often negative for the second resonant mode and above. This indicated that although a standing wave form was present, the amplitude decreased across the site and therefore is likely to be 'lost' amongst the progressive waves, a result consistent with other forms of dynamic response analysis.

Influence of reef type on the generation of resonance

Resonance was generated on a simple reef structure (no lagoon) and on a reef-lagoon structure with the numerical model XBeach. The amplification on a simple reef was found to be greater than for a reef-lagoon structure of the same overall length. The frequency associated with this resonance was also found to increase due to the presence of a lagoon. This was attributed to the increased influence of wave celerity though the lagoon. A reef with a vertical step for the fore-reef was found to have a clearly defined seaward nodal point while the breaking of waves over a

sloping fore-reef was found to result in a less defined nodal point. While it would seem that a vertical step onto the reef would improve the analysis of a practical reef case, this transition was found to cause an overestimation of the low frequency waves and the tide and setup components of the XBeach model when compared to a sloped fore-reef. The analysis demonstrates that with a correctly specified fore-reef, XBeach has the capability to model reef structures.

Influence of geometric parameters on the generation of resonance

An increase in the reef width was found to reduce the frequency of resonance while the depth had less influence on the frequency associated with resonance. A narrower and deeper reef was found to increase the resonant amplification. A similar result may be suggested for the lagoon however this trend was found to be less pronounced.

The resonance response followed the form estimated by the analytical expression. While this expression is a good indicator of phase, it does not provide information about whether a particular mode is resonant. The indicators in the present study provide this information via an analysis of the amplification. This analysis indicates that with the exception of specific cases, the largest amplification occurs for the zero-mode of resonance with only isolated amplifications of significant magnitude observed at higher modes.

The importance of friction

A frictionless model of a simple reef and a reef-lagoon system demonstrated that resonance could be generated for many different reef geometric arrangements. However, the introduction of friction into these systems resulted in the dissipation of the energy at the resonance frequencies. A small frictional value ($C_f = 0.01$) was found to reduce the energy at the peaks considerably. For a coral reef, the frictional coefficient ($C_f = 0.1$) was found to 'flatten' the spectral (and hence amplification) peaks to an energy density equivalent to the progressive waves. This indicates that under the conditions tested in the present study, low-frequency wave resonance is unlikely to occur due to dissipation and the de-tuning of the incident and reflected waves by friction.

Resonance at Ningaloo Reef

Analysis of spatially lagged data at Ningaloo Reef could not identify a resonance signal rather progressive waves were found to dominate. This was demonstrated by the absence of the necessary phase relationship between the spatially lagged data at the (limited) high coherence instances in the data. The results of this study suggest that this result is due to the high friction at the site.

7.3   Recommendations

Resonance indicators

This study has demonstrated the steps required to fully describe resonance on a reef, with three indicators proposed. Further research is required to understand why bands of high coherence and appropriate phase relations are generated in the frictionless case as well as how these bands relate to the formation of standing waves.

Definition of coral reef roughness

This study, along with the previous study by Trang (2010) defined the dissipation and frictional parameters against hydrodynamic and bathymetry data obtained from Ningaloo Reef. Further analysis of the relationship between the defined frictional values and the physical coral on a reef would enable a spatially variable friction parameter to be defined and a more correct calibration of the model to be achieved.

XBeach development

There is scope for further development in the description of friction within XBeach. This study has demonstrated that XBeach describes the hydrodynamic processes well. However, for complex systems such as a reef, the application of one or two frictional parameters is unlikely to fully describe the processes in the system. In particular, the application of a single flow friction parameter may not be completely accurate throughout the model domain. On this basis, implementation of a spatially varying dissipation and breaking parameters is recommended.

Geometric sensitivity

This analysis was undertaken in relation to a reference case (Ningaloo Reef) with specific wave boundary conditions. It is recommended that a four variable analysis be conducted to determine the inter-dependencies of each of the variables particularly with the inclusion of friction. This would enable a more detailed evaluation of the analytical solution. The application of a range of wave boundary conditions to such a study is also recommended.

2D effects

The present study has been conducted in one-dimension and therefore many two and three-dimensional processes have been omitted from this analysis. There is scope to undertake an analysis, which builds upon the methodology and results of the present study but with the inclusion of (in particular) two dimensional processes which are likely to affect the generation of standing waves.

Physical model

Finally, there is a case for the construction of a physical model experiment. Considerable research has been undertaken into a number of different processes on a reef, which have typically been calibrated against specific site studies. However, due to the size of reef systems (physically) it is often not possible to investigate the whole system. The construction of a wave-basin type physical model test would contribute greatly to the evaluation of the existing state on knowledge on many different processes on a system scale. It is acknowledged that such a project would be expensive and complex but its contribution to knowledge and verification of many different processes is likely to be significant.

REFERENCES

BATTJES, J. A. 2006. Developments in coastal engineering research. *Coastal Eng,* 53**,** 121-132.

BATTJES, J. A., BAKKENES, H. J., JANSSEN, T. T. & VAN DONGEREN, A. R. 2004. Shoaling of subharmonic gravity waves. *J. Geophys. Res.,* 109**,** C02009.

BATTJES, J. A. & JANSSEN, J. Energy loss and set-up due to breaking of random waves. Proceedings of the 16th international conference on coastal engineering, 1978. 569-587.

BENDAT, J. S. & PIERSOL, A. G. 1986. *Random Data: Analysis and Measurement Procedures,* John Wiley & Sons.

BENDAT, J. S. & PIERSOL, A. G. 1993. *Engineering applications of correlation and spectral analysis,* J. Wiley.

DALY, C. 2009. *Low Frequency Waves in the Shoaling and Nearshore Zone - A Validation of XBeach.* Erasmus Mundus Master in Coastal and Marine Engineering and Management (CoMEM), Delft University of Technology.

DARWIN, C. R. 1842. *The structure and distribution of coral reefs. Being the first part of the geology of the voyage of the Beagle, under the command of Capt. Fitzroy, R.N. during the years 1832 to 1836. ,* London, Smith Elder and Co.

DEAN, R. G. & DALRYMPLE, R. A. 1991. *Water wave mechanics for engineers and scientists,* World Scientific.

ELGAR, S., HERBERS, T. H. C., OKIHIRO, M., OLTMAN-SHAY, J. & GUZA, R. T. 1992. Observations of Infragravity Waves. *J. Geophys. Res.,* 97**,** 15573-15577.

EMERY, K. O. & KUHN, G. G. 1982. Sea cliffs - their processes, profiles and classification. *GEOL SOC AM BULL,* 93**,** 644-654.

GERRITSEN, F. Wave attenuation and wave set-up on a coastal reef. 17th International Conference on Coastal Engineering, 1980. ASCE, 444-461.

GOURLAY, M. R. 1994. Wave transformation on a coral reef. *Coastal Eng,* 23**,** 17-42.

GOURLAY, M. R. 1996a. Wave set-up on coral reefs. 1. Set-up and wave-generated flow on an idealised two dimensional horizontal reef. *Coastal Eng,* 27**,** 161-193.

GOURLAY, M. R. 1996b. Wave set-up on coral reefs. 2. set-up on reefs with various profiles. *Coastal Eng,* 28**,** 17-55.

GOURLAY, M. R. & COLLETER, G. 2005. Wave-generated flow on coral reefs--an analysis for two-dimensional horizontal reef-tops with steep faces. *Coastal Eng,* 52**,** 353-387.

GUZA, R. T., THORNTON, E. B. & HOLMAN, R. A. Swash on steep and shallow beaches. 19th Coastal Engineering Conference, 1984 Houston. Am. Soc. of Civ. Eng.

HARDY, T. A. & YOUNG, I. R. 1996. Field study of wave attenuation on an offshore coral reef. *J. Geophys. Res.,* 101**,** 14311-14326.

HARKINS, G. S. & BRIGGS, M. J. Resonant forcing of harbors by infragravity waves. Proceedings of the 24th International Conference on Coastal Engineering. Part 1 (of 3), October 23, 1994 - October 28, 1994, 1995 Kobe, Jpn. ASCE, 806-820.

HEARN, C. J. 1999. Wave-breaking hydrodynamics within coral reef systems and the effect of changing relative sea level. *J. Geophys. Res.,* 104**,** 30007-30019.

HEARN, C. J. & PARKER, I. N. Hydrodynamic Processes on the Ningaloo Coral Reef, Western Australia. 6th International Coral Reef Symposium, 1988 Australia. 497-502.

HINWOOD, J. B. & LUICK, J. L. 2001. Long-period waves in an island reef harbor. *Coral Reefs,* 20**,** 423-432.

JANSSEN, T. T., BATTJES, J. A. & VAN DONGEREN, A. R. 2003. Long waves induced by short-wave groups over a sloping bottom. *J. Geophys. Res.,* 108**,** 3252.

KAMPHUIS, J. W. 2010. *Introduction to Coastal Engineering and Management*, World Scientific Pub.

KARUNARATHNA, H., CHADWICK, A. & LAWRENCE, J. 2005. Numerical experiments of swash oscillations on steep and gentle beaches. *Coastal Eng,* 52**,** 497-511.

KIRBY, J. T., ÖZKAN-HALLER, H. T. & HALLER, M. C. Seiching in a large wave flume. *In:* MCKEE SMITH, J., ed. Coastal Engineering, 2006 San Diego, California. World Scientific.

KOSTENSE, J. K. Measurements of surf beat and set-down beneath wave groups. *In:* EDGE, B. L., ed. Ninetheenth International Conference of Coastal Engineering, 1984 Houston. ASCE, 724-740.

KRAINES, S. B., SUZUKI, A., YANAGI, T., ISOBE, M., GUO, X. & KOMIYAMA, H. 1999. Rapid water exchange between the lagoon and the open ocean at Majuro Atoll due to wind, waves, and tide. *J. Geophys. Res.,* 104**,** 15635-15653.

LEE, T. T. & BLACK, K. P. 1978. The Energy Spectra of Surf Waves on a Coral Reef. *Coastal Eng***,** 588-608.

LONGUET-HIGGINS, M. S. & STEWART, R. W. 1962. Radiation stress and mass transport in gravity waves, with application to 'surf beats'. *J Fluid Mech,* 13**,** 481-504.

LOWE, R. J. 12/01/2011 2011. *RE: Ningaloo Reef field study and analysis (pers. comm.).*

LOWE, R. J., FALTER, J. L., BANDET, M. D., PAWLAK, G., ATKINSON, M. J., MONISMITH, S. G. & KOSEFF, J. R. 2005. Spectral wave dissipation over a barrier reef. *J. Geophys. Res.,* 110**,** C04001.
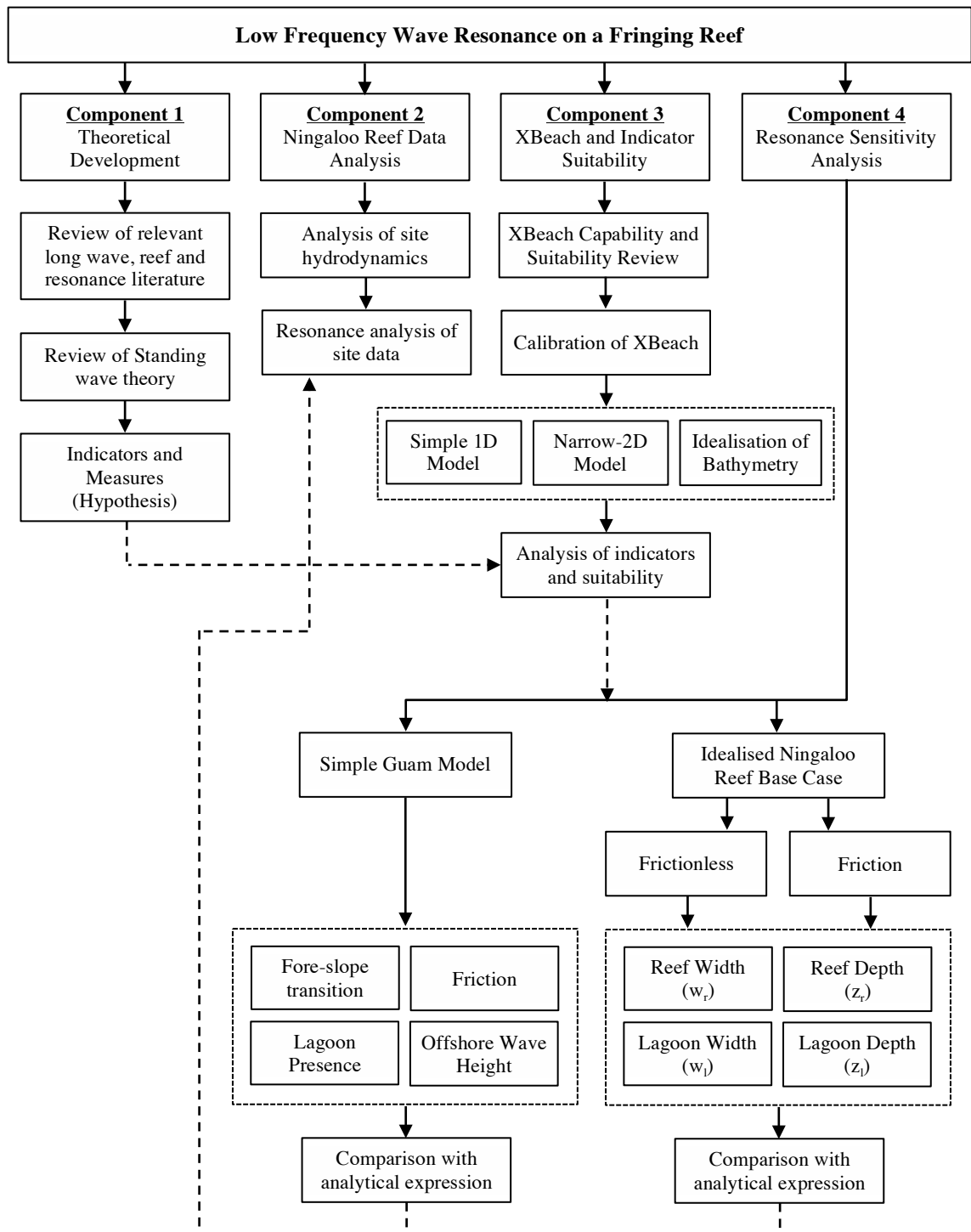
LOWE, R. J., FALTER, J. L., MONISMITH, S. G. & ATKINSON, M. J. 2009a. A numerical study of circulation in a coastal reef-lagoon system. *J. Geophys. Res.,* 114**,** C06022.

LOWE, R. J., FALTER, J. L., MONISMITH, S. G. & ATKINSON, M. J. 2009b. Wave-Driven Circulation of a Coastal Reef-Lagoon System. *J Phys Oceanogr,* 39**,** 873-893.

LOWE, R. J., HART, C. & PATTIARATCHI, C. B. 2010a. Morphological constraints to wave-driven circulation in coastal reef-lagoon systems: A numerical study. *J. Geophys. Res.,* 115**,** C09021.

LOWE, R. J., SYMONDS, G., MOORE, C., IVEY, G., PATTIARATCHI, C. B., VAN DONGEREN, A. R., MINH TRANG, D. & ROELVINK, D. Dynamics of infragravity waves in fringing reef systems. *In:* A., D. K., ed. 2010 Australian Wind Waves Symposium, 2010b Gold Coast, Queensland, Australia.

LUGO-FERNÁNDEZ, A., ROBERTS, H. H., WISEMAN JR, W. J. & CARTER, B. L. 1998. Water level and currents of tidal and infragravity periods at Tague Reef, St. Croix (USVI). *Coral Reefs,* 17**,** 343-349.

LUICK, J. L. & HINWOOD, J. B. 2008. Water levels in a dual-basin harbour in response to infragravity and edge waves. *Prog Oceanogr,* 77**,** 367-375.

MASSEL, S. R. & GOURLAY, M. R. 2000. On the modelling of wave breaking and set-up on coral reefs. *Coastal Eng,* 39**,** 1-27.

MILES, J. W. 1974. Harbor Seiching. *Ann. Rev. Fluid. Mech.,* 6**,** 17-33.

MONISMITH, S. G. 2007. Hydrodynamics of Coral Reefs. *Ann. Rev. Fluid. Mech.,* 39**,** 35-55.

MUNK, W. H. 1949. Surf Beats. *EOS Trans AGU,* 30**,** 849-854.

MUNK, W. H. & SARGENT, M. C. 1948. Adjustment of Bikini Atoll to Ocean Waves. *Trans Am Geophys Union,* 29**,** 855-860.

NAESS, A. 2007. An introduction to random vibrations. Trondheim: Norwegian University of Science and Technology.

NAKAZA, E. & HINO, M. 1991. Bore-like surf beat in a reef zone caused by wave groups of incident short period waves. *Fluid Dyn Res,* 7**,** 89-100.

NWOGU, O. & DEMIRBILEK, Z. 2010. Infragravity Wave Motions and Runup over Shallow Fringing Reefs. *J Waterw Port C-ASCE,* 136**,** 295-305.

OKIHIRO, M., GUZA, R. T. & SEYMOUR, R. J. 1993. Excitation of Seiche Observed in a Small Harbor. *J. Geophys. Res.,* 98**,** 18201-18211.

ÖZKAN-HALLER, H. T., VIDAL, C., LOSADA, I. J., MEDINA, R. & LOSADA, M. A. 2001. Standing edge waves on a pocket beach. *J. Geophys. Res.,* 106**,** 16981-16996.

PÉQUIGNET, A. C., BECKER, J., MERRIFIELD, M. & BOC, S. 2011. The dissipation of wind wave energy across a fringing reef at Ipan, Guam. *Coral Reefs***,** 1-12.

PÉQUIGNET, A. C. N., BECKER, J. M., MERRIFIELD, M. A. & AUCAN, J. 2009. Forcing of resonant modes on a fringing reef during tropical storm Man-Yi. *Geophys. Res. Lett.,* 36**,** L03607.

PRIESTLEY, M. B. 1982. *Spectral analysis and time series*, Academic Press.

ROELVINK , D. 2011. *RE: Ningaloo Reef Site Visit (pers. comm.).*

ROELVINK , D., RENIERS, A., VAN DONGEREN, A., VAN THIEL DE VRIES, J., LESCINSKI, J. & MCCALL, R. T. 2010. XBeach Model Description and Manual. Delft: Unesco-IHE Institute for Water Education, Deltares and Delft University of Technology.

ROELVINK, D., RENIERS, A., VAN DONGEREN, A., VAN THIEL DE VRIES, J., MCCALL, R. & LESCINSKI, J. 2009. Modelling storm impacts on beaches, dunes and barrier islands. *Coastal Eng,* 56**,** 1133-1152.

ROELVINK, D. & STIVE, M. 1989 Bar‑Generating Cross‑Shore Flow Mechanisms on a Beach. *J. Geophys. Res.,* 94.

ROELVINK, J. A. 1993. Dissipation in random wave groups incident on a beach. *Coastal Eng,* 19**,** 127-150.

RUESSINK, B. G., MILES, J. R., FEDDERSEN, F., GUZA, R. T. & ELGAR, S. 2001. Modeling the alongshore current on barred beaches. *J. Geophys. Res.,* 106**,** 22451-22463.

SCHAEFFER, H. A. 1993. Infragravity waves induced by short wave groups. *J Fluid Mech,* 247**,** 551-588.

SCHAFFER, H. A. 1993. Infragravity waves induced by short-wave groups. *J Fluid Mech,* 247**,** 551-588.

SEELIG, W. N. 1983. Laboratory Study of Reef-Lagoon System Hydraulics. *J Waterw Port C-ASCE,* 109**,** 380-391.

SHEREMET, A., GUZA, R. T., ELGAR, S. & HERBERS, T. H. C. 2002. Observations of nearshore infragravity waves: Seaward and shoreward propagating components. *J. Geophys. Res.,* 107**,** 3095.

SORENSEN, R. M. 2006. *Basic coastal engineering*, Springer Science+Business Media.

SUHAYDA, J. N. 1974. Standing Waves on Beaches. *J. Geophys. Res.,* 79**,** 3065-3071.

SYMONDS, G., BLACK, K. P. & YOUNG, I. R. 1995. Wave-driven flow over shallow reefs. *J. Geophys. Res.,* 100**,** 2639-2648.

SYMONDS, G. & BOWEN, A. J. 1984. Interactions of nearshore bars with incoming wave groups. *J. Geophys. Res.,* 89**,** 1953-1959.

SYMONDS, G., HUNTLEY, D. A. & BOWEN, A. J. 1982. Two dimensional surfbeat: Long wave generation by a time varying breakpoint. *J. Geophys. Res.,* 87**,** 492-498.

TAEBI, S., LOWE, R. J., PATTIARATCHI, C. B., IVEY, G. N., SYMONDS, G. & BRINKMAN, R. 2011. Nearshore circulation in a tropical fringing reef system. *J. Geophys. Res.,* 116**,** C02016.

TAYLOR, J. G. & PEARCE, A. F. 1999. Ningaloo Reef currents: implications for coral spawn dispersal, zooplankton and whale shark abundance. *Journal of the Royal Society of Western Australia,* 82**,** 57-65.

THORNTON, E. B. & GUZA, R. T. 1983. Transformation of Wave Height Distribution. *J. Geophys. Res.,* 88**,** 5925-5938.

TRANG, D. M. 2010. *Modelling infragravity waves and currents across a fringing reef: Ningaloo Reef, Western Australia (using XBeach).* Master of Science, UNESCO-IHE.

TRANG, D. M., VAN DONGEREN, A. R., LOWE, R. J., ROELVINK, D., RANASINGHE, R. & SYMONDS, G. in prep. Modelling infragravity waves and currents across a fringing reef: Ningaloo Reef, Western Australia.

TUCKER, M. J. 1950. Surf Beats: Sea waves of 1 to 5 min. period. *Proceedings of the Royal Society of London*, Series A, 202**,** 565-573.

VAN DONGEREN, A., BATTJES, J., JANSSEN, T., VAN NOORLOOS, J., STEENHAUER, K., STEENBERGEN, G. & RENIERS, A. 2007. Shoaling and shoreline dissipation of low-frequency waves. *J. Geophys. Res.,* 112**,** C02011.

WILSON, B. W. 1966. The Encyclopedia of Oceanography. FAIRBRIDGE, R. W. (ed.) Reinhold Pub. Co.(pp. 804 - 817)

WU, J.-K. & LIU, P. L.-F. 1990. Harbour excitations by incident wave groups. *J Fluid Mech,* 217**,** 595-613.

YOUNG, I. R. 1989. Wave Transformation Over Coral Reefs. *J. Geophys. Res.,* 94**,** 9779-9789.

Appendix A STRUCTURE OF THIS STUDY

Low Frequency Wave Resonance on a Fringing Reef

Component 1
Theoretical Development

Component 2
Ningaloo Reef Data Analysis

Component 3
XBeach and Indicator Suitability

Component 4
Resonance Sensitivity Analysis

Review of relevant long wave, reef and resonance literature

Analysis of site hydrodynamics

XBeach Capability and Suitability Review

Review of Standing wave theory

Resonance analysis of site data

Calibration of XBeach

Indicators and Measures (Hypothesis)

Simple 1D Model

Narrow-2D Model

Idealisation of Bathymetry

Analysis of indicators and suitability

Simple Guam Model

Idealised Ningaloo Reef Base Case

Frictionless

Friction

Fore-slope transition

Friction

Lagoon Presence

Offshore Wave Height

Reef Width (w_r)

Reef Depth (z_r)

Lagoon Width (w_l)

Lagoon Depth (z_l)

Comparison with analytical expression

Comparison with analytical expression

Appendix B **NINGALOO REEF RESONANCE RESULTS**

## B.1   Results of analysis: Stations C3 and C4

The coherence between variations in surface elevation at C3 and C4 (on the reef flat) was shown to be highly coherent. High coherence across most frequencies was found to occur over the period of the storm (14 June 2009 – 19 June 2009) while on either side of this event, only three distinct bands of coherence were observed (0 Hz to 0.0025 Hz; 0.004Hz to 0.009 Hz and 0.12 Hz to 0.17 Hz).

Both the co-spectrum and the quad-spectrum alternate between a high positive and negative density. Together these spectra confirm a progressive wave pattern across the reef flat.

B.2   Results of analysis: Stations C4 and C5

The analysis of stations C4 (inner reef edge) and C5 (in the lagoon) indicated strong coherence between the two stations throughout the storm (14 June 2009 – 19 June 2009). However, outside this period the coherence was significantly less (0 – 0.4). Two distinct bands of coherence could be identified over the frequencies 0 Hz to 0.001 Hz and 0.004 Hz to 0.008 Hz.

The co-spectrum and quad-spectrum are characterised by highly positive to highly negative values. This indicates that although coherence was high at some times and frequencies, a standing wave was not generated between stations C4 and C5.
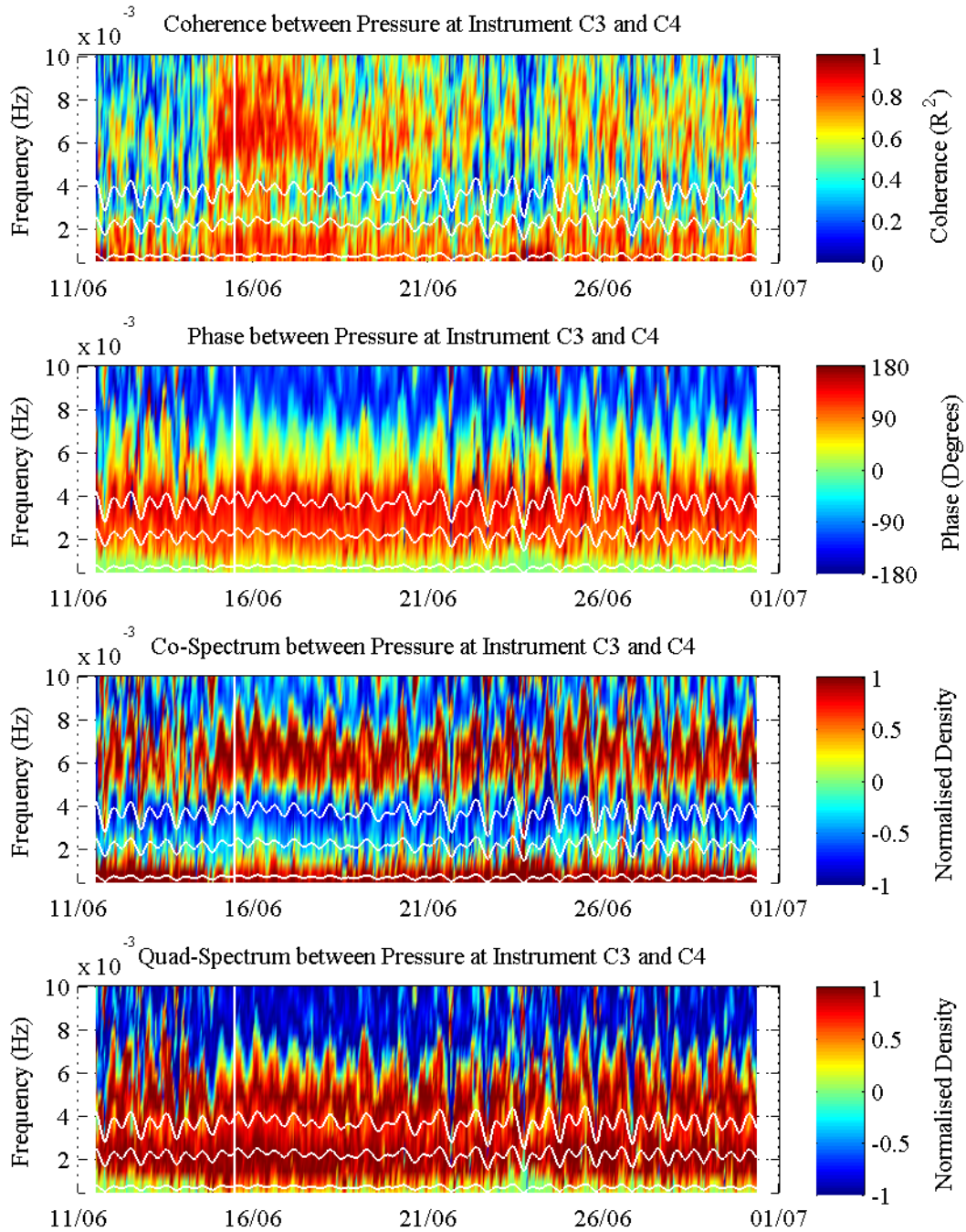
Coherence, phase, co- and quad-spectra between instruments C3 and C4
Frequencies higher than 0.01 Hz have been omitted for clarity. The vertical (white) line represents the peak storm observed at the site. The first three modes of natural resonance frequencies are also plotted.

110
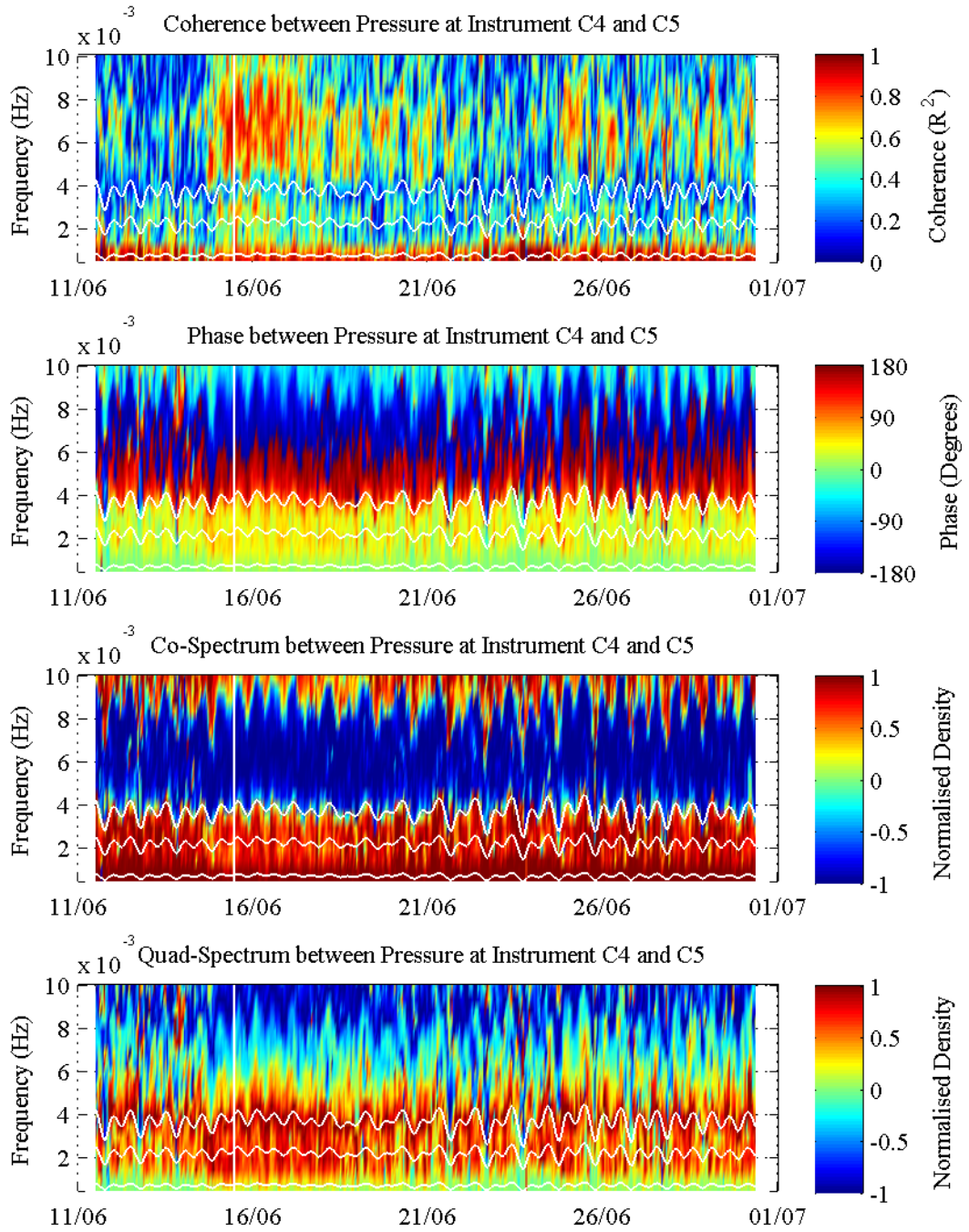
Coherence, phase, co- and quad-spectra between instruments C4 and C5
Frequencies higher than 0.01 Hz have been omitted for clarity. The vertical (white) line represents the peak storm observed at the site. The first three modes of natural resonance frequencies are also plotted.

Appendix C

CALCULATION OF THE COHERENCE BETWEEN TWO SIGNALS

C.1 Introduction

Correlation functions are used to compare two sets of data and form the basis for other measures of analysis such as coherence and co-spectra. There are many good references on this topic and the reader is referred to such texts (eg. Priestley, 1982; Bendat and Piersol, 1986; Bendat and Piersol, 1993) for a complete analysis. The theoretical basis and procedure to evaluate the correlation and coherence, particularly with respect to the current project, is summarised in this appendix. This appendix commences in C.2 with a brief review of the classical basis of correlation and coherence. This basis is extended to time history discussion in C.3 with a brief discussion related to instrument locations in C.4. The last two topics are particularly relevant to the present study.

C.2 Classical basis

Classically, correlation evaluates the relationship between two sets of data such as x and y or one set of data with itself. These sets of data typically consist of measurements that are independent of time, for example $x_i, i = 1,2,3 \dots N$.

To evaluate the degree of linear relationship within a data set, the *auto-variance* (or simply *variance*) is calculated. This function measures how much a variable changes in relation to itself and is defined, for example in the case of x, as:

$$
\begin{aligned}
\sigma_{xx}^2 &= E[(x - u_x)(x - u_x)] \\
&= \lim_{N \to \infty} \frac{1}{N} \sum_{i=1}^{N} x_i^2 - u_i^2
\end{aligned}
$$

Analogous to this, the same approach can be adopted to determine the degree of linear relationship between the two sets of data. In this case, the *covariance* is calculated:

$$
\begin{aligned}
\sigma_{xy} &= E\big[(x - u_x)(y - u_y)\big] \\
&= \lim_{N \to \infty} \frac{1}{N} \sum_{i=1}^{N} (x_i - u_x)(y_i - u_y)
\end{aligned}
$$

This function is a measure of how much two variables change together and relates the two sets of data in the following way:

- If the sum of the positive products of $(x - u_x)$ and $(y - u_y)$ equal the sum of the negative products, there is no linear relationship between the data and $\sigma_{xy} = 0$.

- If the positive products of $(y - u_y)$ are always positive when $(x - u_x)$ is positive (or the case exists when both are negative), $\sigma_{xy} = \sigma_x \sigma_y$.

- Between these two cases are various levels of linear correlation.

It is common to express the degree of linear correlation on a scale from -1 to +1 by calculating the *correlation coefficient* (ρ_{xy}):

$$
\rho_{xy} = \frac{\sigma_{xy}}{\sigma_x \sigma_y}
$$

The full derivation of this expression along with the domain can be mathematically proven (Bendat and Piersol, 1986).

C.3 Time history random data

The concepts from the classical basis are extended to analyse time history random data with the assumption that the two (sampled) data sets $\{x(t)\}$ and $\{y(t)\}$ are stationary (ergodic) random processes. The classical concepts are applied by the introduction of a new variable (such as a time or spatial lag τ).

Covariance Function

In this new context, the variance function (defined with the inclusion of the new variable) is referred to as an *auto-covariance* and describes the variance of a signal against a time (or space) shifted version of itself:

$$
\begin{aligned}
C_{xx}(\tau) &= E\big[\{x(t) - u_x\}\{x(t + \tau) - u_x\}\big] \\
&= \lim_{T \to \infty} \frac{1}{T} \int_0^T \{x(t) - u_x\}\{x(t + \tau) - u_x\}dt \\
&= R_{xx}(\tau) - u_x^2
\end{aligned}
$$

114

The function (in the present example in terms of x) is composed of two components, $R_{xx}(\tau)$ and u_x^2. The first component is defined as the *auto-correlation function* and describes the similarity of the signal time shifted against itself.

$$R_{xx}(\tau) = \lim_{T \to \infty} \frac{1}{T} \int_0^T x(t)x(t + \tau)dt$$

The second component is the square of the mean of the signal. By extension, the *covariance* function describes the variance of a signal against a time (or space) shifted second signal:

$$
\begin{aligned}
C_{xy}(\tau) &= E\big[\{x(t) - u_x\}\{y(t + \tau) - u_y\}\big] \\
&= \lim_{T \to \infty} \frac{1}{T} \int_0^T \{x - u\}\{y - u\}dt \\
&= R_{xy}(\tau) - u_x u_y
\end{aligned}
$$

Where:

$$R_{xy}(\tau) = \lim_{T \to \infty} \frac{1}{T} \int_0^T x(t)y(t + \tau)dt$$

In this case, $R_{xy}(\tau)$ is referred to as the *cross-correlation function* and describes the similarity of the two sets of data with one set of data having a time (or space) shift applied.

Spectral Density Functions

Spectral density functions are related to correction functions. At the most specific level, the spectral density function is a Fourier transform of a correlation function. A broader application of spectra is in generalized Fourier analysis, which is regularly employed in hydrodynamic applications.

The spectra density function of two time history records can be calculated by a Fourier transform of the correlation function between the two sets of data and is referred to as the *cross-spectral density function* (or simply *cross-spectrum*) between $x(t)$ and $y(t)$. This function describes how the variance between the two signals varies with frequency.

$$S_{xy}(f) = \int_{-\infty}^{\infty} R_{xy}(\tau)e^{-j2\pi f\tau}d\tau$$

For the case when $y(t) = x(t)$, the spectrum is defined as the *auto-spectral density function* (also known as the *auto- spectrum*, *power spectral density function* or the *variance spectrum*).

As for the cross-spectral density function, the auto-spectral density function describes how the variance of a signal is distributed with frequency.

$$S_{xx}(f) = \int_{-\infty}^{\infty} R_{xx}(\tau)e^{-j2\pi f\tau}d\tau$$

According to this definition, these spectra are defined over all frequencies and are therefore referred to as *two sided spectra*. It can be shown (Bendat and Piersol, 1986) that the symmetry properties of the auto-spectrum are different than for the cross-spectrum. The auto-spectra are real functions (symmetrical) while the cross-spectra are complex.

$$S_{xx}(-f) = S_{xx}^*(f) = S_{xx}(f) \quad and \quad S_{xy}(-f) = S_{xy}^*(f) = S_{yx}(f)$$

The Cross- and Auto-Correlation Function

Generally, negative frequencies are undesirable for analysis and therefore for the ease of analysis and for better practical understanding, *one-sided spectra* are used.

Since the auto-spectra are real functions, these functions can be re-expressed as the one-sided function:

$$\begin{aligned}
G_{xx}(f) \quad &= 2S_{xx}(f) \\
&= 2\int_{-\infty}^{\infty} R_{xx}(\tau)e^{-i2\pi f\tau}d\tau \\
&= 2\int_{-\infty}^{\infty} R_{xx}(\tau)\cos 2\pi f\tau\, df \\
&= 4\int_{0}^{\infty} R_{xx}(\tau)\cos 2\pi f\tau\, df
\end{aligned}$$

The cross-correlation is a complex function. The one-sided function therefore becomes:

$$\begin{aligned}
G_{xy}(\tau) \quad &= 2\int_{-\infty}^{\infty} R_{xy}(\tau)e^{-j2\pi f\tau}df \\
&= C_{xy}(f) - jQ_{xy}(f)
\end{aligned}$$

The cross-spectrum is shown to consist of two parts: a *coincident spectral density function (Co-spectrum)* and the *quadrature spectral density function (Quad spectrum)*. These are the real and imaginary parts of the cross-correlation function respectively.

$$C_{xy}(f) = 2\int_{-\infty}^{\infty} R_{xy}(\tau)\cos(2\pi f\tau)\, d\tau$$

$$Q_{xy}(f) = 2\int_{-\infty}^{\infty} R_{xy}(\tau)\sin(2\pi f\tau)\, d\tau$$

The cross-correlation function can therefore be defined to the fullest extent as:

$$
\begin{aligned}
R_{xy}(\tau) \quad &= \int_{-\infty}^{\infty} S_{xy}(f) e^{-i2\pi f\tau}\, d\tau \\
&= \frac{1}{2}\int_{0}^{\infty} G_{xy}(f) e^{-i2\pi f\tau}\, df + \frac{1}{2}\int_{0}^{\infty} G_{xy}^{*}(f) e^{-i2\pi f\tau}\, df \\
&= \int_{0}^{\infty} \left[C_{xy}(f)\cos 2\pi f\tau + Q_{xy}(f)\sin 2\pi f\tau \right] df
\end{aligned}
$$

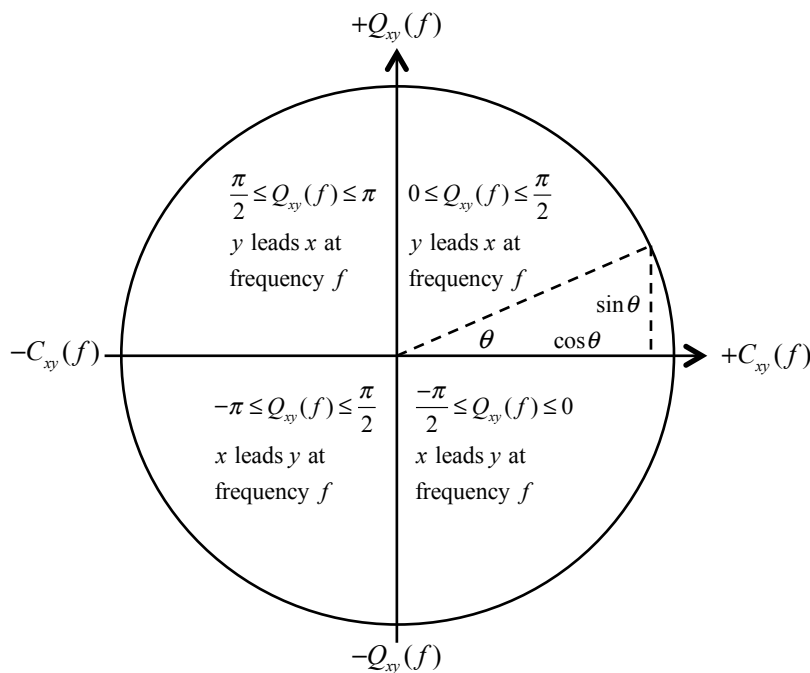The cross-spectra can be represented using polar coordinates (a magnitude and a phase angle).

$$
G_{xy}(f) = G_{xy}^{*}(f) = \left| G_{xy}(f) \right| e^{-j\theta_{xy}(f)}
$$

where:

$$
\left| G_{xy}(f) \right| = \sqrt{C_{xy}^{2}(f) + Q_{xy}^{2}(f)}
$$

$$
\theta_{xy}(f) = \tan^{-1}\left[\frac{Q_{xy}(f)}{C_{xy}(f)} \right]
$$

When $\theta_{xy}(f)$ is positive, y follows x at frequency f.

Cross-Spectrum Inequality and the (Squared) Coherence Function

The cross-spectrum inequality is analogous to the cross-correlation inequality:

$$
\left| G_{xy}(f) \right|^{2} \le G_{xx}(f) G_{yy}(f)
$$

From this inequality, the (Squared) Coherence Function is defined:

$$\gamma_{xy}^2(f) = \frac{\left|G_{xy}(f)\right|^2}{G_{xx}(f)G_{yy}(f)}$$

The (squared) coherence function describes how well two data sets are correlated, as measured by the cross-correlation function. In practice, this informally described the extent to which $y(t)$ may be predicted by $x(t)$.

Coherence, Co-Spectrum and Quad Spectrum

The three statistical measures, coherence, co-spectrum and quad-spectrum can be used to describe the relationship between two signals separated in the field.

The **(squared) coherence function** describes how well the two signals are correlated (exhibit a predictive function). If the (squared) coherence is + 1, the two signals have a direct relationship (one signal can be predicted from the other). If (squared) coherence between the two signals is not high, the co-spectrum and quad-spectrum do not provide any additional information.

Between the two stations, a phase difference may exist between the measurements at each location. The **co-spectrum** describes how 'in-phase' the two signals are and is described by a cosine function. The **quad-spectrum** describes how 'out-of-phase' the two signals are and is described by a sine function. Together, these spectra define the phase difference (an angle in polar coordinates) between the two signals.

If the two signals are in-phase (zero phase difference), the co-spectrum will indicate a strong positive density and the quad-spectrum will be near zero. Similarly, if the signals are 180 degrees out of phase, the co-spectrum will indicate a strong negative density and the quad-spectrum will be near zero. In these two cases, a standing wave is demonstrated.

If the two signals are partially out of phase (progressive), the co-spectrum and the quad-spectrum will both possess some degree of density which describes how much one instrument will lead the other instrument.

In a spectral density plot that consists of co-spectral density on the y-axis and frequency on the x-axis, a standing wave will be demonstrated at a particular frequency when the co-spectral density is near $\pm$ 1. At the same frequency a quad spectrum, constructed with the quadrature density on the y-axis and frequency on the x-axis, must be near zero.

A plot in which phase is on the y-axis and frequency is on the x-axis, is expected to show a progressive change in phase across the frequency axis. In contrast, for a standing wave, the plot

is expected to exhibit a jump discontinuity between 0 and 180 degrees consistent with the co-spectrum.

C.4 Position of the instruments

The position of the instruments relative to the nodes associated with the standing wave will determine the value of the co-spectrum (+1 or -1). If the two sampling stations are positioned between two nodes, the co-spectrum is expected to be unity (phase shift = 0 degrees). However, if the two stations are positioned such that a node is located between them, the co-spectrum is expected to be minus one because the time series is 180 degrees out of phase. In summary, for n nodes between the station pair:

$$co\,(f) = \begin{cases} 1 \text{ if n nodes} = 0, 2, 4 \ldots \\ -1 \text{ if n nodes} = 1, 3, 5 \ldots \end{cases}$$
$$quad\,(f) = \quad 0$$

Appendix D

THE XBEACH MODEL

The equations that drive the XBeach model are transparent and have been subjected to rigorous development (Roelvink et al., 2009). The numerical basis of the wave propagation and flow modules is contained within three groups of equations: the wave action balance, roller energy balance and the shallow wave equations. In addition to these equations, there are two boundary condition sources: wave boundary and flow boundary. These equations are cast into a Generalised Lagrangian Mean (GLM) form. The Eulerian shallow water velocity (u^E), the short-wave-averaged velocity observed at a fixed point, is related to the lagrangian equivalent (u^L) by:

$$u^L = u^E + u^S \quad \text{and} \quad v^L = v^E + v^S$$

The Stokes (drift) component is represented in the x- and y-direction by u^S and v^S respectively:

$$u^S = \frac{E_w \cos \theta}{\rho h c} \quad \text{and} \quad v^S = \frac{E_w \sin \theta}{\rho h c}$$

This approach, in which the lagrangian velocity is defined as the distance a water particle travels in one wave period, divided by that period, enables the wave induced mass-flux and the (subsequent) return flow to be modelled. This enables the wave-current interaction process to be incorporated into the model.

D.1 Wave action balance equations

The wave action equation balances the spatial transport and temporal change in wave action with sources and sinks of action. The equation, which consists of three groups of terms: one

group of terms describe the local changes in wave action, the second the propagation of wave action and the third the generation and dissipation of wave action. From this equation, the wave action and consequently the (group) wave energy can be derived. This enables the wave forcing to be determined from radiation stress tensors.

Wave Action

Wave Action is best described as a density of (group) wave energy and is defined by the (group) wave energy (E_w), within a directional bin, divided by the intrinsic frequency (σ):

$$A(x, y, \theta) = \frac{E_w(x, y, \theta)}{\sigma(x, y)}$$

The intrinsic frequency is a 'representative' frequency for the spatial location. This assumption (simplification) reduces the computational complexity associated with the use of the full frequency spectrum. This frequency is best represented the spectral parameter $f_{m,-1}$, which 'weights' the lower frequencies within the frequency spectrum. This 'weighting' better describes the frequencies associated with wave group motions; the scale in which the wave action balance equation is solved. An alternative frequency can be obtained from the linear dispersion relation:

$$\sigma = \sqrt{gk \tanh kh}$$

Wave Action Balance Equation

The wave action balance equation adopted in XBeach is similar to that adopted in other models such as the HISWA model. The equation equates the spatial transport and temporal change in wave action with sources and sinks of action:

$$\frac{\partial A}{\partial t} + \frac{\partial c_x A}{\partial x} + \frac{\partial c_y A}{\partial y} + \frac{\partial c_\theta A}{\partial \theta} = S_A - D_A$$

The equation consists of three groups of term: the local rate of change of the spectral action density $\left(\frac{\partial A}{\partial t}\right)$; propagation terms $\left(\frac{\partial c_x A}{\partial x} + \frac{\partial c_y A}{\partial y} + \frac{\partial c_\theta A}{\partial \theta}\right)$; and a source and sink term which is a function that accounts for the generation and dissipation of wave action $(S_A - D_A)$.

The wave action represents a form of (group) wave energy and therefore the equation is solved in the scale of wave group motion (discussed in the previous section). This means that the equation solves the time-varying amplitude variation over the wave group rather than the

variation in amplitude for an individual wave. The structure provides a simulation time advantage when compared to other numerical schemes.

Local Rate of Action Change

The first term of the wave action balance equation, the local rate of change in wave action density $\left(\frac{\partial A}{\partial t}\right)$, describes how the wave action varies with time. This term allows non-stationary conditions to be modelled. In the HISWA model, this term is omitted as one of the simplifications, making the HISWA model a stationary model.

Wave Action Propagation

The wave action propagation terms $\left(\frac{\partial c_x A}{\partial x} + \frac{\partial c_y A}{\partial y} + \frac{\partial c_\theta A}{\partial \theta}\right)$ describe the spatial transportation of wave action in x- and y-space at a specific location and in a specific direction (x, y, θ). It is well known from wave mechanics (eg. Snell's Law), that as a wave propagates into shallow water, the wave ray refracts; the (group) wave energy continually changes direction while travelling through x- and y-space. This process is represented in the wave action balance equation by the three wave action propagation terms. These terms describe wave action propagation through x- and y-space and simultaneously through θ-space, with the θ-space representing refraction.

The transportation of wave action is explained by the x- and y-component of the wave action propagation speeds $\left(C_x, C_y\right)$ for the first two terms (analogous to the concept of following wave energy along a wave ray). The θ-space wave action propagation speed $\left(C_\theta\right)$ describes the rate at which direction changes as a particle travels with the group velocity along the curving ray.

The propagation speeds in the x- and y-direction consist of the propagation group velocity and the current velocity (cross and along-shore depth-averaged Lagrangian velocities):

$$c_x(x, y, t, \theta) = c_g \cos\theta + u^L$$
$$c_y(x, y, t, \theta) = c_g \sin\theta + v^L$$

with (from Linear Wave Theory):

$$c_g = nc = \left(\frac{1}{2} + \frac{kh}{\sinh 2kh}\right)\frac{\sigma}{k}$$

In the θ-space, the propagation speed is defined as:

$$c_\theta(x, y, t, \theta)$$

$$= \frac{\sigma}{\sinh 2kh} \left(\sin\theta \frac{\partial h}{\partial x} - \cos\theta \frac{\partial h}{\partial y} \right) + \cos\theta \left(\sin\theta \frac{\partial u}{\partial x} - \cos\theta \frac{\partial u}{\partial y} \right)$$

$$+ \sin\theta \left(\sin\theta \frac{\partial v}{\partial x} - \cos\theta \frac{\partial v}{\partial y} \right)$$

Wave Generation and Dissipation

Sources and sinks of wave action are represented by the third group of terms in the wave action balance equation that consists of a source function (S_A) and a sink function (D_A). These functions are the directionally distributed source and sink functions that are derived from expressions for the total source action $(\overline{S_A})$ and sink action $(\overline{D_A})$ by:

$$S_A(x, y, \theta) = \frac{S_w(x, y, \theta)}{E_w(x, y)} \overline{S_A} \quad \text{and} \quad D_A(x, y, \theta) = \frac{S_w(x, y, \theta)}{E_w(x, y)} \overline{D_A}$$

The current release of XBeach does not include any source expressions however it does include four different expressions for wave dissipation and one expression for bed friction dissipation. The reader is referred to Roelvink et al. (Roelvink et al., 2009) for more information regarding each model.

Wave Forcing

XBeach determines, using the wave action balance equation, the spatial distribution of the wave action (A). Consequently, the spatial distribution of the (group) wave energy (S_w) can be determined.

The radiation stress tensors can be evaluated using Linear Wave Theory:

$$S_{xx}(x, y, t) = \int \left(\frac{c_g}{c} (1 + \cos^2\theta) - \frac{1}{2} \right) S_w d\theta$$

$$S_{xy}(x, y, t) = \int \sin\theta \cos\theta \frac{c_g}{c} S_w d\theta$$

$$S_{yy}(x, y, t) = \int \left(\frac{c_g}{c} (1 + \sin^2\theta) - \frac{1}{2} \right) S_w d\theta$$

These radiation stress tensors are used, along with the roller energy radiation stress tensors (Section D.2), to determine the wave forces for input into the shallow water equations (Section D.3).

D.2 Roller energy equation

As waves approach the nearshore and breaking occurs, there is a transportation and dissipation of the breaking wave energy via a roller. This process is not included in the wave action balance previously described (Section D.1). To model the roller process, XBeach uses a roller action balance equation structured in the same way as the wave action balance and couples it with the wave action balance equation by including the energy dissipation term (D_w) as a source term in the roller action balance equation:

$$\frac{\partial A_R}{\partial t} + \frac{\partial c_x A_R}{\partial x} + \frac{\partial c_y A_R}{\partial y} + \frac{\partial c_\theta A_R}{\partial \theta} = D_{A,w} - D_{A,r}$$

where:

$$A_R(x, y, \theta) = \frac{S_r(x, y, \theta)}{\sigma(x, y)}$$

Like the wave action balance, the roller action balance consists of three terms: the local rate of change of the roller action $\left(\frac{\partial A_R}{\partial t}\right)$; propagation terms $\left(\frac{\partial c_x A_R}{\partial x} + \frac{\partial c_y A_R}{\partial y} + \frac{\partial c_\theta A_R}{\partial \theta}\right)$; and source and sink terms which are a series of functions that accounts for the generation and dissipation of roller energy.

Local Rate of Action Change and Propagation

The first two terms represent the same processes as for the wave action balance equation. It is assumed that the roller action is propagating in the same direction as the waves and that the propagation speed in the x- and y-direction is based upon the phase velocity rather than the group velocity:

$$c_x(x, y, t, \theta) = c \cos \theta + u^L$$
$$c_y(x, y, t, \theta) = c \sin \theta + v^L$$

with (from Linear Wave Theory):

$$c = \frac{\sigma}{k}$$

The propagation speed in θ-space is the same expression as for the wave action balance equation (Equation X) and is based on the same principles that were discussed in Section X.

Roller Generation and Dissipation

Sources and sinks of roller action are represented by the third group of terms in the roller action balance equation that consists of a source function (D_A) and a sink function (D_R). These functions are the directionally distributed source and sink functions that are derived from expressions for the total source action $(\overline{D_A})$ and sink action $(\overline{D_R})$.

$$D_R(x, y, \theta) = \frac{S_{waves}(x, y, \theta)}{E_{waves}(x, y)} \overline{S_A} \quad \text{and} \quad D_A(x, y, \theta) = \frac{S_{waves}(x, y, \theta)}{E_{waves}(x, y)} \overline{D_A}$$

The source term is the dissipation term from the wave action balance equation. This couples the two equations and results in the assumption that the energy dissipated during the breaking process is transferred into the roller process where it is further dissipated according to the dissipation model by Reiners et al.(2004) that combines the concepts of Deigaard (1993) and Svendsen (1984).

In this combined model, the dissipation of the roller action is governed by a shear stress term (τ_{roller}) that travels at the phase velocity:

$$\overline{D}_{roller} = c\tau_{roller}$$

The shear stress term describes the shear stress experienced by the roller at the surface and defined by Svendsen (1984) as:

$$\tau_{roller} = \frac{\rho g R}{L} \beta_r$$

The roller area is represented by R while the roller length is represented by L. The slope of the breaking wave (typically between 0.05 and 0.10) is defined by β_r. The total energy of the roller trough is related to the roller area by the expression:

$$E_r = \frac{1}{2} \frac{\rho R c^2}{L}$$

Roller Forcing

XBeach determines, like for the wave action balance equation, the spatial distribution of the wave action (A). Consequently, the spatial distribution of the (group) wave energy (S_w) can be determined.

The roller contributes to the wave forcing and therefore a radiation stress tensor representing this forcing is calculated. This roller radiation stress contribution is added to the wave-induced radiation stresses to obtain the total radiation stress gradient.

The radiation stress tensors and hence the wave forcing can be evaluated using Linear Wave Theory:

$$S_{xx,r}(x, y, t) = \int \cos^2 \theta \, S_r d\theta$$

$$S_{xy,r}(x, y, t) = S_{yx,r}(x, y, t) = \int \sin \theta \cos \theta \, S_r d\theta$$

$$S_{yy,r}(x, y, t) = \int \sin^2 \theta \, S_r d\theta$$

The wave forces can be determined from radiation stress tensors from the wave action balance and the roller action balance. These forces are used as an input into the shallow water equations (Section D.3).

$$F_x(x, y, t) = -\left(\frac{\partial S_{xx,w} + \partial S_{xx,r}}{\partial x} + \frac{\partial S_{xy,w} + \partial S_{xy,r}}{\partial y} \right)$$

$$F_y(x, y, t) = -\left(\frac{\partial S_{xy,w} + \partial S_{xy,r}}{\partial x} + \frac{\partial S_{yy,w} + \partial S_{yy,r}}{\partial y} \right)$$

D.3 Shallow water equations solver

XBeach uses depth-averaged shallow water equations to solve for low-frequency waves and mean flow. The equations are based on the principle of conservation of momentum and are expressed as:

$$\frac{\partial u}{\partial t} + u \frac{\partial u}{\partial x} + v \frac{\partial u}{\partial y} - fv - v_h \left(\frac{\partial^2 u}{\partial x^2} + \frac{\partial^2 u}{\partial x^2} \right) = \frac{\tau_{sx}}{\rho h} - \frac{\tau_{bx}}{\rho h} - g \frac{\partial \eta}{\partial x} + \frac{F_x}{\rho h}$$

$$\frac{\partial v}{\partial t} + u \frac{\partial v}{\partial x} + v \frac{\partial v}{\partial y} - fu - v_h \left(\frac{\partial^2 v}{\partial x^2} + \frac{\partial^2 v}{\partial x^2} \right) = \frac{\tau_{sy}}{\rho h} - \frac{\tau_{by}}{\rho h} - g \frac{\partial \eta}{\partial x} + \frac{F_y}{\rho h}$$

$$\frac{\partial \eta}{\partial t} + \frac{\partial hu}{\partial x} + \frac{\partial hv}{\partial y} = 0$$

The wave induced mass-flow and the subsequent (return) flow are accounted for using the Generalized Lagrangian Mean (GLM) formulation. The euleren velocities are used in the

evaluation of the bottom shear stress. In addition, the effects of Coriolis, viscosity and surface stresses are not implemented in XBeach. The resulting GLM-momentum equations are:

$$\frac{\partial u^L}{\partial t} + u^L \frac{\partial u^L}{\partial x} + v^L \frac{\partial u^L}{\partial y} = -\frac{\tau_{bx}^E}{\rho h} - g\frac{\partial \eta}{\partial x} + \frac{F_x}{\rho h}$$

$$\frac{\partial v^L}{\partial t} + u^L \frac{\partial v^L}{\partial x} + v^L \frac{\partial v^L}{\partial y} = -\frac{\tau_{bx}^E}{\rho h} - g\frac{\partial \eta}{\partial x} + \frac{F_y}{\rho h}$$

D.4 Boundary conditions

XBeach requires the input of two boundary conditions to commence the model run. These are the wave boundary conditions and the flow boundary conditions.

Wave Boundary Conditions

To specify the wave boundary condition at the offshore boundary, function of y, θ and time is defined. This can be generated using a set of given spectral parameters or using directional spectrum information.

The lateral wave boundary conditions are specified based upon two assumptions:

- In the stationary case, the alongshore gradient of the wave energy is zero; and
- In the in-stationary case, the gradient along the crest of the wave group is zero. The direction of the crest is derived from the local mean wave direction and the values at the boundary are determined by interpolation around a virtual point.

Flow Boundary Conditions

At the seaward (and in the case of a bay the landward) boundary, radiating boundary conditions are prescribed. The lateral boundary conditions, by default, use the 'Neumann Boundary' condition in which the longshore water level gradient is set to be zero.

A detailed description of XBeach is freely available (Roelvink et al., 2010) to which the reader is referred for a full description of the model.
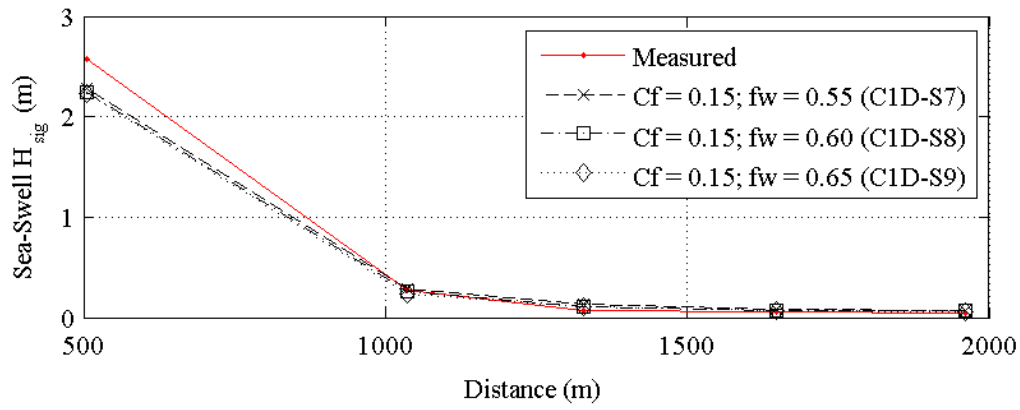
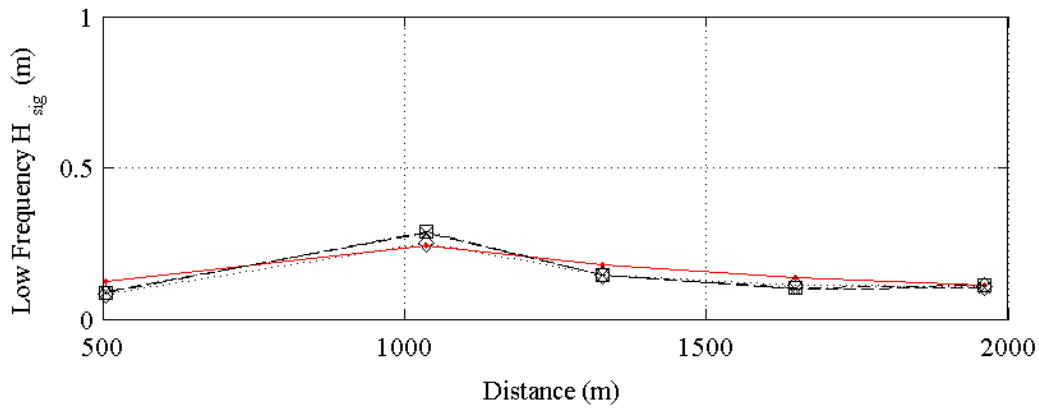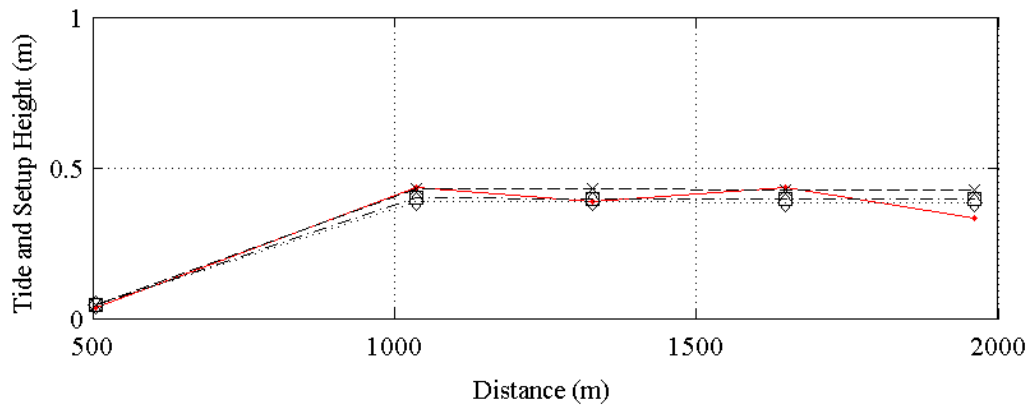# Appendix E

ADDITIONAL 1D CALIBRATION RESULTS
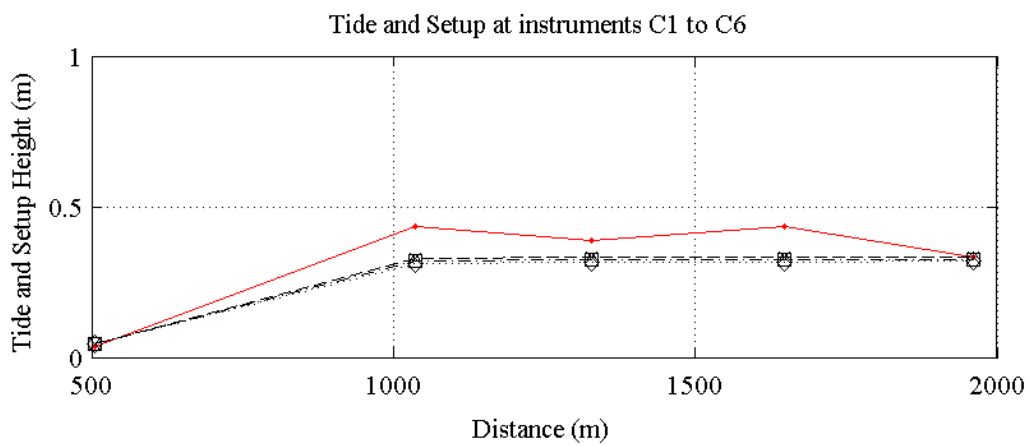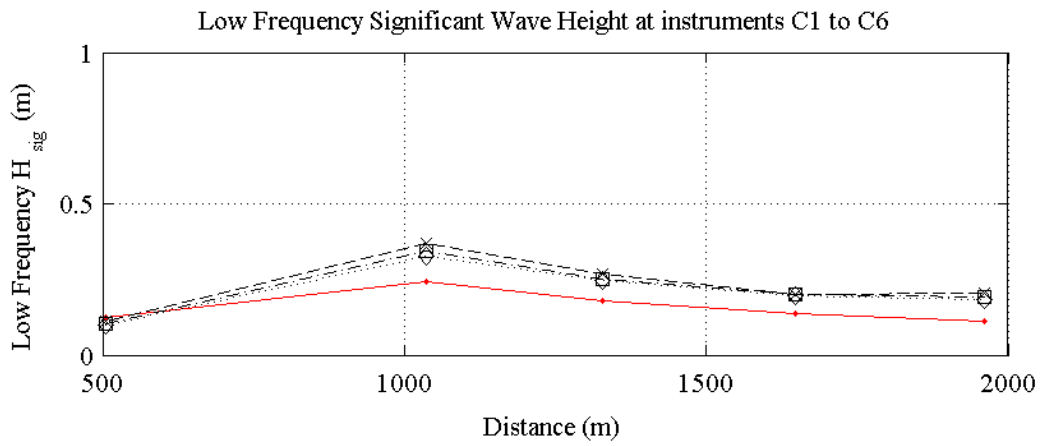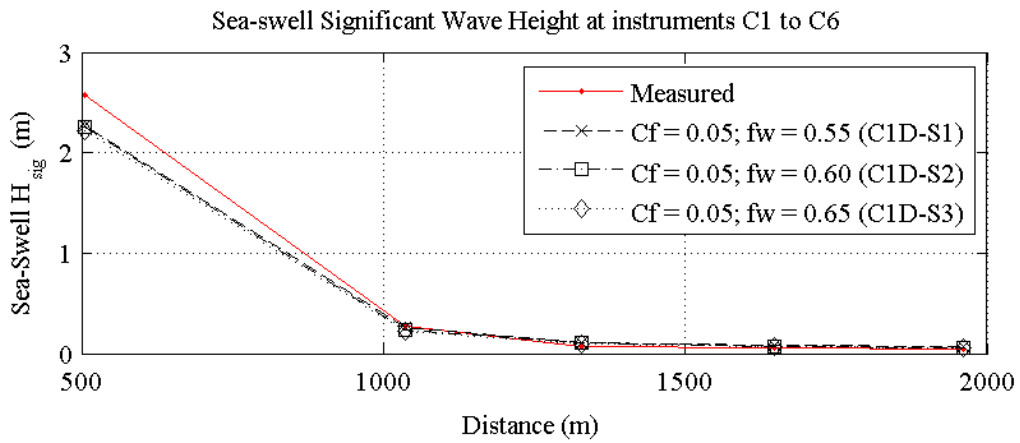
Sea-swell Significant Wave Height at instruments C1 to C6

Low Frequency Significant Wave Height at instruments C1 to C6

Tide and Setup at instruments C1 to C6

Sea-swell Significant Wave Height at instruments C1 to C6

Low Frequency Significant Wave Height at instruments C1 to C6

Tide and Setup at instruments C1 to C6

Appendix F

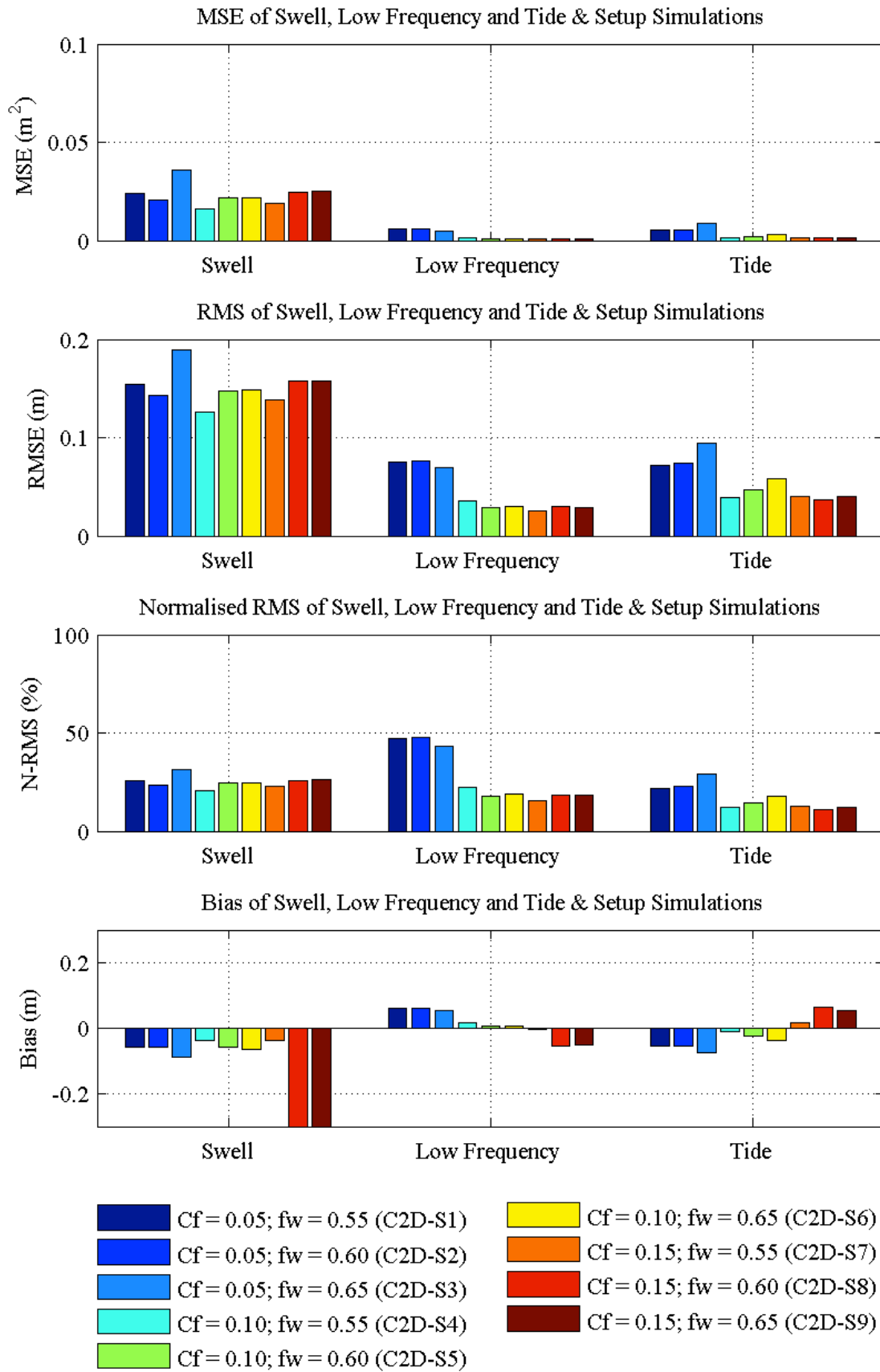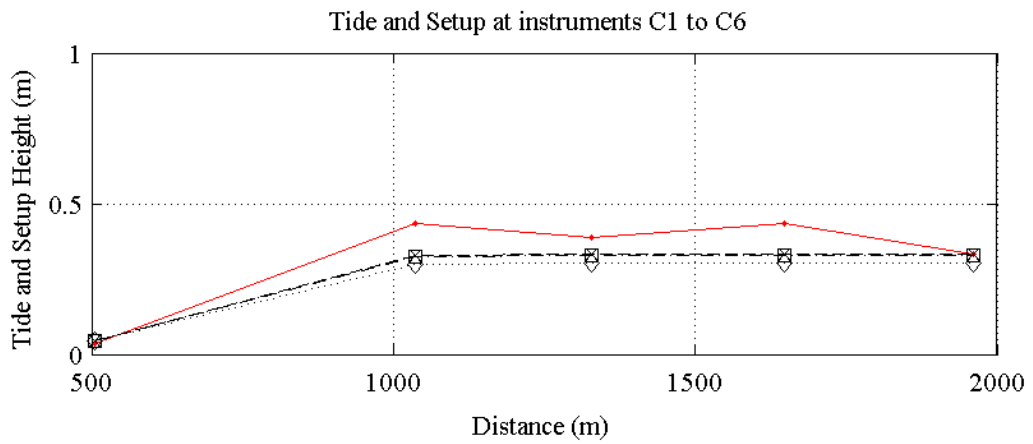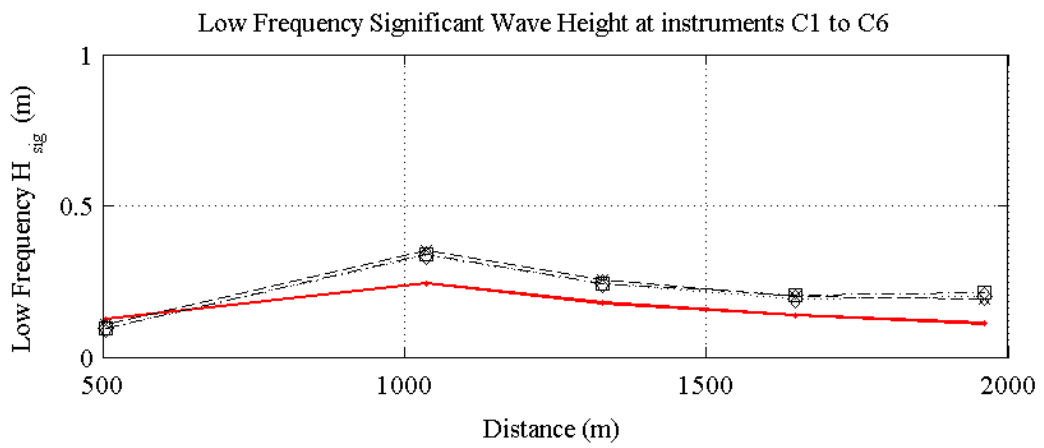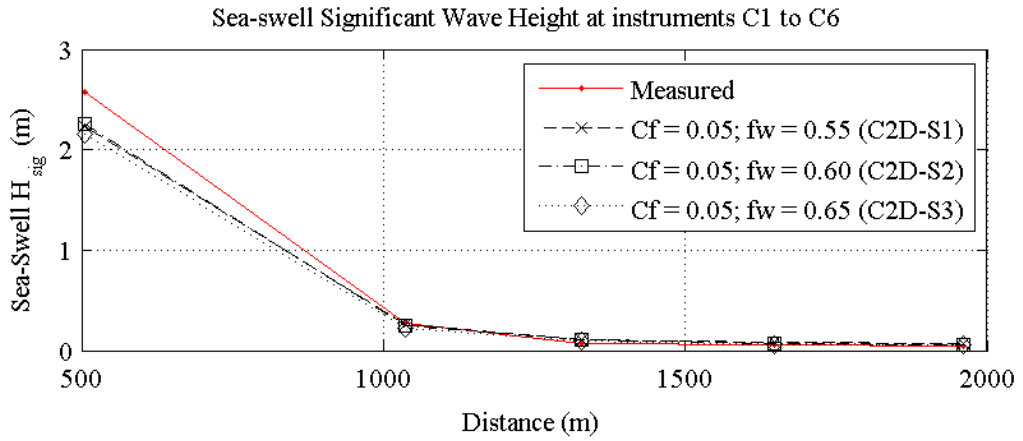## THREE-CELL CALIBRATION RESULTS AND COMPARISION WITH 1D MODEL

F.1   Assessment of calibration results

The statistical and spatial distribution results of the three-cell model were consistent with the 1D model results and for this reason will not be discussed. This demonstrates that the two model types are consistent.
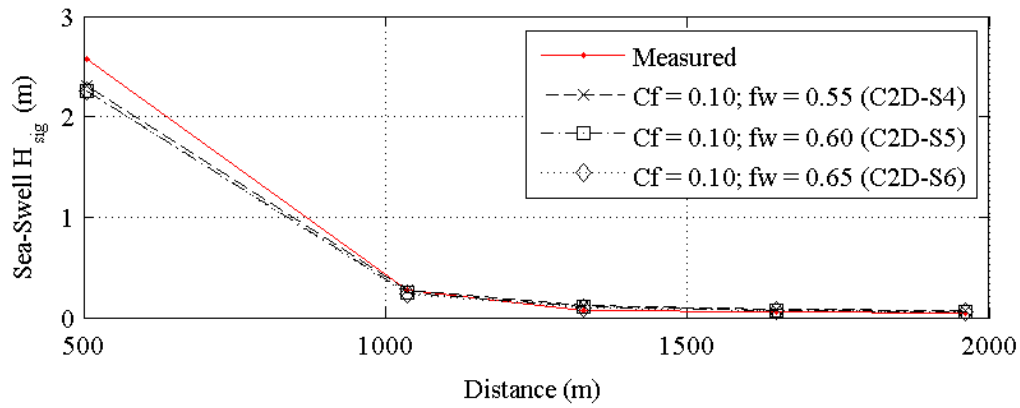
1D and three cell simulations (site profile)			
ID	Type	c_f	f_w
C2D-S1	2D	0.05	0.55
C2D-S2	2D	0.05	0.60
C2D-S3	2D	0.05	0.65
C2D-S4	2D	0.10	0.55
C2D-S5	2D	0.10	0.60
C2D-S6	2D	0.10	0.65
C2D-S7	2D	0.15	0.55
C2D-S8	2D	0.15	0.60
C2D-S9	2D	0.15	0.65

1D and three cell comparison			
ID	Type	c_f	f_w
CC-S1	1D	0.1	0.6
CC-S2	2D	0.1	0.6

MSE of Swell, Low Frequency and Tide & Setup Simulations

RMS of Swell, Low Frequency and Tide & Setup Simulations

Normalised RMS of Swell, Low Frequency and Tide & Setup Simulations

Bias of Swell, Low Frequency and Tide & Setup Simulations

Cf = 0.05; fw = 0.55 (C2D-S1)
Cf = 0.05; fw = 0.60 (C2D-S2)
Cf = 0.05; fw = 0.65 (C2D-S3)
Cf = 0.10; fw = 0.55 (C2D-S4)
Cf = 0.10; fw = 0.60 (C2D-S5)
Cf = 0.10; fw = 0.65 (C2D-S6)
Cf = 0.15; fw = 0.55 (C2D-S7)
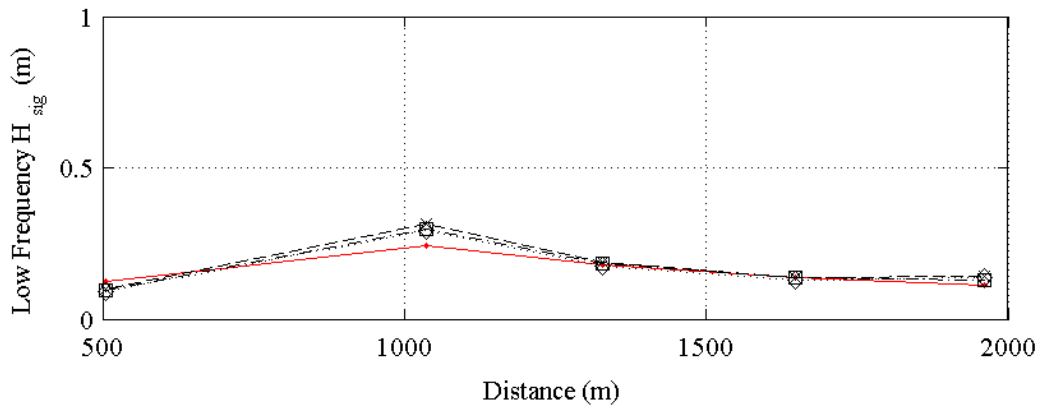Cf = 0.15; fw = 0.60 (C2D-S8)
Cf = 0.15; fw = 0.65 (C2D-S9)

136

Sea-swell Significant Wave Height at instruments C1 to C6

Low Frequency Significant Wave Height at instruments C1 to C6

Tide and Setup at instruments C1 to C6
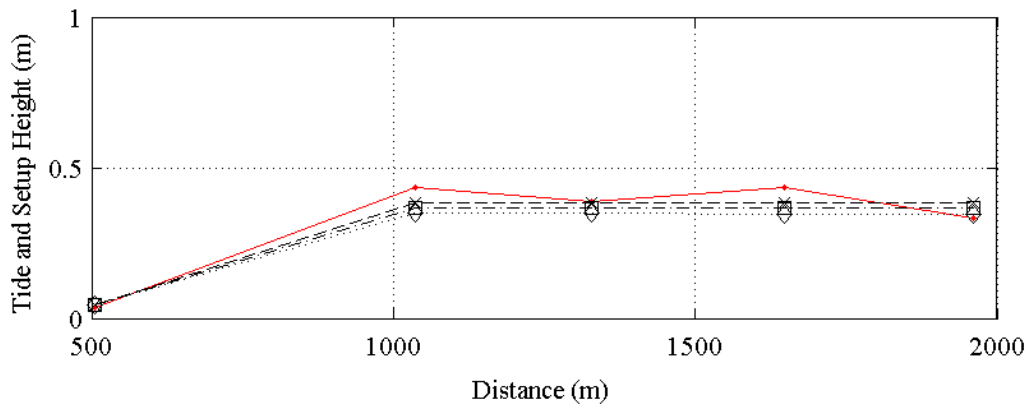
Sea-swell Significant Wave Height at instruments C1 to C6

Low Frequency Significant Wave Height at instruments C1 to C6

Tide and Setup at instruments C1 to C6
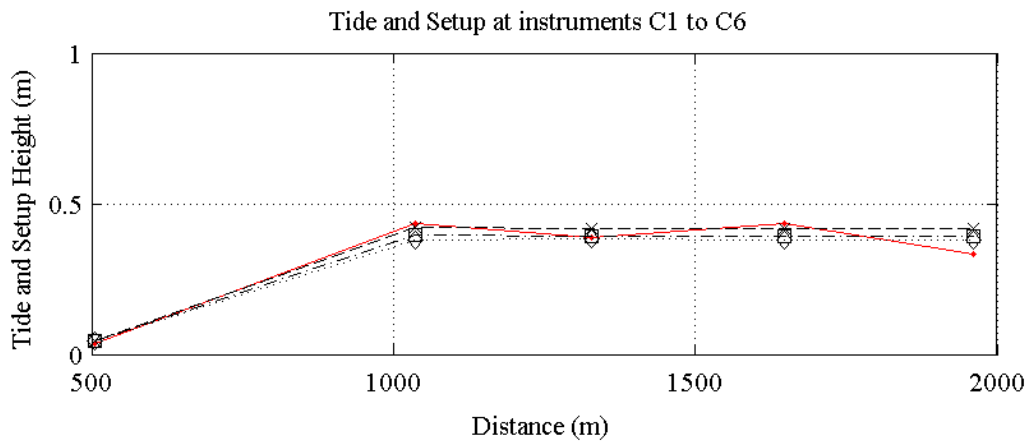
138

Sea-swell Significant Wave Height at instruments C1 to C6
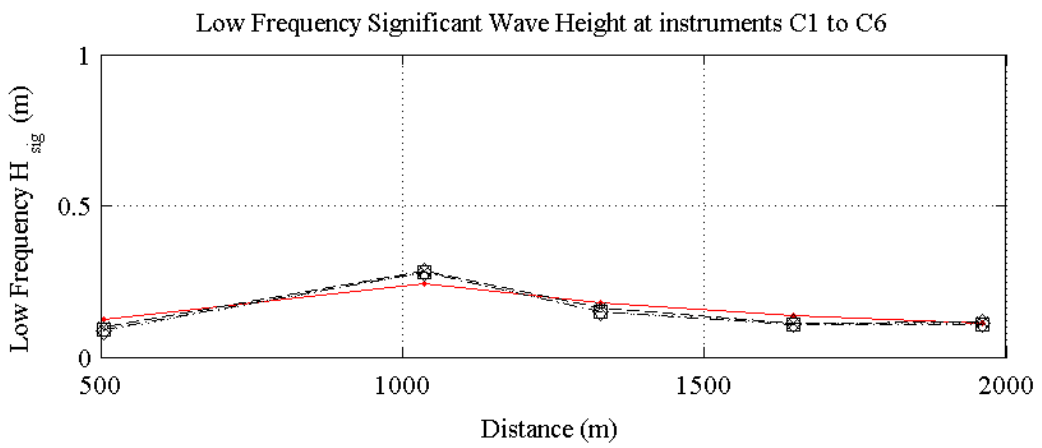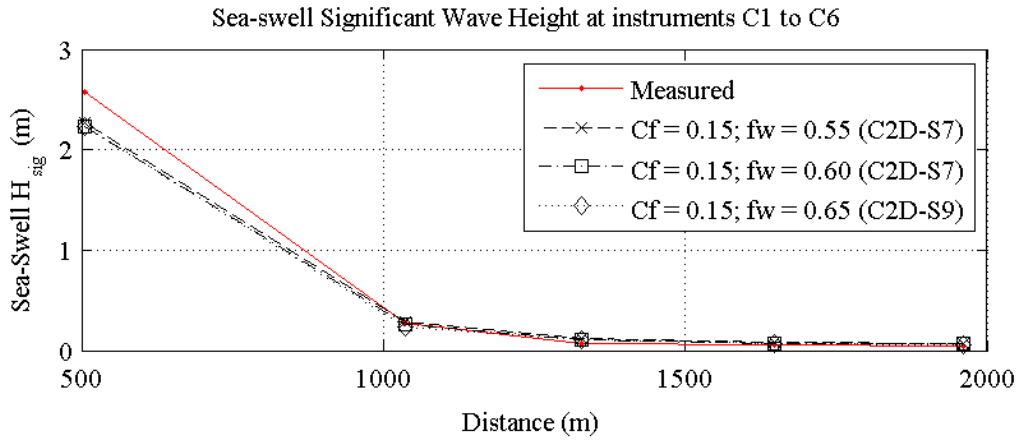
Low Frequency Significant Wave Height at instruments C1 to C6

Tide and Setup at instruments C1 to C6

F.2 Comparison of three cell and 1D model results (Site Profile)

Confirmation of consistency between the three-cell and 1D models was demonstrated by the comparison of the statistical and spatial results obtained for the best-fit case of $C_f = 0.1$ and $f_w = 0.6$.

The analysis indicates that for this best-fit model, the three-cell 1D simulations produced the same results. The sea-swell waves were found to be underestimated (RMSE: 0.1470 m, BIAS: -0.0566 m) at the offshore measurement station but consistent with the measured results across the reef and lagoon. The statistical results indicated the that low-frequency waves were slightly overestimated (RMSE: 0.0295 m, BIAS: 0.0077 m) however the spatial distribution indicated that the wave heights were underestimated offshore and overestimated on the reef crest. Across the reef and into the lagoon the low-frequency waves agreed with the measured data. A slight overestimation was observed near the shoreline. The tide and setup component was statistically underestimated (RMSE: -0.0273 m, BIAS: -0.0273 m), a result observed spatially except at the shoreline where this component is found to be slightly overestimated.

MSE of Swell, Low Frequency and Tide & Setup Simulations

RMS of Swell, Low Frequency and Tide & Setup Simulations

Normalised RMS of Swell, Low Frequency and Tide & Setup Simulations

Bias of Swell, Low Frequency and Tide & Setup Simulations

Sea-swell Significant Wave Height at instruments C1 to C6: Cf = 0.10, fw = 0.60

Low Frequency Significant Wave Height at instruments C1 to C6

Tide and Setup at instruments C1 to C6